



**NTNU – Trondheim**  
Norwegian University of  
Science and Technology

# Study on the Swelling Potential of some Selected Rocks

**Catrine Pettersen**  
**Skippervik**

Geology

Submission date: July 2014

Supervisor: Krishna Kanta Panthi, IGB

Co-supervisor: Filip Dahl, IGB

Norwegian University of Science and Technology  
Department of Geology and Mineral Resources Engineering



# Acknowledgements

---

The master thesis has been carried out during the fall/winter 2013 and spring/summer 2014 at the Department of Geology and Mineral Resources Engineering, Norwegian University of Science and Technology (NTNU), Trondheim, Norway. The cooperating partner for this thesis has been SINTEF Building and Infrastructure, Trondheim, Norway.

Associate professor Krishna K. Panthi, at the Department of Geology and Mineral Resources Engineering, Geological engineering at NTNU, has been my main supervisor in this work. A special thanks to him for his great knowledge and guidance during this period and for making the project task.

Laboratory manager, Filip Dahl, at SINTEF Building and Infrastructure, Geological engineering laboratory, SINTEF/NTNU has been my co-supervisor. I am grateful for his good and useful contributions during the laboratory work and for his guidance and knowledge during the entire period.

Senior engineer, Erik Endre, at the Norwegian Geotechnical Institute, Oslo, Building, Construction and Transportation, Rock Engineering has been so kind and contributed with procurement of the alum shale.

Rock technician, Simon A. Hagen, at SINTEF Building and Infrastructure, Geological engineering laboratory, SINTEF/NTNU has been very helpful and supervised the laboratory work. Also thanks to all the good and useful contributions on the work.

Rock technician, Kjartan Følke, at SINTEF Building and Infrastructure, Geological engineering laboratory, SINTEF/NTNU has been very helpful in the preparation of the rock cubes.

Senior engineer, Gunnar Vistnes, at the Department of Geology and Mineral Resources Engineering, has been very helpful with the sample preparations. He has also been consultative in the laboratory testing.

Laboratory technician, Joakim Eggen, at SINTEF Building and Infrastructure, Geological engineering laboratory, SINTEF/NTNU has been very patient and has answered all my questions. He has also prepared and cut the rock cubes for the laboratory testing.

Laboratory technician, Niklas Haugen, at SINTEF Building and Infrastructure, Geological engineering laboratory, SINTEF/NTNU has helped me when ever needed and guided me and answered all my questions.

Staff Engineer, Arild Monsøy and Kjetil Eriksen, at the Department of Geology and Mineral Resource Engineering, Sliplaboratorium, helped preparing the rock cylinders and the thin sections for the laboratory testing.

Senior Engineer, Laurentius Tjihuis, at the Department of Geology and Mineral Resource Engineering, Chemical-/Mineralogical laboratory has been performing the XRD analysis for the test material.

Associate Professor, Bjørn Eske Sørensen, at the Department of Geology and Mineral Resource Engineering, Microscopy laboratory, has contributed with his knowledge and been very helpful regarding the thin section analysis.

I also have to thank my husband Runar Skippervik for his patience and good mood, and his invaluable support during the work of my master thesis. I appreciate his constructive inputs and advices, and also the proofreading of my thesis. Finally I give my thanks to my precious little son; because of him I have worked very hard to complete my work.

## Abstract

---

Weaknesses zones consisting of sheared and fractured rock mass have a swelling potential in the presence of clays rich in montmorillonite. When it comes to intact rocks there are questions regarding both the swelling potential and the main reasons for swelling in the different rock types. This is experienced in several projects, where swelling of intact rock has been different than what was expected.

To better understand what is causing the behaviour of intact rock when exposed to water a comprehension on the water impact on the swelling potential is required. For clay minerals the swelling mechanisms and factors influencing on the swelling potential is explained and confirmed by comprehensive research. Four types of clay minerals are discussed to describe the swelling potential of these minerals in contact with water.

The extensive laboratory work performed for this thesis addresses a study on the expansive character of intact rock. Three different rock types are tested; alum shale, greenschist and tuff and the rocks vary in both structure and mineral composition. The rocks were selected in dialog with the supervisors at SINTEF and NTNU.

Three traditional test methods, swelling pressure determination performed on dust powder and rock cylinders and free swelling, have been used in the previous testing on both gouge material and intact rocks. The measured values for swelling pressure have been low even though observations would indicate otherwise. For this reason a new approach has been made and a new test apparatus is developed by SINTEF/NTNU. This method for determination on the swelling strain of rocks cubes when submerged in water gives measurements in three directions. When exposed to water the displacement in all three directions is recorded over time. The mentioned swelling test methods are combined with mineralogical analysis and rock mechanical tests to determine the swelling potential of intact rock and to find correlations that might explain the mechanisms of swelling in a larger scale. The applicability of this new method and comparisons to the other test methods is discussed.

Following conclusions on the basis of the test results are drawn:

- All three rocks show swelling potential of varying degree and some correlations between swelling potential and rock mechanical properties are found.
- The testing method for rock cube is by far the best in terms of execution and presentation of the results. This method is the most tangible regarding criterias and behaviour of expansive rocks as it results in values for actual displacement of the rock mass which may relate to the in situ conditions.

## Sammendrag

---

Svakhetssoner som består av knust og oppsprukket bergmasse har et svellepotensiale dersom det er tilstedeværelse av leire rik på montmorillonitt. Når det kommer til intakt berg er det fortsatt en del spørsmål knytte til både svellepotensialet og hovedårsaker til svelling for de ulike bergarter. Dette er erfart i flere prosjekter, hvor svelling av intakt berg har vært ulikt det som var forventet.

For å bedre kunne forstå hvordan intakt berg oppfører seg ved kontakt med vann er det nødvendig med en forståelse av vannets påvirkningskraft på svellepotensialet. For leireminerale finnes omfattende forskning og utallige forklaringer på svellemekanismene og de faktorer som påvirker svellepotensialet. Fire typer leirminerale blir drøftet for å beskrive svellepotensialet disse har i kontakt med vann.

Laboratoriearbeidet utført i forbindelse med denne masteroppgave omhandler en studie på intakt bergs ekspansjonskarakter. Tre forskjellige bergarter er testet; alunskifer, grønnskifer og tuff og bergartene varierer i både struktur og mineralsammensetning. Bergartene ble valgt i dialog med veilederne ved SINTEF og NTNU.

Tre tradisjonelle testmetoder, svelletrykk bestemmelse utført på pulver og intakt skive og fri svelling, har vært brukt i tidligere testing på både sleppemateriale og intakt berg. De målte verdier for svelletrykk har vært lave selv om observasjoner skulle tilsi noe annet. Av denne grunn har en foretatt en ny tilnærming og en nytt testapparat har blitt utviklet av SINTEF/NTNU. Denne metoden bestemmer utvidelsen av en intakt kube i tre retninger etter at det er tilført vann. De nevnte svellestene kombineres med mineralogiske analyser og bergmekaniske tester for å kunne bestemme svellepotensialet av intakt berg og for å finne korrelasjoner som kan forklare mekanismene av svelling i større skala. Anvendbarheten av denne nye testen samt sammenligninger med de andre testmetodene er diskutert.

Følgende konklusjoner basert på testresultatene er:

- Alle tre bergarter viser et svellepotensiale av ulike grad og noen korrelasjoner mellom svellepotensiale og bergmekaniske egenskaper er funnet.
- Test metoden for kube er den desidert beste når det gjelder utførelse og presentasjon av resultater. Denne metode er den mest håndgripelige vedrørende kriterier og oppførsel av ekspanderende bergarter siden den gir verdier for faktisk utvidelse av bergmassen som kan relateres til forholdene in situ.

# Table of contents

---

<b>Acknowledgements</b> .....	<b>i</b>
Abstract .....	iii
Sammendrag.....	iv
<b>List of Symbols and Abbreviations</b> .....	<b>viii</b>
<b>1 Introduction</b> .....	<b>1</b>
1.1 Background.....	1
1.2 Introduction to swelling potential.....	1
1.2.1 Project background .....	1
1.2.2 Swelling characteristics of clay minerals .....	1
1.2.3 Swelling characteristics of intact rock .....	2
1.3 Purpose and scope of the work.....	2
1.4 Constraints of the laboratory work .....	2
<b>2 Swelling characteristics of clay minerals</b> .....	<b>5</b>
2.1 The mechanisms of swelling in clay minerals.....	5
2.1.1 Formation of clay minerals .....	5
2.1.2 Properties and structure of clay minerals .....	6
2.1.3 Swelling process .....	7
2.1.4 Classification of the clay minerals .....	7
2.2 Clay minerals .....	9
2.2.1 Montmorillonite .....	9
2.2.2 Vermiculite .....	10
2.2.3 Illite .....	11
2.2.4 Kaolinite.....	13
2.3 Instability issues.....	14
<b>3 Review of two tunnel instability cases</b> .....	<b>17</b>
3.1 Tunnel 1 – The Frøya subsea tunnel.....	17
3.1.1 Issues .....	18
3.1.2 Swelling potential .....	22
3.1.3 Rock support and tunnelling progress.....	23
3.2 Tunnel 2 – The Hanekleiv tunnel .....	24
3.2.1 Issues .....	25
3.2.2 Swelling potential .....	27

3.3.3 Rock support and tunneling progress .....	28
<b>4 Selected rocks and sample preparations .....</b>	<b>31</b>
4.1 Rock type .....	31
4.1.1 Alum shale .....	31
4.1.2 Greenschist .....	33
4.1.3 Tuff.....	34
4.2 Sample types .....	35
4.2.1 Dust powder .....	35
4.2.2 Rock cylinders.....	36
4.2.3 Rock cubes .....	38
4.2.4 Rock pieces .....	39
4.2.5 Thin sections.....	40
<b>5 Methodology and standards .....</b>	<b>41</b>
5.1 Standards suggested by the ISRM .....	41
5.1.1 The ISRM suggested method for determination of the swelling pressure index.....	41
5.1.2 The ISRM suggested method for determination of the swelling strain .....	44
5.1.3 The ISRM suggested method for determination of the slake-durability index.....	45
5.1.4 The ISRM suggested method for point load strength determination .....	47
5.2 Method for swelling pressure determination - constant volume, axial swelling.....	49
5.3 Petrographic and mineralogical test methods .....	50
5.3.1 X-ray diffraction analysis .....	50
5.3.2 Thin section analysis.....	52
5.4 Rock mechanical test methods.....	53
5.4.1. Density test.....	53
<b>6 Results from laboratory work .....</b>	<b>55</b>
6.1 Swelling tests.....	55
6.1.1 Swelling pressure index – bulk material and free swelling .....	55
6.1.2 Swelling pressure - rock cylinders .....	58
6.1.3 Swelling strain - undisturbed and unconfined rock cubes .....	63
6.2 Mineralogical tests .....	65
6.2.1 X-ray diffraction – bulk material.....	65
6.2.2 Thin sections – customized rock cores .....	68
6.3 Rock mechanical testing .....	76
6.3.1 Point load strength – rock pieces .....	76



6.3.2 Slake-durability index – rock pieces .....	78
6.3.3 Density – irregular rock pieces .....	80
<b>7 Evaluations and comparisons.....</b>	<b>81</b>
7.1 Mechanical properties of the tested rocks .....	81
7.1.1 Evaluation of the test results.....	81
7.1.2 Comparisons with competent crystalline rocks .....	82
7.2 Swelling characteristics of the tested rocks .....	84
7.2.1 Evaluation of the test results.....	84
7.2.2 Comparison in relation with dust powder, rock cylinders and rock cubes .....	85
7.2.3 Comparison with swelling clays.....	91
7.3 Applicability of the testing methods for rock cylinders and rock cubes .....	94
7.3.1 Evaluation and discussion of the sample preparation .....	94
7.3.2 Evaluation and discussion of the performance and results of the testing.....	94
7.3.3 Comparison of the applicability for the two testing methods .....	95
<b>8 Discussion .....</b>	<b>97</b>
8.1 Swelling characteristics .....	97
8.2 Swelling potential based on test results.....	99
8.3 Strength and limitations of the laboratory work.....	102
<b>9 Conclusions and recommendations.....</b>	<b>103</b>
9.1 Conclusions.....	103
9.2 Recommendations.....	104
<b>References.....</b>	<b>105</b>
<b>Appendix A: Tunnel profile.....</b>	<b>109</b>
<b>Appendix B: Geological timescale - chronostratigraphic chart.....</b>	<b>113</b>
<b>Appendix C: Classification of swelling parameters of gouge material .....</b>	<b>115</b>
<b>Appendix D: Classification of rock composition, grain size, texture and silicate minerals. ....</b>	<b>117</b>
<b>Appendix E: Classification of point load strength.....</b>	<b>121</b>
<b>Appendix F: Classification of slake-durability index .....</b>	<b>125</b>
<b>Appendix G: Classification of density and compressive strength .....</b>	<b>127</b>

## List of Symbols and Abbreviations

---

A	Angstrom/Ångström (Å), $1\text{Å} = 10^{-10}\text{ m}$
AADT	Annual average daily traffic
DTA	Differential thermal analysis
D&B	Drill and Blast
rpm	Revolutions per minute
SEM	Scanning electron microscope
Strike & Dip	Orientation of a rock layer, fault etc.
XRD	X-ray diffraction

# 1 Introduction

---

## 1.1 Background

The research topic for this master thesis is “*Study on the swelling potential of some selected rocks*”. This implies a research of the swelling potential of intact rocks that have an expansive character, compared to the more comprehensive research of swelling potential for clay minerals. The swelling potential might have an adversely effect on the stability of tunnels, slopes and foundations. There exists more research on the determination of swelling potential of clays and gouge materials and less on the swelling potential of intact rock. In the recent years, the focus on the latter case has increased, and this entails both the development of already existing test methods, as well as an adjustment to the new methods (Dahl. et. al, 2013).

## 1.2 Introduction to swelling potential

### 1.2.1 Project background

Challenges and problems related to the swelling potential of clays and rock material entail the need for quantifying the swelling characteristics by laboratory testing. This master thesis will compare the traditionally test methods for determining swelling behaviour of gouge materials and clays with the new apparatus developed for testing on intact rock, see chapter 5.

The selected rocks for this thesis are alum shale, greenschist and tuff. The tests regarded to determining swelling potential are free swelling, swelling pressure by oedometer and 3D free swelling. Chapter 5 gives a further elaboration of these topics.

A thoroughly sample preparation involving drilling, slicing, cutting and crushing of the selected rock material is performed, providing cores, cored cylinders, cubes, pieces and milled dust, see chapter 4. The laboratory test methods mentioned above and both mineralogical and rock mechanical test methods are carried out, chapter 5.

The test results will then be evaluated and presented, and comparisons between the different test methods and the sample types will be discussed, to find correlations between them. Also the applicability of the testing methods for rock cylinders and rock cubes is to be discussed. Finally the test results for intact rock will be compared to the ones for clays. Chapter 7 gives a detailed discussion of these evaluations and comparisons.

### 1.2.2 Swelling characteristics of clay minerals

Clays such as smectite, that is rich in montmorillonite, may in contact with water expand, this meaning the material may have a swelling potential. The swelling characteristics and the degree of expansion depend on the material exposed, the presence of swelling minerals and the amount of water accessible. The swelling potential may result in stability issues and threats to foundations, slopes and tunnels if the

swelling potential is mobilized. Section 2 provides a detailed discussion on the factors listed and other factors influencing on the swelling mechanisms.

### **1.2.3 Swelling characteristics of intact rock**

Intact rocks with swelling potential may also result in stability problems in tunnels, slopes and foundations. The knowledge on the cause and how this swelling potential may affect the in situ stability is still inadequate, so a new and improved test apparatus and methods have been developed (Dahl. et. al, 2013).

## **1.3 Purpose and scope of the work**

The main purpose of this master thesis is to study some selected rocks and their potential to swell, including their swelling characteristics. This study will be based on extensive laboratory work and for this thesis, various rock mechanical tests and mineralogical analysis also will be performed. The scope of the MSc Project Task is:

- *A description of the swelling characteristics of some clay minerals and instability caused by swelling to foundations, slopes and tunnels performed by a literature review*
- *Two tunnel cases where stability problems are caused by swelling*
- *Free swelling and swelling pressure tests of black shale, green schist and andesite shall be carried out, for milled dust, cored rock cylinders and rock cubes*
- *For the same rock types, mineralogical tests using XRD and thin sections analysis*
- *Mechanical tests, like density, Brazilian tensile and slake durability shall be carried out*
- *Evaluation and presentation of the mechanical properties. Comparison of the results against competent crystalline rocks, and evaluation of the differences*
- *Evaluation and presentation of the swelling characteristics of the tested rocks. Comparison of the results in relation with dust powder, rock cylinders and rock cubes. Comparison of the results with swelling clays*
- *Evaluation and discussion on the applicability of the testing methods for rock cylinders and rock cubes*

The background information for the study is:

- *Relevant information and data from SINTEF*
- *The information provided by the supervisors*
- *Scientific papers, reports and books related to the subject*

## **1.4 Constraints of the laboratory work**

The constraints of the work are due to the difference between the laboratory test results and the actual in situ test conditions. The test methods are index tests using small rock samples, hence not representative for full scale testing. The quantities and the condition of the samples depend on the

sampling and the preparations prior to the laboratory testing, see section 4.2 and the main reasons for this difference are as follows (Dahl et.al, 2013):

- Sampling and preparation might damage the structure and compaction of the specimen.
- Only a small amount is tested.
- The time between excavation and installation of the rock support and the rock support behaviour have an impact on the in situ swelling pressure.
- The laboratory testing is based on ideal conditions; dry materials representing the highest swelling potential and for clays: fractions representing the most active part of the gouge material.



## 2 Swelling characteristics of clay minerals

---

For clay minerals to expand, and further cause stability problems in tunnels, slopes and foundations, certain assumptions and factors have to be fulfilled. There has to be a potential for swelling and the potential need to be mobilized, a swelling pressure is required. The factors having a significant impact on the swelling potential are described as internal factors and the factors affecting the mobilization of the swelling potential as external factors (Brekke and Selmer-Olsen, 1965), these are discussed in the following sections. The clay minerals ability to swell is closely related to the formation of them, their capture- and emits capability of available water and the types of exchangeable cations in the sheet silicate (Selmer-Olsen and Palmstrøm, 1989).

The chemical composition of the clay minerals, the structure of them, the conditions and processes forming them and the existence of water, will influence on the degree of expansion and the swelling characteristics. The clay minerals capacity to swell (Brekke and Selmer-Olsen, 1965) and the cause of swelling are thus of great importance regarding to the extent of the stability issues and problems.

Section 2.1 deals with the general understanding of swelling mechanisms and section 2.2 addresses two expansive clay minerals; montmorillonite and vermiculite and two nonexpansive clay minerals; kaolinite and illite. These minerals ability to swell will be assessed against potentially instability factors, section 2.3.

### 2.1 The mechanisms of swelling in clay minerals

#### 2.1.1 Formation of clay minerals

Clay minerals are often found in gouges and weakness zones, known as swelling clay zones. These swelling clay zones consist of faults and joints filled with clay minerals, and altered rock masses where the gouge material are part of the formation of the rock (Selmer-Olsen and Palmstrøm, 1989).

The clay minerals are either formed by hydrothermal deposition or as a result of transformation of crushed side rock. Factors influencing the formation of clay minerals are the composition and temperature of the fluid and the permeability of the rock mass. This subject will not be addressed further. The latter formation of clay minerals involves a hydrolysis of feldspar of varying composition, which transforms the original structure of the crystal to clay. The highly expandable montmorillonite mineral is formed from the hydrolysis of albite, a member of the feldspar group, by the given, simplified, chemical reaction formula (Nilsen and Broch, 2009) as following;



The albite reacts with water and montmorillonite, silicon dioxide and positively charged cations, in this case sodium ions, are the reaction product. Formation of the various types of clay minerals depends on the reactants, the temperature and the water flow.

## 2.1.2 Properties and structure of clay minerals

Clay minerals have a distinct structure, and the kaolinite mineral is shown in figure 2-1. Typical structure of swelling clay minerals is given by sheets of  $\text{SiO}_4$ -tetrahedrons and  $\text{Al}(\text{OH})_3$ -octahedrons bonded by oxygen molecules and combined with interlayers, of free and exchangeable cations and water molecules, of various thickness and ratios (Nilsen, 2010), figure 2-2 and 2-3. These silicate minerals are composed of a number of sheets assembled in unit layers and the specific combination of the unit layers and the forces between the layers defines the type of clay mineral.

Most expandable clay minerals have a 2:1 ratio of tetrahedrons and octahedrons and the interlayer spaces (The Cooperative Soil Survey, 2014) are capable of storing cations and water molecules. The difference between the various expandable clay minerals and thus the capability to swell is the size of the interlayer spaces, the greater spacing the greater change in the shrink and swell behaviour.

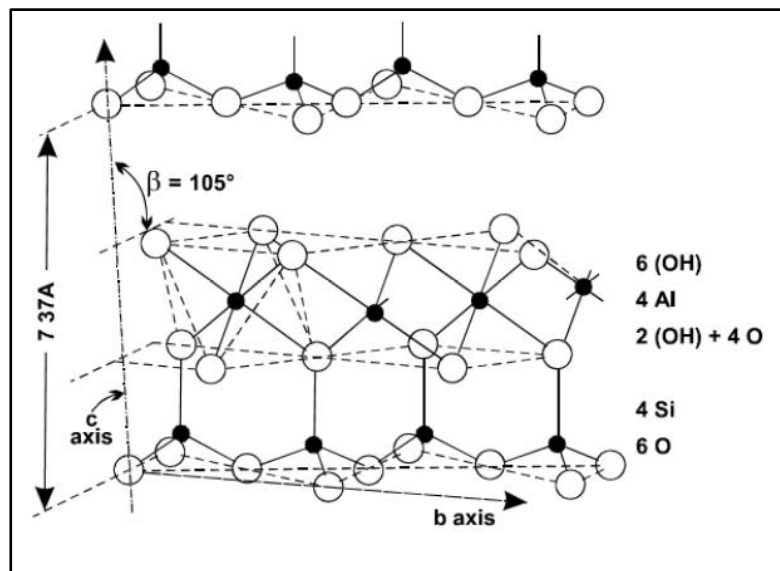


Figure 2-1: Typical structure of a kaolinite mineral (Nilsen, 2010).

As mentioned above some factors and assumptions have to be met for swelling to happen and further causing stability threats to structures and underground works. The internal factors refer to the properties of the clay minerals and cations in the clays, while the external factors refer to the properties of available pore water and the ions in the water (Brekke and Selmer-Olsen, 1965). The type, structure, particle size, amount and dry density of the clay minerals are essential internal factors, as well as the concentration of the ions and type of cations in the clay and finally the initial water content. External factors are the amount of available pore water, the pore water chemistry and properties, the concentration and valence of the ions and the type and strength of the particle bonding (Pusch, 2012).

Clay minerals are relatively small and have large reactive surface areas which imply a potential for swelling (Nilsen, 2010) provided that the previously mentioned factors are fulfilled. The greater the average specific surface area the more surface forces are acting and causing a higher volume change and a higher swelling pressure (Pusch, 2012). The swelling pressure and the volume changes have significant influence on the behaviour and the properties of the clay minerals and are indications of



increased swelling. The clays are likely to experience deformations of the crystal structure and changes in the mineral strength and in the hydraulic conductivity (Pusch, 2012). The amount and dry density of the clay minerals, the forces between the clay particles and the composition and amount of the pore water are affecting the swelling degree (Nilsen and Broch, 2009).

The positively charged cations, with more protons than electrons, have attractive forces acting on the exchangeable positions of the negatively charged surface of the clay minerals and the concentration and valence of the cations reflect the magnitude of the mobilized swelling pressure (Pusch, 2012). The attractive forces towards the exchangeable positions on the clay surface increase with increased concentration of the specific cations where;  $\text{Li}^+ < \text{Na}^+ < \text{Mg}^{2+} < \text{Ca}^{2+} < \text{H}^+$  (Pusch, 2012). The most common cations (Nilsen and Broch, 2009) are the divalent calcium ions ( $\text{Ca}^{2+}$ ), the monovalent potassium ions ( $\text{K}^+$ ), the divalent magnesium ions ( $\text{Mg}^{2+}$ ) and the monovalent sodium ions ( $\text{Na}^+$ ).

### **2.1.3 Swelling process**

The swelling potential presupposes in most cases wet conditions and the material undergoes both shrinkage and swelling as a result of drying and wetting cycles from water content changes (Pusch, 2012). An important factor is the dissimilar behaviour the various clay minerals have according to the water content changes, and will thus be a source of different volume changes which in turn might affect the stability.

When the conditions for a swelling potential are present a mobilization of this potential will initiate the swelling process. For most expandable clay minerals the swelling process first takes place as a hydration where water molecules are attached to the negatively charged clay surfaces. A transition of highly bonded water molecules on the clay surface to freely pore water is gradually taking place and major swelling might occur. The hydration stadium is followed by an osmotic swelling where water will flow in the direction of highest ion concentration due to differences in the ion concentration between the unit layers and in the pore water (Nilsen and Broch, 2009). Water molecules will be flowing towards the interlayers of the clay minerals and the swelling degree depends on a number of factors like the interlayer spacing, ion concentration and valence and water availability.

A significant factor limiting the volume increase when clays are subjected to swelling is the cementation of clay minerals caused by attractive forces between the clay particles and organic and inorganic adhesives, such as carbonates and hydroxides (Nilsen and Broch, 2009 and Pusch, 2012). The cementation of the particles entails the formation of molecular bindings making the interlayers in the clay minerals impenetrable for cations and water molecules which impair the clays ability to expand.

### **2.1.4 Classification of the clay minerals**

Clay minerals are divided according to their capability to expand and are classified as nonexpansive, moderately expansive or highly expansive. Kaolinite and illite are classified as nonexpansive clay minerals, and vermiculite and montmorillonite as respectively moderately expansive and highly

expansive clay minerals (The Cooperative Soil Survey, 2014). The degree of swelling is related to the degree of volume change, that is high swelling clays indicate a high volume change as opposed to low swelling clays indicating a limited volume change, see table 2-1.

High swelling clays like montmorillonite undergo repeated cycles of shrinking and swelling and have a greater interlayer space between the unit layers which makes it easier for the water molecules and the cations to enter. The positively charged cations are bonded to the negatively charged surfaces causing an expansion of the lattice structure of the clay minerals. The low swelling clays like kaolinite and illite shows a small volume change due to low swelling when rewetted after drying (Pusch, 2012).

Table 2-1: Size and swelling of some clay minerals (Modified after Pusch, 2012).

<b>Mineral</b>	<b>Approximate particle thickness [nm]</b>	<b>Average specific surface area [m<sup>2</sup>/g]</b>	<b>Observed volume change</b>
Montmorillonite	2,0	700-800	High
Illite	20	80-120	Medium
Kaolinite	100	10-15	Low

Table 2-1 shows the correlation between clay particles size and degree of swelling. The montmorillonite minerals are relatively small compared to the ones for illite and the kaolinite and are nevertheless showing the highest observed volume change. The high volume change indicates a high swelling degree due to greater average surface area which enables attachment of a number of water molecules and exchangeable cations.

In table 2-2 a classification of the clay minerals activity based on the values for free swelling and swelling pressure is given.

Table 2-2: A classification of the clay minerals activity based on free swelling and swelling pressure values (Nilsen, 2010).

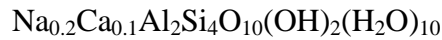
	<b>Free swelling [%]</b>	<b>Swelling pressure [MPa]</b>
Inactive	40-70	< 0,15
Active	100-170	> 0,30
Extremely active	~ 250	~2

As indicated in table 2-2 the clay minerals are divided into three groups where the lowest values for free swelling and swelling pressure indicate inactive clay minerals as opposed to the extremely active clay minerals having the highest free swelling and swelling pressure values. Results from the swelling test methods are given in section 6.1.

## 2.2 Clay minerals

### 2.2.1 Montmorillonite

Montmorillonite is a mineral in smectite and has the empirical formula (Mineralogy Database, 2014):



The clay mineral is the most commonly found expandable clay mineral in gougematerial and weaknesszones. The specific structure and composition of this swelling mineral is causing the greatest concern regarding stability problems. Figure 2-2 shows the structure of the montmorillonite mineral.

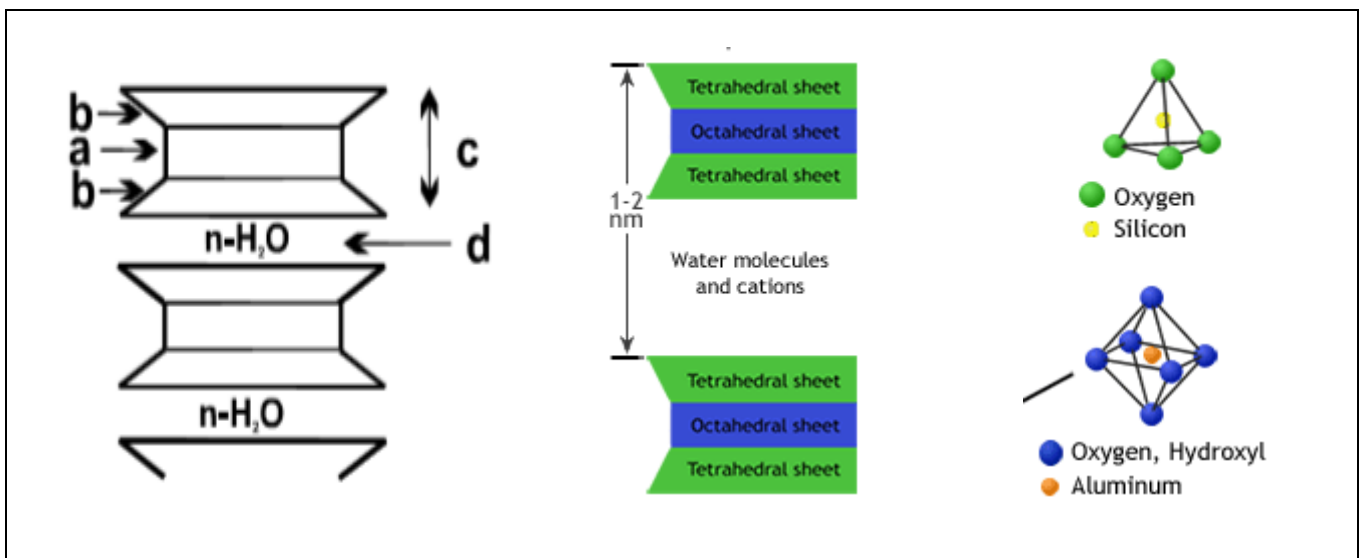


Figure 2-2: Mineral structure of the montmorillonite mineral, showing **a** as an  $\text{Al}(\text{OH})_3$ -layer (blue), **b** as a  $\text{SiO}_4$ -layer (green), **c** as the length of one unit layer and **d** as the interlayer consisting of water molecules and cations (Selmer-Olsen and Palmstrøm, 1989). Also shown are the  $\text{SiO}_4$ -tetrahedron and the  $\text{Al}(\text{OH})_3$ -octahedron, right (The Cooperative Soil Survey, 2014).

The sheet silicate is composed of unit layers of tetrahedrons and octahedrons in a 2:1 ratio with interlayers capable of storing exchangeable cation and water molecules. The total length of a unit layer and an interlayer is 1-2 nanometres (The Cooperative Soil Survey, 2014) and this relatively large spacing implies weak bonds between the unit layers. This allows for a free flow of water molecules and cations in between the unit layers and if the repulsive forces are greater than the attractive forces the unit layers are drawn apart causing a great volume change. The high volume change will in turn results in considerable swelling and the concentration and type of the dominant cation influences the swelling capacity of the clay mineral. This highly expansive mineral is classified as high swelling clay due to the reversible shrinking and swelling behaviour on redrying and rewetting cycles (Pusch, 2012).

Table 2-3 presents the composition of the montmorillonite minerals and is showing both elements and chemical compounds (Mineralogy Database, 2014).

Table 2-3: Composition of the montmorillonite mineral showing both elements and chemical compounds (Modified after Mineralogy Database, 2014).

Element	[%]	Chemical compounds	[%]
Sodium (Na)	0,84	Na <sub>2</sub> O	1.13
Calcium (Ca)	0,73	CaO	1.02
Aluminium (Al)	9,83	Al <sub>2</sub> O <sub>3</sub>	18.57
Silicon (Si)	20,46	SiO <sub>2</sub>	43.77
Hydrogen (H)	4,04	H <sub>2</sub> O	36.09
Oxygen (O)	64,11		

According to table 2-3 the silicon and the oxygen elements constitute as the main parts of the montmorillonite mineral and aluminium oxide, silicon oxide and water molecules as main chemical compounds of the clay mineral (Mineralogy Database, 2014).

### 2.2.2 Vermiculite

Vermiculite has the empirical formula (Mineralogy Database, 2014):



The mineral is a less commonly clay mineral compared to the montmorillonite, and is nevertheless associated with stability problems due to the expansive characters of the mineral. Vermiculite is formed as a result of hydrothermal alteration or weathering of phlogopite or biotite (Mineralogy Database, 2014). Figure 2-3 shows the structure of the vermiculite mineral

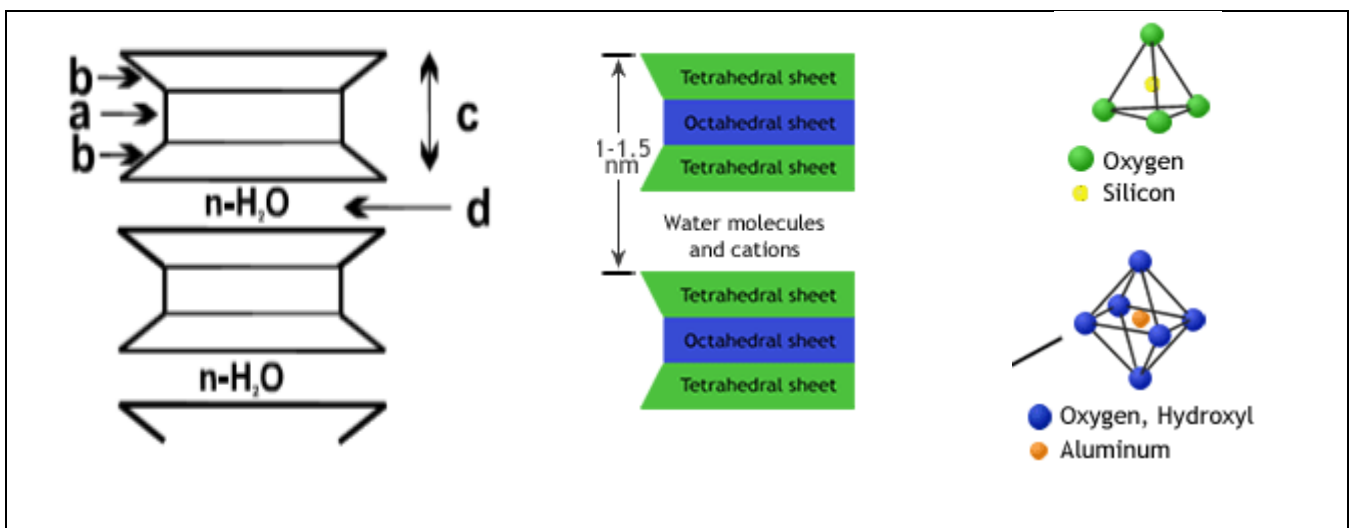


Figure 2-3: Mineral structure of the vermiculite mineral showing **a** as an Al(OH)<sub>3</sub>-layer (blue), **b** as a SiO<sub>4</sub>-layer (green) and **c** as the length of one unit layer and **d** as the interlayer consisting water molecules and cations (Selmer-Olsen and Palmstrøm, 1989). Also shown are the SiO<sub>4</sub>-tetrahedron and the Al(OH)<sub>3</sub>-octahedron, right (The Cooperative Soil Survey, 2014).

The vermiculite mineral is like the montmorillonite mineral composed of unit layers of tetrahedrons and octahedrons in a 2:1 ratio. The inter layers are capable of storing exchangeable cation and water molecules and the total length of a unit layer and an interlayer is 1-1.5 nanometres (The Cooperative Soil Survey, 2014). The spacing between the unit layers let the water molecules and cations enter freely and the unit layers are drawn apart as a result of high repulsive forces. A volume change occurs which implies a swelling of the clay minerals. The vermiculite is classified as moderately expansive and is termed as moderate swelling clay (Pusch, 2012).

Table 2-4 presents the composition of the vermiculite mineral and is showing both elements and chemical compounds (Mineralogy Database, 2014).

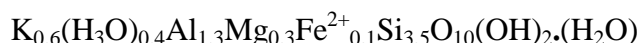
Table 2-4: Composition of the vermiculite mineral showing both elements and chemical compounds (Modified after Mineralogy Database, 2014).

Element	[%]	Chemical compounds	[%]
Magnesium (Mg)	8,68	MgO	14,39
Aluminium (Al)	23,01	Al <sub>2</sub> O <sub>3</sub>	43,48
Iron (Fe)	9,97	FeO	12,82
Silicon (Si)	5,57	SiO <sub>2</sub>	11,92
Hydrogen (H)	2,00	H <sub>2</sub> O	17,87
Oxygen (O)	50,77		

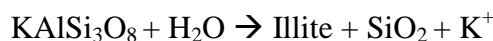
Table 2-4 shows that the hydrogen and aluminium element constitute as the main parts of the vermiculite mineral. Aluminium oxide, water molecules and magnesium oxide are the main chemical compounds of the clay mineral (Mineralogy Database, 2014).

### 2.2.3 Illite

Illite is a nonexpansive clay mineral with the empirical formula (Mineralogy Database, 2014):



The clay mineral is a reaction product from the hydralysis of potassium feldspar. A simplified chemical reaction formula is shown below (Nilsen and Broch, 2009):



The potassium feldspar reacts with water and illite, silicon dioxide and positively charged potassium ions are the reaction product. Figure 2-4 shows the structure of the kaolinite mineral

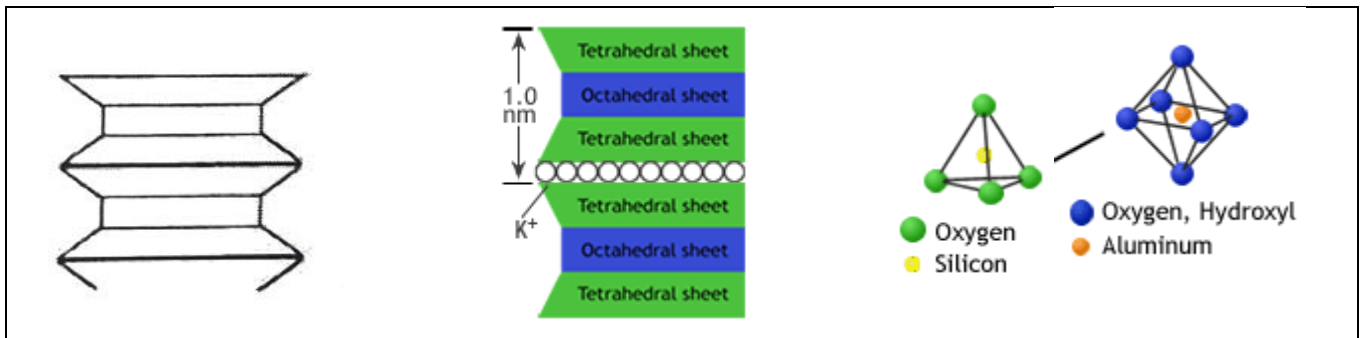


Figure 2-4: Mineral structure of the illite mineral showing  $\text{SiO}_4$ -tetrahedrons (green),  $\text{Al}(\text{OH})_3$ -octahedrons and the interlayer consisting of positively charged potassium ions. Also shown are the  $\text{SiO}_4$ -tetrahedron and the  $\text{Al}(\text{OH})_3$ -octahedron, right. (Selmer-Olsen and Palmstrøm, 1989 and The Cooperative Soil Survey, 2014)

Illite is a 2:1 ratio clay mineral composed of unit layers of two tetrahedrons and one octahedron with interlayers consisting of positively charged potassium ions. The unit layers are drawn towards one another by the potassium ions and thus preventing other cations with higher hydration capability to enter (Prestvik, 2001 and Pusch, 2012). This entails both low capacity of cation exchange and low shrink and swell behaviour. The kaolinite mineral is thus a nonexpansive clay mineral.

Table 2-5 presents the composition of the illite minerals and is showing both elements and chemical compounds.

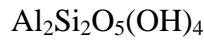
Table 2-5: Composition of the illite mineral showing both elements and chemical compounds (Modified after Mineralogy Database, 2014).

Element	[%]	Chemical compounds	[%]
Potassium (K)	6,03	$\text{K}_2\text{O}$	7,26
Magnesium (Mg)	1,87	$\text{MgO}$	3,11
Aluminium (Al)	9,01	$\text{Al}_2\text{O}_3$	17,02
Iron (Fe)	1,43	$\text{FeO}$	1,85
Silicon (Si)	25,25	$\text{SiO}_2$	54,01
Hydrogen (H)	1,35	$\text{H}_2\text{O}$	12,03
Oxygen (O)	55,06		

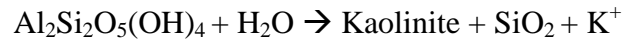
Table 2-5 shows that the oxygen and silicon elements are given as the main parts of the illite mineral. Silicon oxide, aluminium oxide and hydrogen are the main chemical compounds of the clay mineral (Mineralogy Database, 2014).

## 2.2.4 Kaolinite

Kaolinite is a nonexpansive clay mineral with the empirical formula (Mineralogy Database, 2014):



The clay mineral is, like the illite in section 2.2.3, a reaction product from the hydralysis of potassium feldspar under the condition of higher temperatur and greater flow rate of the water. A simplified chemical reaction formula is shown below (Nilsen and Broch, 2009):



The potassium feldspar reacts with water and kaolinite, silicon dioxide and positively charged potassium ions are the reaction product. Figure 2-5 shows the structure of the kaolinite mineral.

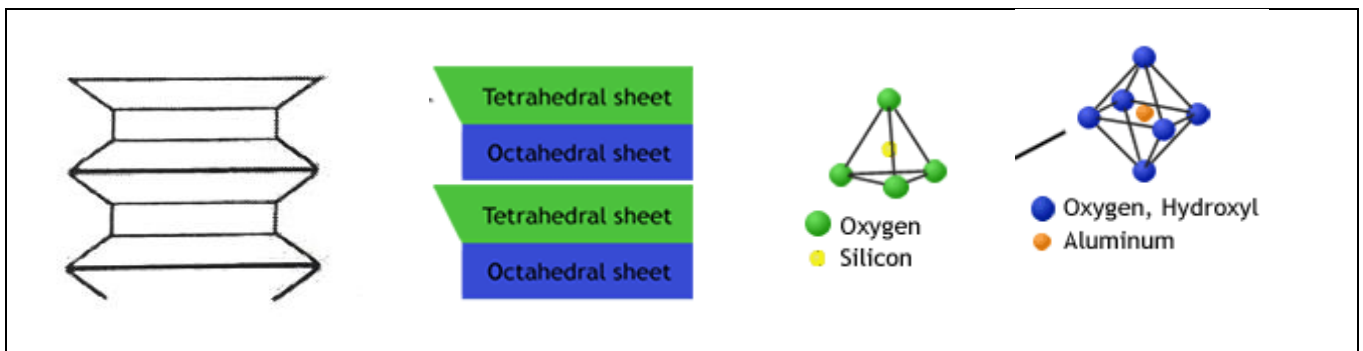


Figure 2-5: Mineral structure of the kaolinite mineral showing  $\text{SiO}_4$ -tetrahedrons (green) and  $\text{Al}(\text{OH})_3$ -octahedrons. Also shown are the  $\text{SiO}_4$ -tetrahedron and the  $\text{Al}(\text{OH})_3$ -octahedron, right. (Selmer-Olsen and Palmstrøm, 1989 and The Cooperative Soil Survey, 2014)

Kaolinite is a 1:1 ratio phyllosilicate with one tetrahedron for each octahedron in the unit layer of the sheet silicate. The closely packed unit layers provide limited or no available surface areas and the capability of holding water molecules and cations are of minor extend. This entails both low capacity of cation exchange and low shrink and swell behaviour. The kaolinite mineral is thus a nonexpansive clay mineral and will not pose stability threats to underground works or the like.

Table 2-6 presents the composition of the kaolinite mineral and is showing both elements and chemical compounds.

Table 2-6: Composition of the kaolinite mineral showing both elements and chemical compounds (Modified after Mineralogy Database, 2014).

Element	[%]	Chemical compounds	[%]
Aluminium (Al)	20,90	$\text{Al}_2\text{O}_3$	39,50
Silicon (Si)	21,76	$\text{SiO}_2$	46,55
Hydrogen (H)	1,56	$\text{H}_2\text{O}$	13,96
Oxygen (O)	55,78		

In table 2-6 the oxygen, silicon and aluminium element are given as the main parts of the kaolinite mineral. Silicon oxide and aluminium oxide are the main chemical compounds of the clay mineral (Mineralogy Database, 2014).

## **2.3 Instability issues**

Swelling of clay minerals may cause stability problems in tunnels, slopes or foundations and further result in time delays and cost overruns, in worst cases a total closure of the work. Certain factors and assumptions, section 2.1 and 2.2, have to be met for a swelling potential to be established and mobilized and further cause instability threats to the construction works. The clay minerals ability to swell and the degree of swelling affect the extent of stability issues.

The stability problems might occur during construction of the works, after the project completion and throughout the entire operational life (Selmer-Olsen and Palmstrøm, 1989). A combination of two or more factors is often the case and there are a number of factors influencing the stability. Essential factors influencing the stability are the ones mentioned in previous sections and factors such as the quality of the rock mass, rock stresses, the influence of groundwater, and the orientation, location, size and shape of the construction work (Panthi, 2006). Influencing factors and conditions may vary from one construction work to another, making it difficult to provide real correlations between them. Every project need to be considered individually, which enables a specific interpretation of the given factors and conditions for each case.

Gouge material, mostly found in faults or weakness zones and consisting of both clay minerals and rock fragments in various fractions, is causing the greatest concern with regard to stability threats on foundations, tunnels and slopes. The swelling character of the clay minerals and the highly disturbed rock mass consisting gouge material of low quality and in the interaction with high water pressures represents the most difficult working conditions. The combination of these conditions and an underestimation of the swelling pressure may result in an inadequate rock support and problems with lateral movement and collapse and sliding of the rock mass.

Stability problems in slopes associated by swelling clays are closely related to the factors and conditions previous listed. Other factors of interest are the geometry of the slope, the discontinuity infilling properties and the influence of groundwater. The height, angle and orientation determine the geometry of the rock slope and infillings found in faults and joints vary in type, amount, and thickness and may have differing shear strength properties. Groundwater conditions of interest are the amount of water and the orientation of joints relative to swelling clay zones. The geometry of the slope, the groundwater properties and infilling properties will thus influence the stability in different ways and to a varying degree.

Foundations positioned on expansive soils are subjected to uplift pressures and forces due to repeated cycles of shrinking and swelling caused by swelling minerals. Stresses applied to the structures and buildings from these forces may cause great damages such as fracturing of walls and floors (Rogers et.al, 2014).



Both consolidation and unloading of the rock mass, respectively before and after an excavation, are of great significance as they are seen as potential instability factors. The affect these factors have on the stability of underground excavations are recreated by performing laboratory test methods, section 6.

As mentioned in section 1.4 the laboratory tests are index test carried out on prepared rock samples and thus not representative for full scale testing. For a complete analyses of the potential stability problems field investigations and use of previous experience is required.



### **3 Review of two tunnel instability cases**

---

Stability problems in tunnels may lead to tunnelling collapses and the one of the main causes may be instabilities related to the presence of swelling rocks and clay minerals, mainly smectite, in both rocks and the fracture/fault zones within the rock mass. The knowledge and experiences with swelling mechanism have increased in the recent years because of the advanced development of testing methods (Dahl et.al, 2013).

Rock falls and cave-ins are infrequent instability problems in tunnelling. However, severe cave-in incidences in Norway are primarily associated to swelling characteristics of the fractured rock mass and some schistose rocks. The stability problems occur either during the excavation of the tunnel or after the project completion and the geological conditions are often related to weakness zones and faults with the presence of swelling minerals and high water pressures. Even though thorough surveys and adequately planning and excavation stages are carried out, incidents may nevertheless occur. For this reason it is required to have an ongoing investigation during the project life and a contingency plan is worked out (Nilsen, 2010).

The stability problems caused by swelling leads to an adverse impact on the projects time- and cost estimates, which are related to delays in construction completion and cost overruns. The cost overruns include the need for additional reinforcement of the tunnels, and this in many cases may correspond to as high as 75 percent of the total cost (Selmer-Olsen and Palmström, 1989). In the following, two undersea tunnel cases are reviewed where severe instability was confronted during tunnel excavation.

#### **3.1 Tunnel 1 – The Frøya subsea tunnel**

Significant challenges associated with the excavation of subsea road tunnels are the crossing of weakness zones, faults and thrusts and the possible leakage from the overlying reservoir (Palmström et. al, 2000). For subsea tunnels the challenges linked to the weakness zones are due to the location of them, mainly in the deepest part of the fjords. The subsea tunnels are inclined from both sides, resulting in even more complicated working conditions and stability issues (Nilsen and Palmström, 2013 and Nilsen, 2012).

Figure 3-1 is a sketch of a subsea road tunnel, in deep rock, showing regional weakness zones (Nilsen and Palmström, 2013).

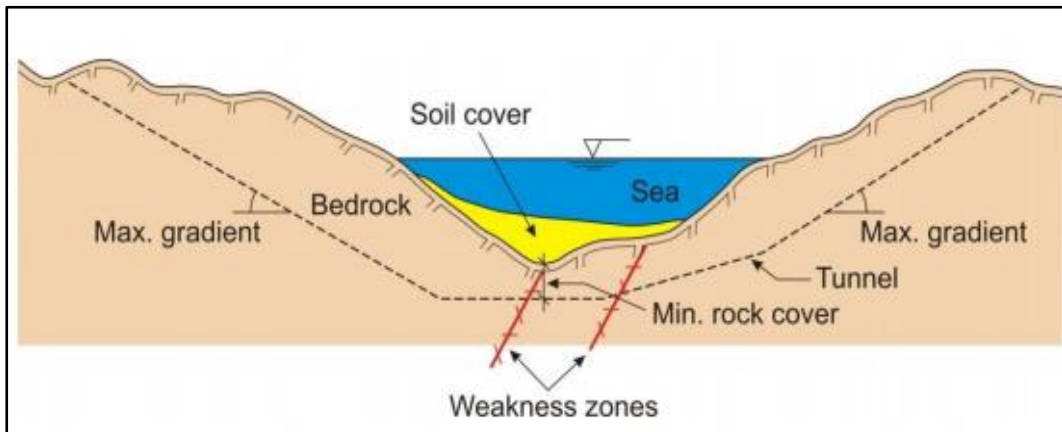


Figure 3-1: Subsea road tunnel, in deep rock, showing regional weakness zones (Nilsen and Palmström, 2013).

As can be seen from figure 3-1 requirements for the maximum gradient and minimum rock cover is given to ensure a good and safe tunnelling work.

### 3.1.1 Issues

The Frøya tunnel is a subsea road tunnel located under the Frøyfjord in Sør-Trøndelag County, Norway and is the second subsea tunnel in the Hitra-Frøya project. Figure 3-2 is showing the location of the Frøya tunnel and the main weakness zones.

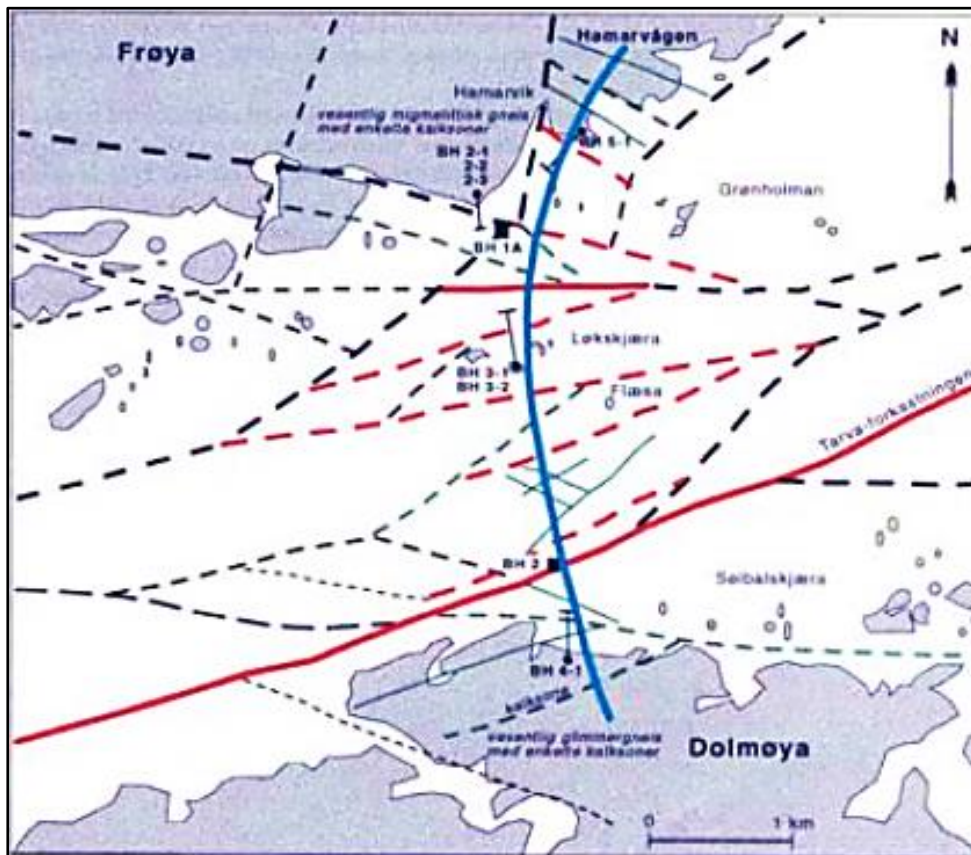


Figure 3-2: Situation map of the Frøya tunnel, including the main weakness zones and faults (Palmstrøm et.al 2000).

A classification of the dashed lines, indicating the weakness zones, was based on stability estimates and ranges from class A to class D. After thorough field investigations, preliminary measurements and changes because of the detection of a weakness zone, the tunnel alignment was selected, shown as a blue line in the situation map.

The total length of the two-lane tunnel is 5.3 km and it has a cross section of 50 m<sup>2</sup> that gives a T8 tunnel profile (Appendix A). The rock cover above the road tunnel is ranging from 37-155 m and the maximum depth below sea level is 155 m (Palmström et.al, 2000). Figure 3-3 shows the longitudinal profile of the Frøya subsea tunnel, and the major weakness zones, the low velocity zones and the soil locations (Nilsen, 2012).

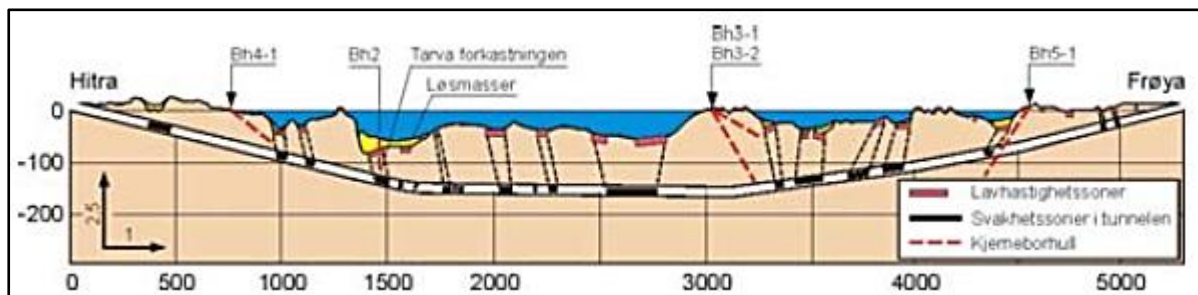


Figure 3-3: Longitudinal profile of the Frøya tunnel, showing the topography, major weakness zones, the low velocity zones and the soil locations (Nilsen, 2012).

The main rock type in the Hitra- Frøya area is Precambrian metamorphic gneiss, such as *granitic gneiss*, *micagneiss* and *migmatite* (Palmström et. al, 2000). The geological surveys also identified layers of *limestone* and the strike and dip of the rocks are primarily ENE-WSW/NW. A number of thrusts and faults indicate that the area has undergone substantial faulting dating back to the Precambrian Eon (International Union of Geological Science, 2013).

Figure 3-4 shows a geological map over Norway and the Frøya – Hitra area.

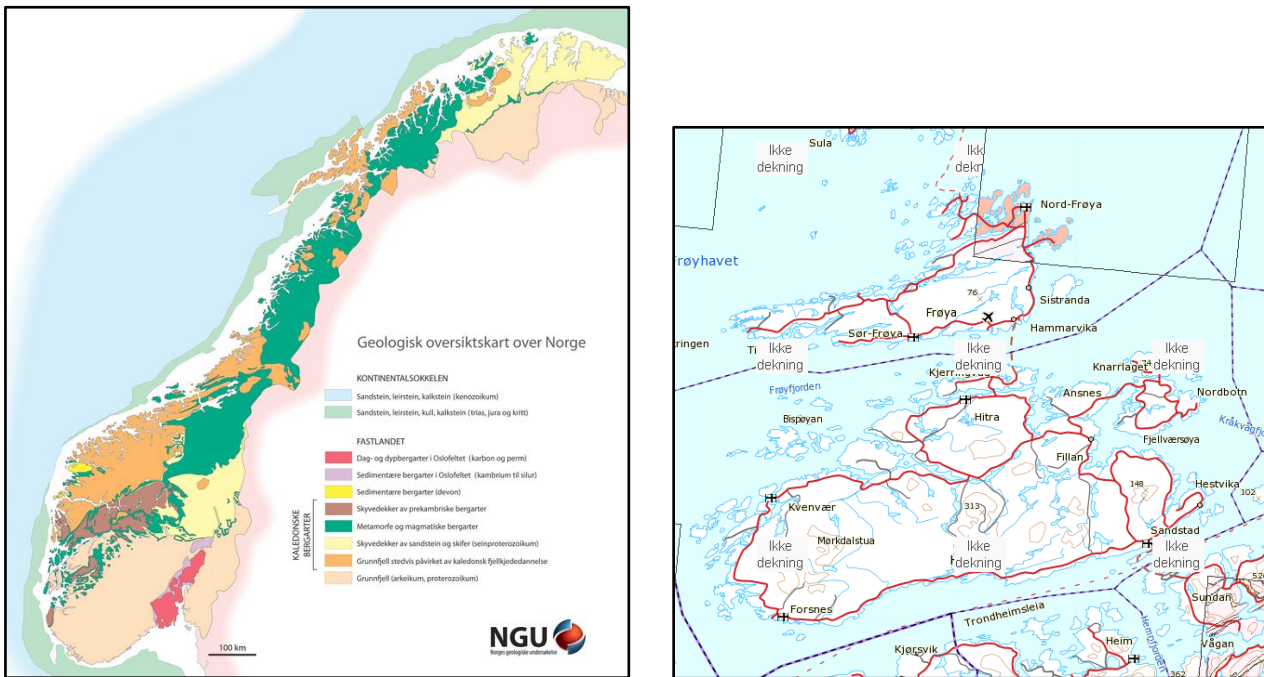


Figure 3-4: Geological map over Norway, and the Frøya – Hitra area (NGU, 2014).

Core drillings and reflection seismic measurements conducted in the early stages of the project showed weakness zones with high degree of alteration and low velocity, containing seams of clay with varying thickness (Palmström et. al, 2000). The material in the weakness zones ranges from clay fraction to sand fraction, and is classified as a soil material. The seismic velocity (Cecil, 1971) is a measure of the rock quality and the velocity ratio is compared to the required tunnel support, table 3-1.

Table 3-1: Seismic velocity ratio compared to support requirements (Cecil, 1971).

Seismic Velocity Ratio	Support Requirement
> 0.90	None to spot rock bolting
0.80 - 0.90	Light shotcrete (< 5 cm), frequently in combination with rock bolting
< 0.80	Rock bolting, heavy shotcrete (> 5 cm, two or more applications)

From table 3-1, we see that the lower velocity measured, the more rock support is necessary (Cecil, 1971).

The challenging geological ground conditions at the site, such as major faults, thrusts and weakness zones, entailed the establishment of two different experts groups, independent of each other. The final reports, including the determination of excavation method and rock support, and an evaluation on the time, cost and risk estimates, gave a green light to the commencement of the project (Palmström et. al, 2000). Figure 3-5 shows the actual rock mass conditions encountered in the Frøya tunnel.



Figure 3-5: Actual rock mass conditions in the Frøya tunnel; fractured core samples to the left and excavation of the tunnel to the right (Nilsen, 2013).

In figure 3-5 poor rock quality by fractured core samples are seen and this actual condition differed from what was expected (Nilsen, 2013).

The Frøya tunnel was excavated by the drill and blast method, that is a cost effective excavation method, and flexible and adaptable to any variations in the rock mass. For most subsea tunnels this excavation method is the preferred one (Nilsen, 2012). Figure 3-6 shows the drill and blast excavation at the tunnel face.





Figure 3-6: D&B excavation at the tunnel face (Nilsen, 2012).

### 3.1.2 Swelling potential

The detection of several weakness zones, consisting of soil material, by probe drilling and reflection seismic, lead to an extensive evaluation of the field investigations prior to the construction of the tunnel. The routines and control during both planning and construction were emphasized considering the uncertainties and risks related to the project.

The main concerns were on the possible unstable ground conditions, which might lead to a collapse of the ground, and the leakage of water. For this reason a number of probe drillings, figure 3-7, were performed to prepare for the ground conditions behind the tunnel face. 3 to 5 drill holes for each 20 meter of excavated tunnel were carried out.

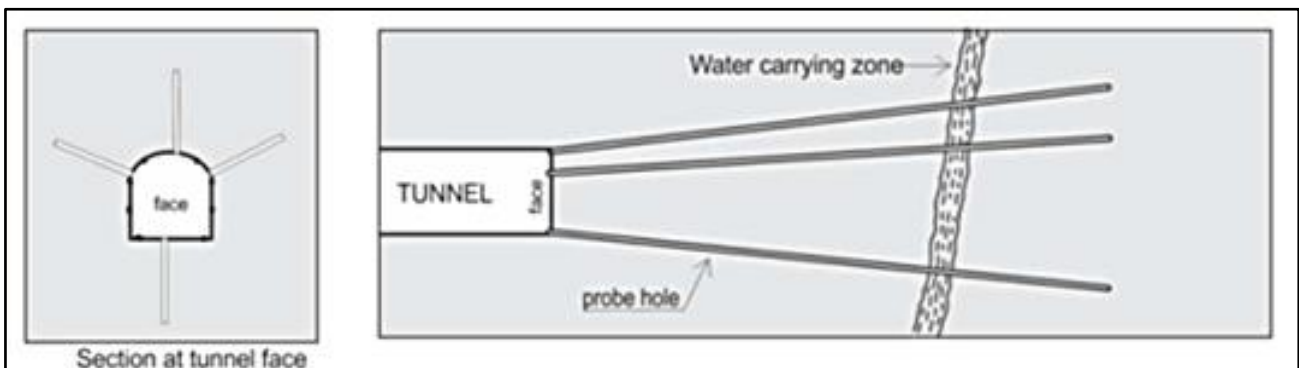


Figure 3-7: Principles of probe drilling ahead of the tunnel face (Nilsen and Palmström, 2013)



The probe holes, as seen in figure 3-7, are drilled through the water carrying zone to determine the ground conditions behind the tunnel face.

The water leakage in the probe holes was stopped by grouting and this led to a control of the water and a stability increase of the rock mass (Nilsen and Palmström, 2013). In figure 3-8 both pre-grouting and grouting are shown, and the pre-grouting entailed the drilling of holes with a length of 10 to 20 m. The procedure was performed by high pressure injection (International Union of Geological Science, 2013; Palmström et. al, 2000).

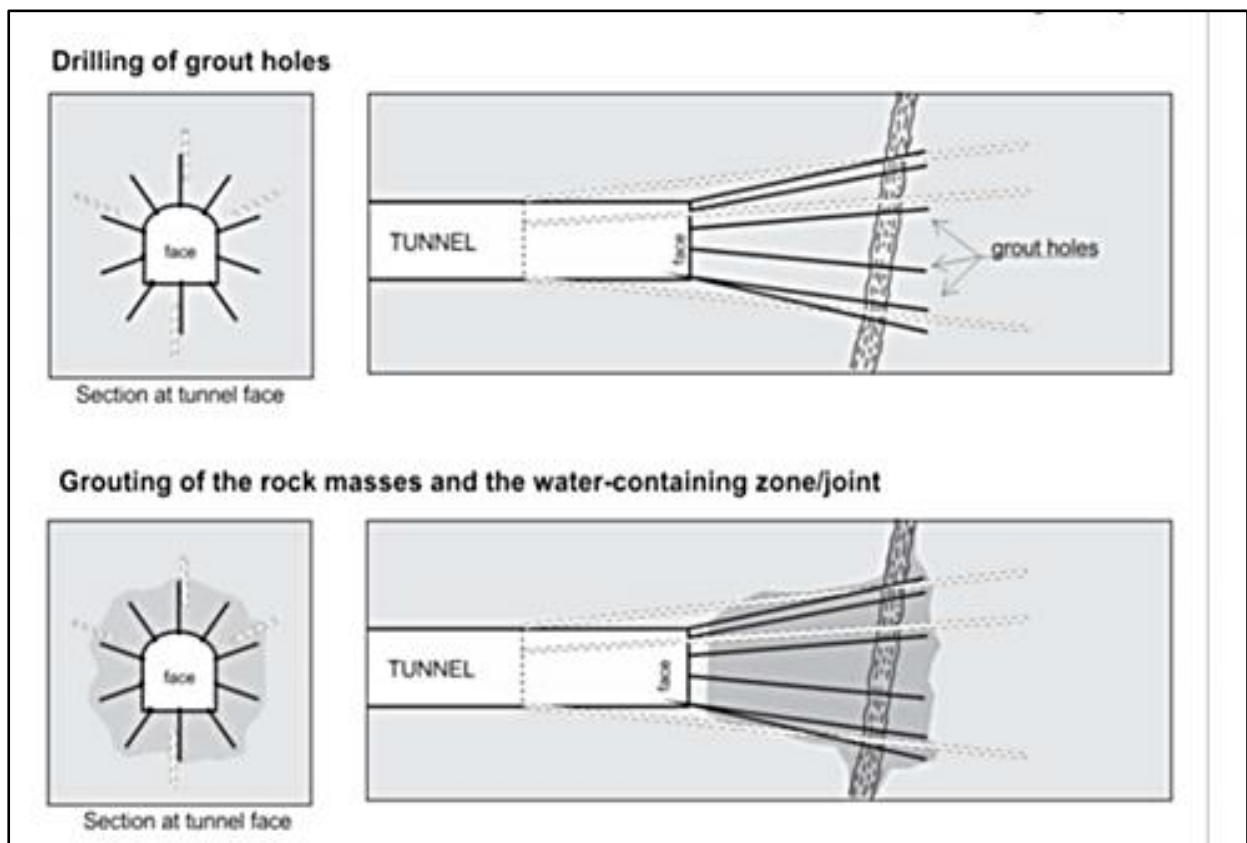


Figure 3-8: Pre-grouting and grouting ahead of the tunnel face (Nilsen and Palmström, 2013).

As can be seen in figure 3-8 is the drilling of grout holes followed by the grouting of the rock masses and the water-containing water carrying zone

The swelling pressures in weakness zones in the Frøya tunnel were measured to be very active; 1.55 MPa (Appendix C-2) and even though many of them contained smectite, not all caused problems due to the decrease in permeability of the rock mass and the sealing of the rock joints (Nilsen, 2010).

### 3.1.3 Rock support and tunnelling progress

The Frøya subsea tunnel was driven from both the north and the south side, and the progress for the south drive was somewhat higher than the north side, 39 m/week compared to 35 m/week (Palmström et. al, 2000). The good tunnelling progress brought forward the opening of the tunnel, so the time and cost estimates were accomplished (Nilsen, 2010 and Palmström et. al, 2000).

Table 3-1 gives the relationship between the seismic velocity ratio and needed rock support for a tunnel. As mentioned in section 3.1.1, the lower velocity measured, the heavier rock support is essential for the stability. The field investigations prior to the tunnel works of the Frøya tunnel revealed weakness zones with low velocities and an extensive rock support was carried out.

In figure 3-9 excavation and rock support in ground with weakness zones and difficult conditions are illustrated (Nilsen and Palmström, 2013).

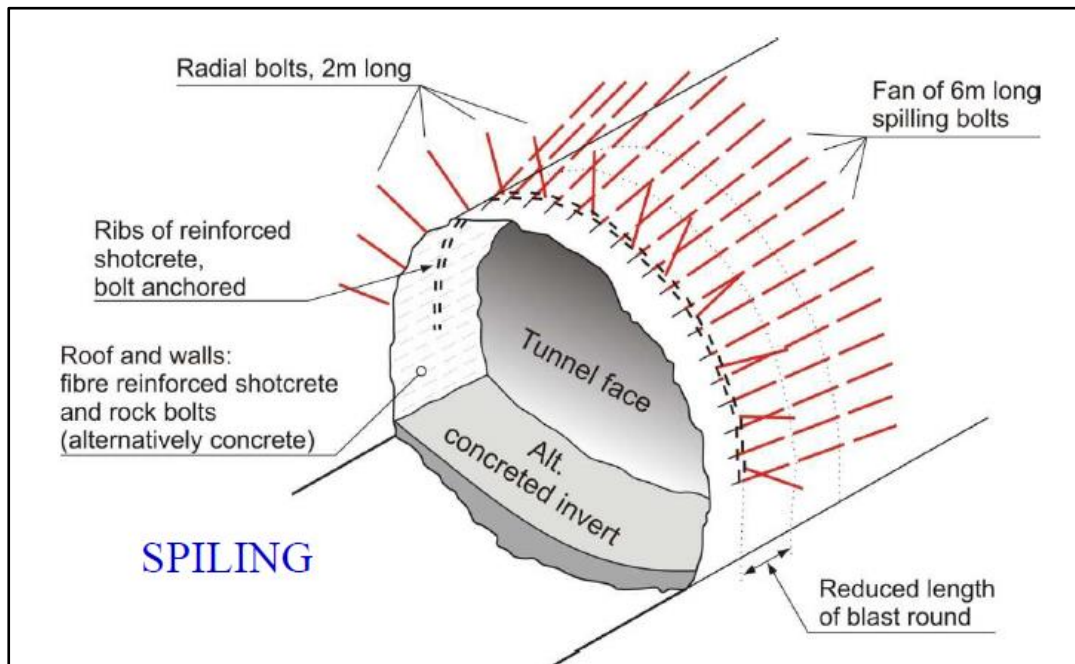


Figure 3-9: Excavation and rock support in ground with weakness zones and difficult conditions (Nilsen and Palmström, 2013).

The principles shown in figure 3-9 correspond well to the actual excavation and rock support performed for this subsea tunnel. For the Frøya tunnel, fibre reinforced shotcrete was applied as the main type and the average number of bolts were 4.97 for each meter of tunnel excavated and part of the invert and tunnel lining was concreted, respectively 375 m and 270 m (Palmström et.al, 2000).

The Frøya subsea tunnel was completed in 2000, the stability of the tunnel is good and so far no substantial issues have been connected to it (Nilsen, 2010).

### 3.2 Tunnel 2 – The Hanekleiv tunnel

The Hanekleiv highway tunnel is one of many examples where stability problems occur several years after the project complete, even though the stability was apparently good and no significant issues were detected (Nilsen, 2010).

### 3.2.1 Issues

The Hanekleiv tunnel is part of the E18 highway and it is located between Sande and Holmestrand in Vestfold County, Norway (Nilsen, 2012). Figure 3-10 shows the location of the tunnel and the topography of the area.

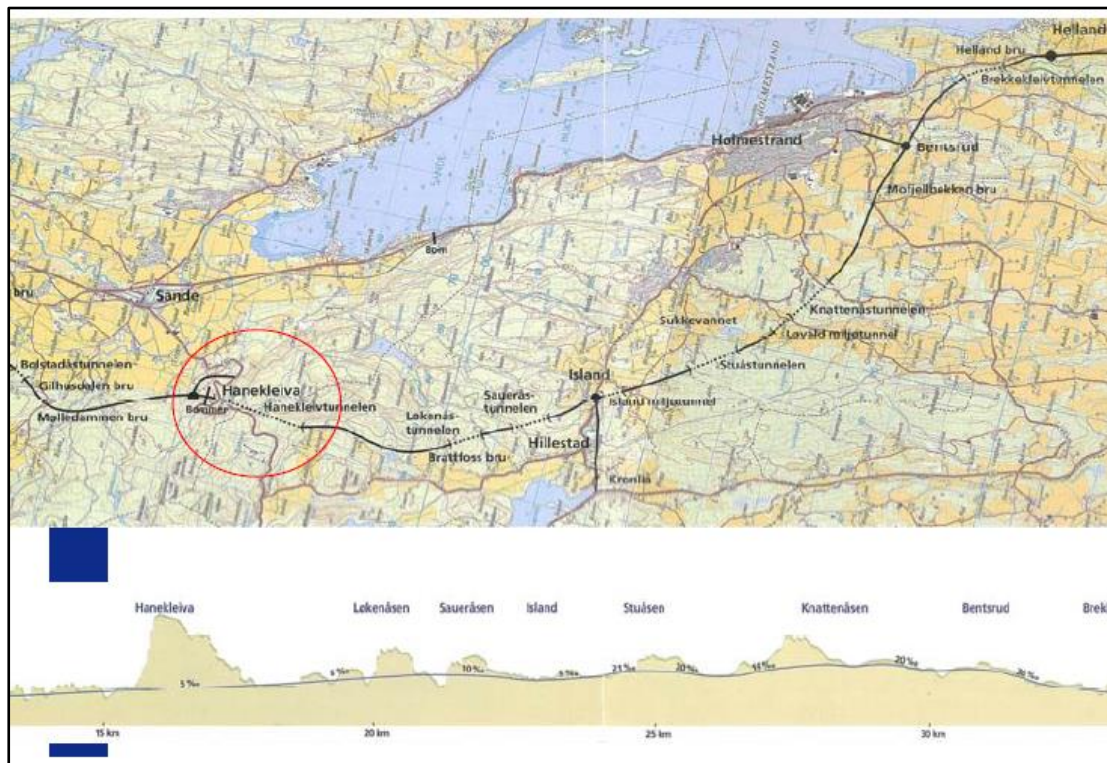


Figure 3-10: Location of the Hanekleiv tunnel and topography of the area (Nilsen, 2012).

The Hanekleiv tunnel has a total length of 1,765 m and the two tube tunnel, each with a cross section of  $65 \text{ m}^2$ , has a T9 tunnel profile (Appendix A). The tunnel was constructed between 1996 and 1998, and no major stability problems had yet occurred until Christmas Day 2006, when a cave-in of rock mass led to a repair of the tunnel and the need for extra rock support (Nilsen, 2012).

Figures 3-11 and 3-12 shows the geology of the rock mass and the bedrock along the tunnel is divided into a northern and a southern part. Also shown in figure 3-11 is the cross-section trace of both the tunnel and road, and the location of the cave-in is illustrated, yellow mark (Nilsen, 2010).

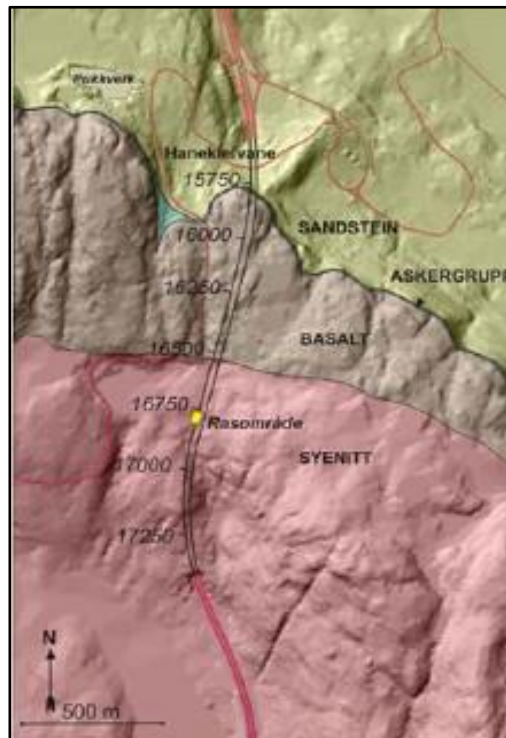


Figure 3-11: Situation map of the Hanekleiv tunnel with the geology of the bedrock, the cross-section trace of both the tunnel and road, and the location of the cave-in (Nilsen, 2012 and Rønning et.al, 2013).

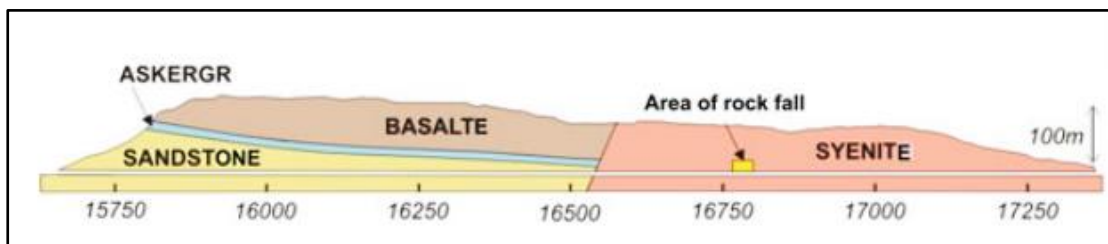


Figure 3-12: Longitudinal profile of the Hanekleiv tunnel, showing both the geology and the topography (Rønning et.al, 2013).

In the northern part of the Hanekleiv tunnel the Ringerike sandstone from the Silurian Period is the main rock type. Above the sandstone a shale and conglomerate layer from the Carboniferous Period, the Askergrupp, and Permian basalt were identified. In the southern part of the Hanekleiv tunnel the field investigations showed syenite from the Permian Period (International Union of Geological Science, 2013).

The tunnel was excavated from the northern side where the most challenging conditions were anticipated, due to the jointed and flat bedded sandstone. The tunnel was located below the shale and conglomerate layer, and thereby eliminating further issues, figure 3-11. In August 1996, during the excavation of the south bound tube, swelling clay was detected in a fault zone, and measures were made to prevent unstable conditions to occur. Both fibre reinforced shotcrete, a total of 25 cm thickness, and rock bolts were used to seal the fault zone (Nilsen, 2010).



On the December 25th in 2006, a cave-in occurred in the Hanekleiv tunnel, resulting in a 250 m<sup>3</sup> rock burst on to the tunnel floor, figure 3-13. The incident caused the need for repairs and additional rock support before re-opening of the tunnel (Nilsen, 2010).



Figure 3-13: Photo of the collapsed area in the roof of the tunnel and the material from the cave-in on the floor of the tunnel (Nilsen, 2012).

As can be seen in figure 3-13 is the massive cave-in in the Hanekleiv tunnel where an area of the tunnel roof collapsed due to the weight of the overlying masses. The rock burst covered a part of the tunnel floor.

### 3.2.2 Swelling potential

The location of the rock fall in December 2006 is the same as the area of the fault zone described in section 3.2.1. The 25 m long weakness zone was composed by two parallel joint faults, each with a thickness of 5-10 cm and filled with smectite (Rønning et.al, 2013). Between the two joint faults, about 2-2.5 m, both weathered and fresh syenite was identified (Nilsen, 2010). Figure 3-14 gives a schematic presentation of the collapsed area in both the south bound tube and the north bound tube, showing both a longitudinal and a transverse sketch of the tunnel tubes (modified after Bollingmo et.al, 2007 and Nilsen, 2010).

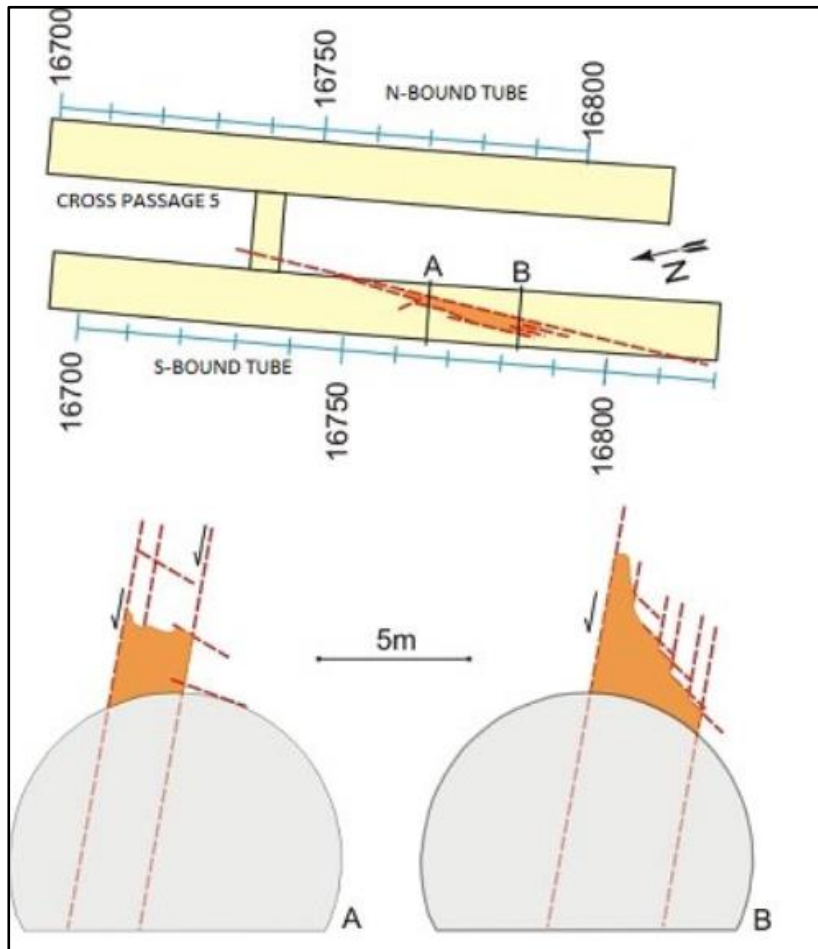


Figure 3-14: Illustration of the collapsed area in the south bound tube, longitudinal sketch of the tunnel tube (upper) and transvers sketch of the tunnel tube (lower) (modified after Bollingmo et.al, 2007; Nilsen, 2010).

In the north bound tube the width of the collapsed area was greater than for the south bound tube. The smectite detected in the fault zone showed a free swelling percentage of 150 and a swelling pressure of 0.18 MPa, indicating the swelling clay as moderately active (Appendix C).

The cave-in in the Hanekleiv tunnel happened as a combination of several causes. The swelling process was of great importance and had a high impact on the stability. Also the high degree of weathering that led to a reduced rock mass strength was crucial for the stability (Mao et.al, 2011) and resulted in the gravitational collapse in the tunnel (Nilsen, 2010) .

### 3.3.3 Rock support and tunneling progress

The good tunneling progress for the Hanekleiv tunnel led to an early break through, i.e. 35 working weeks after the project start, and the tunnel was opened for traffic in 1996 (Nilsen, 2010). The rock conditions in this area were relatively good and no major issues, except the cave-in in 2006, delayed or complicated the tunnel project.

For rock support (Nilsen, 2010) in the Hanekleiv tunnel, 2.4 rock bolts/m, both radial rock bolts and spillingbolts was applied, and 1.3 m<sup>3</sup>/m steel fiber reinforced shotcrete was used. The identification of a weakness zone in the northern side of the tunnel, in the sandstone section, made the installation of a concrete lining essential in order to avoid stability problems. Finally the installation of a water/frost lining was performed.





## 4 Selected rocks and sample preparations

---

For this master thesis three different rock types are selected; alum shale, green schist and tuff. The rock types are prepared as milled dust, cored rock cylinders, rock cubes, rock pieces and thin sections. The following sections give a thorough description of the various rock types and the sample preparations.

### 4.1 Rock type

#### 4.1.1 Alum shale

The sedimentary deposited alum shale selected for this master thesis originates from the Oslo-belt in Norway. The alum shale was sent by Erik Endre at NGI and figure 4-1 shows the rock specimen before the sample preparations. The mineralogical analysis in section 5.3.1 and 5.3.2, respectively XRD analysis and thin section analysis provide a detailed identification of the mineralogy and the petrography of the rock.

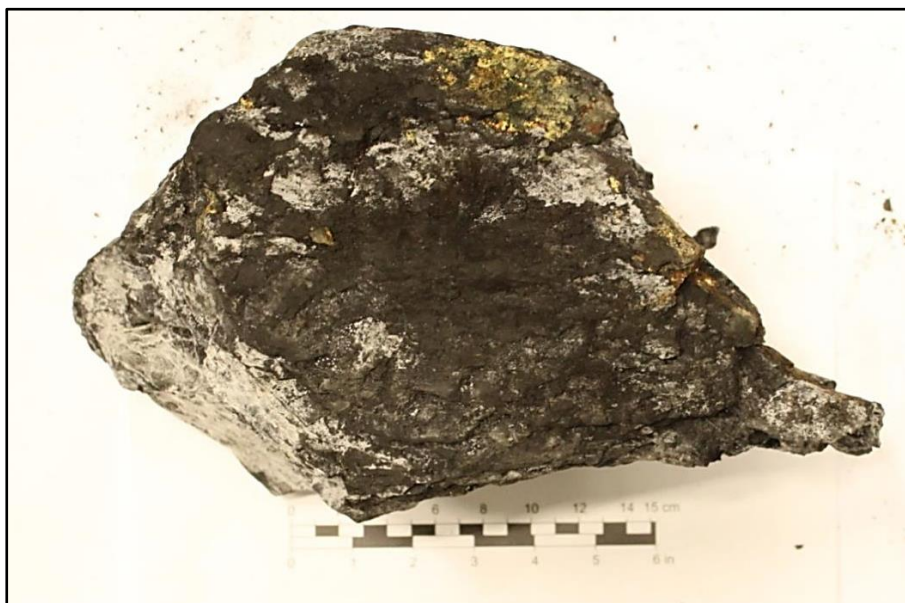


Figure 4-1: Photo of received alum shale.

The received sample, figure 4-1, was greyish black and was wet and very schistose. There were some difficulties in drilling the rock cores due to fractures in the rock sample.

Formation of the clastic sedimentary alum shale was a result of diagenesis caused by compaction, cementation and petrification of oxygen deficient organic mud on the sea bottom 500 million years ago, that is the Cambrian Period. The formation of the alum shale lasted throughout 40 million years (NGI, 2014) to the early Ordovician Period (Appendix B). The mud was deposited in shallow seas as a

result of deglaciation and the sediments may have a high content of uranium, heavy metals and iron sulphur as well as a high content of shells from living microorganisms and organic carbon (NGI, 2014).

Loosely packed minerals grains, in silt- and clay-fractions (Sæther et.al, 2010), were compacted due to the increasing pressure from the overlying layers and high temperatures caused by the formation of the Scandinavian Caledonides (NGI, 2014) in the Silurian Period (Appendix B). This resulted in an out squeezing of water (Mørk, 2008) and further compaction and precipitation of the minerals caused a cementation of the particle grains that led to the formation of this particular clastic rock.

The alum shale is extremely fine grained and highly carbonaceous, the content of organic carbon may constitute up to 50 % (NGI, 2014). High sulphur content is common, about 5-7 %, mainly as pyrite and pyrrhotite (NGI, 2012). The presence of iron sulphur in the alum shale is due to the lava flows and percolation of hot water in fractures and faults during the volcanism between the late Carboniferous Period and the early Triassic Period (Appendix B and NGI, 2014). The distinct colour of the alum shale reflects its grain size and its high content of organic carbon and sulphur (Mørk, 2008).

Alum shale will in contact with water and air easily disintegrate and it may expand, causing stability problems in tunnels, slopes and foundations. The cause of swelling might be related to several factors and the distinct foliation and schistosity of the alum shale might be a reasonable assumption. Capillarity (Dahl et.al, 2013) is enabled when water is added to the dry sample due to absorption of water molecules and further expansion of the rock. Another factor influencing on the swelling potential might be the sulphur content in the alum shale. Formation of sulphates when iron sulphides react with the oxygen in the water and the air (Prestvik, 2005) is of great significance. The most critical is when calcium-sulphate with the chemical formula  $\text{CaSO}_4 \cdot 2\text{H}_2\text{O}$ , also named gypsum, is formed as the result of oxidation of the sulphides into sulphates. The calcite in the rock then reacts with the iron sulphides and swelling pressure due to the volume expansion of the alum shale develops and stability issues might occur (NGI, 2014 and Sæther et.al, 2010).

#### 4.1.2 Greenschist

The greenschist tested for the master thesis is a Norwegian metamorphic rock, deposited from a volcanic rock material such as a lava flow, and the protolith was basalt (NBG, 2000). The mineralogical analysis in section 5.3.1 and 5.3.2, respectively XRD analysis and thin section analysis provide a detailed identification of the mineralogy and the petrography of the rock. Figure 4-2 shows the rock specimen after the core drilling.



Figure 4-2: Photo of greenschist after core drilling.

The light green micaceous sample material is foliated and schistose and the medium to coarse grained minerals are chlorite, epidote, amphibole, biotite and plagioclase (Jensen, 2006 and Prestvik, 2001).

As a result of transformation and recrystallization of the original rock material during the regional metamorphism the greenschist was formed and the rock was exposed to changes in the temperature and the pressure conditions due to the orogenesis process. The relatively low temperature and pressure, the colour of the index minerals and the texture, indicates a low metamorphic grade and the foliated metamorphic rock belongs to the greenschist facies (Jensen, 2006),

The high content and composition of various silicate minerals in the greenschist are of great importance regarding the relationship between swelling potential and instability factors.

### 4.1.3 Tuff

The tuff selected for the thesis is originally an igneous rock deposited as a result from volcanic activity where the ash was ejected by the volcano and solidified at the Earth's surface during rapid cooling (Prestvik, 2001). The mineralogical analysis in section 5.3.1 and 5.3.2, respectively XRD analysis and thin section analysis provide a detailed identification of the mineralogy and the petrography of the rock. 4-3 shows the rock specimen before the sample preparations.



Figure 4-3: Photo of the tuff before testing.

The rock specimen is reddish brown and has relatively large, 5-6 mm, light mineral grains in an otherwise fine-grained matrix and no distinct layering is seen. An accumulation of ash directly from the air gives a mixture of well-crystallized rock fragments and volcanic glass in the size range ash (< 2mm) to lapilli (2-64 mm) and the formation of a lithic pyroclastic rock material.

Due to the pyroclastic texture of the rock and the small fragments in it, this is classified as an intermediate extrusive rock and it might have a quartz content of up to 53-60 % (Jensen, 2006). The quartz content describes the degree of acidity of the igneous rock and the tuff is named after its mineral content and the grain size of the minerals (Prestvik, 2001).

The tuff has also a high content and composition of various silicate minerals and this may be a contributing factor concerning the correlation between swelling potential and stability issues. Section 6 gives a detailed description of the minerals.

## 4.2 Sample types

For the laboratory testing, chapter 5, five different sample types were prepared. This was milled dust, cored rock cylinders, rock cubes, rock pieces and thin sections.

The milled dust samples were applied for free swelling testing, swelling pressure testing using the oedometer and mineralogical analysis using the XRD technique. The cored rock cylinders were applied for swelling pressure testing using the oedometer and the rock cubes were used for 3D free swelling applying the new 3D apparatus developed by SINTEF/NTNU in 2013 (Dahl et.al, 2013). The rock pieces were applied for both slake-durability testing and point-load testing and the thin sections were used for mineralogical analysis.

### 4.2.1 Dust powder

To prepare for the dust powder samples part of the rock specimen was crushed, by hand with a geological hammer, giving a rock piece size of about 10-15 mm. The greenschist entailed the use of more hand power due to the strength of the rock specimen. The crushed bulk material, a total of 40 g, were then placed in the coil mill for 2 minutes, resulting in a milled powder for each of the rock specimens and for each of the testing methods; free swelling, swelling pressure and XRD analysis. This gave a total of 9 dust powder samples. The dust powder was then dried in a heating cabinet, at 105° C for 24 hours, followed by an additional milling in a porcelain mill for 15 minutes. Both coil mill and porcelain mill are shown in figure 4-4.



Figure 4-4: Photo of the coil mill to the left, and the porcelain mill to the right.



The laboratory testing for free swelling, swelling pressure and X-ray diffraction analysis (XRD) was then carried out. Figure 4-5 shows photos of the prepared dust powder.



Figure 4-5: Photos of prepared dust powder for free swelling, swelling pressure and XRD analysis, from left to right; alum shale, greenschist and tuff.

#### 4.2.2 Rock cylinders

The preparation of the discs, involved the drilling of cores from intact rock material at first, followed by the slicing of the rock cores into cored rock cylinders. The discs were cut at the Sliplaboratorium at NTNU, Norway. For the greenschist there was no need for core drilling and slicing because of the available sample material at the Geological Engineering laboratory at NTNU, Norway.

For the drilling of the rock cores a radial drilling machine with compressed air was used, dry drilling, to cool down and remove the drill cuttings. To minimize the amount of drill cuttings, the drilling was conducted at the outer edge of the intact rock specimens, perpendicular to the bedding. The velocity was set to 140 rpm with an automatic feeding of the drill. It was difficult to get good quality and a sufficient length of the rock cores from the alum shale, because the rock material is very schistose, which easily disintegrates. For this reason, the revolution was reduced to 90 rpm, and a gentler drilling of the alum shale was performed.

Figure 4-6 shows a photo of the radial drilling machine and photos of the drilled rock cores are shown in figure 4-7.

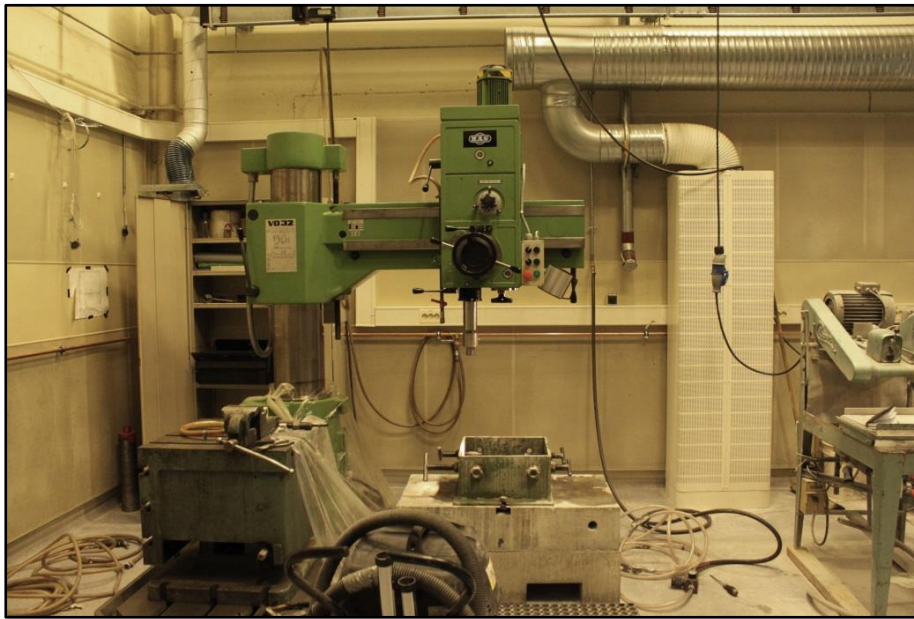


Figure 4-6: Photo of the radial drilling machine used for drilling of the rock cores.



Figure 4-7: Photos of drilled rock cores, from left to right; alum shale, greenschist and tuff.

The rock cores, each with a diameter of approximately 35 mm, were sent to the Sliplaboratorium at NTNU for further preparations and slicing into discs. The discs were cut with respect to the stratification allowing potential swelling perpendicular to the cleavage (Brattli and Broch, 1995). A diamond saw was used to cut the discs and alcohol was used to cool down the cutting process (Dahl, et.al, 2013). The laboratory testing for swelling pressure with axial swelling could be carried out. Figure 4-8 shows the prepared rock discs.



Figure 4-8: Photo of prepared discs for swelling pressure testing.

### 4.2.3 Rock cubes

Preparations of the rock cubes for the new 3D apparatus, with free swelling in 3 directions, involved sawing out the specimens using the cutter machine, figure 4-10. The preparation of the quadratic rock cubes was carried out by the laboratory technicians at the Geological Engineering laboratory at NTNU, Norway.

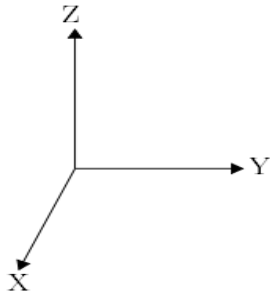


Figure 4-10: Photo of the cutter machine used for cutting of the rock cubes.

The dimensions of the rock cubes were initially set to 50x50x50 mm, and the cubes were prepared so that the cube axis was perpendicular to the foliations and beddings of the rock (ISRM, 1977). Difficulties with the preparation of the rock cubes made it impossible to obtain the standard dimensions. New dimensions for the rock samples are shown in table 4-1 and figure 4-11 show the prepared rock cubes for the 3D free swelling.

Table 4-1: Dimensions of the rock cubes in the X-, Y- and Z-direction

<b>Sample</b>	<b>X (mm)</b>	<b>Y (mm)</b>	<b>Z (mm)</b>
Alum shale	48,16	43,78	49,20
Greenschist	43,80	43,41	43,54
Tuff	50,07	53,08	51,01



From table 4-1 it is seen that the different rock cubes have various dimensions and this is taken into account when plotting the initial dimensions prior to the testing.



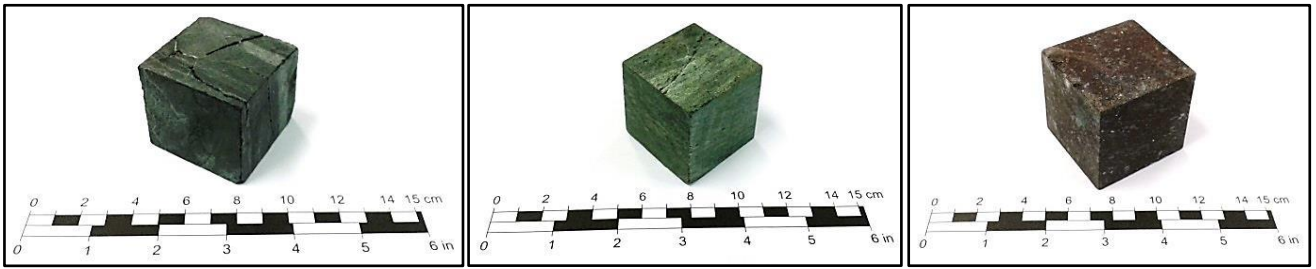


Figure 4-11: Photos of prepared rock cubes for 3D free swelling, from left to right; alum shale, greenschist and tuff.

#### 4.2.4 Rock pieces

Rough spherical rock pieces were prepared for both slake-durability testing and point load testing. Preparing the rock lumps involved a crushing of the specimens, by hand, with a geological hammer.

For the slake-durability testing 10 rock pieces were selected to get a sample mass of 450-550g in total, entailing rock pieces of 40-60 g each (ISRM, 1977). Figure 4-12 show the prepared rock pieces for the slake-durability testing.



Figure 4-12: Photo of prepared rock pieces for slake-durability testing, from left to right; alum shale, greenschist and tuff.

For the point-load testing 10 rock pieces of varying weight were also selected. Unfortunately no photos of the rock pieces were taken, either before or after the testing of them.

## 4.2.5 Thin sections

To prepare for the thin sections, the rock cores mentioned in paragraph 4.2.2 were sent to the Sliplaboratorium at NTNU. The rock cores were customized to fit the microscope slides, figure 4-13, and then glued on to the slides.



Figure 4-13: Photo of customized rock cores for microscope slides, from left to right; alum shale, greenschist and tuff.

After drying of the adhesive, the samples were sawed and grinded until a thickness of 30-35  $\mu\text{m}$  was achieved making the samples transparent. Then the samples were polished to get a smooth surface and to remove any scratches from the grinding/sanding. The thin sections are shown in figure 4-14.

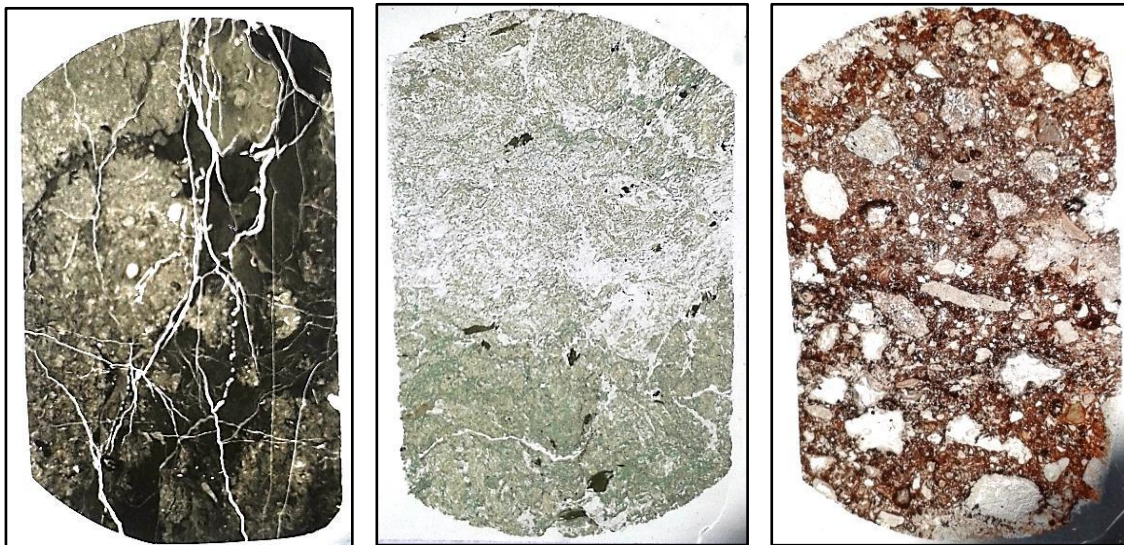


Figure 4-14: Photo of prepared thin sections for thin section analysis, from left to right; alum shale, greenschist and tuff.

## 5 Methodology and standards

---

A number of recommended test methods to determinate swelling behaviour are developed, and these tests address the challenges associated to stability problems caused by swelling of the rock mass. To ensure a good quality control and an unambiguously definition on laboratory test methods, the equipment used for the methods and the sample preparations, several standards are developed. These technical specifications describe the methodology for the various test methods, and frequent updates make it possible to keep up with the developments within the laboratory testing. These traditional procedures are the basis for the new experimental test methods, and describe the practical embodiment of them.

In the following, suggested methods for determination of the swelling pressure for dust powder and rock cube, slake-durability and point load strength durability (ISRM, 1977) recommended by the ISRM Commission on Swelling Rock (Mao et.al, 2011), will be discussed. Further, the methods for determination of swelling pressure for rock discs, the mineralogical analysis, and rock mechanical properties, will be described in detail.

These test methods describe the index properties of the rock, and it is a clear distinction between the index properties and the actual in situ conditions. The index tests are simulations of natural processes and allow for comparison and classification of different rock types. Two factors of great importance to the quality of the final test results are the sample collection and the sample preparations, see section 1.4.

### 5.1 Standards suggested by the ISRM

The International Society for Rock Mechanics (ISRM), established in 1962 in Salzburg, Austria, defines the rock mechanics field *“to include all studies relevant to the physical and mechanical behavior of rocks and rock masses and the application of this knowledge for the better understanding of geological processes and in the fields of engineering”* (NBG, 2000).

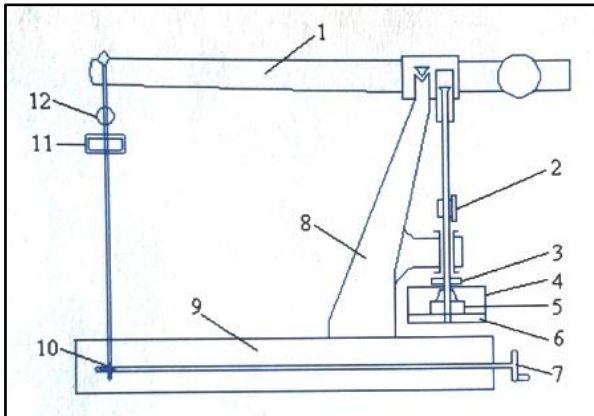
#### 5.1.1 The ISRM suggested method for determination of the swelling pressure index

The ISRM suggested method for swelling pressure index assumes testing of duplicate undisturbed rock specimens. For this thesis testing on remoulded rock specimens without duplicates have been carried out. This test method developed at the Norwegian University of Science and Technology is used due to the difficulties collecting undisturbed samples from the mixed rock mass, see section 2.3.

The swelling pressure test method suggested by the ISRM is widely used when determining the relative swelling potential of a material and potentially instabilities caused by the swelling (Mao et.al, 2011). The test method is also used in the characterization and quantification of the swelling properties of the material (Dahl et.al, 2013).

For swelling pressure determination, an apparatus consisting of several components is used, and this is shown in figure 5-1 and figure 5-2.

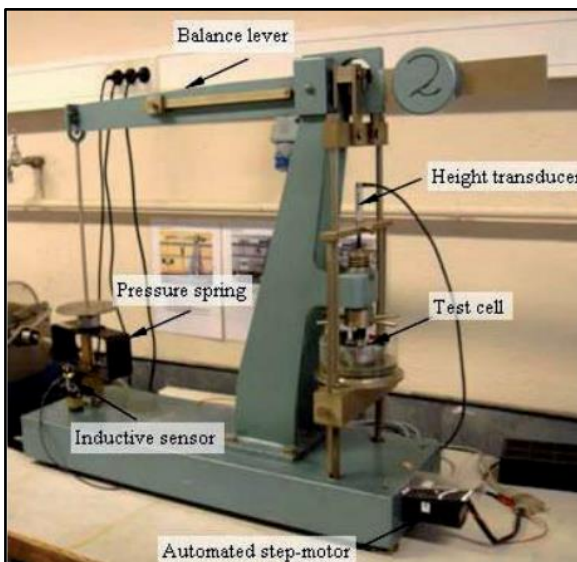
### Components of the test apparatus



- 1 Balance lever, with the ratio 1:10
- 2 Dial gauge to measure the height (volume) of the specimen  
Sensitivity of 0.001 mm
- 3 Adjustment screw
- 4 Container
- 5 Cylindrical test cell
- 6 Steel base plate of the container
- 7 Wheel
- 8 Frame
- 9 Base
- 10 Worm gear
- 11 Pressure ring
- 12 Dial gauge to measure the pressure  
Sensitivity equivalent to 0.05 tons/m<sup>2</sup>

Figure 5-1: Sketch of apparatus and list of components for swelling pressure measurements, traditional version (Mao et.al, 2011).

Figure 5-1 shows a sketch of the traditional apparatus with its constituents listed and figure 5-2 shows the updated version of the oedometer developed at NTNU, used for this master thesis.



### Improvements of the test apparatus

The dial gauge for measuring specimen height is replaced by a height transducer

The dial gauge for measuring specimen pressure is replaced by an inductive sensor

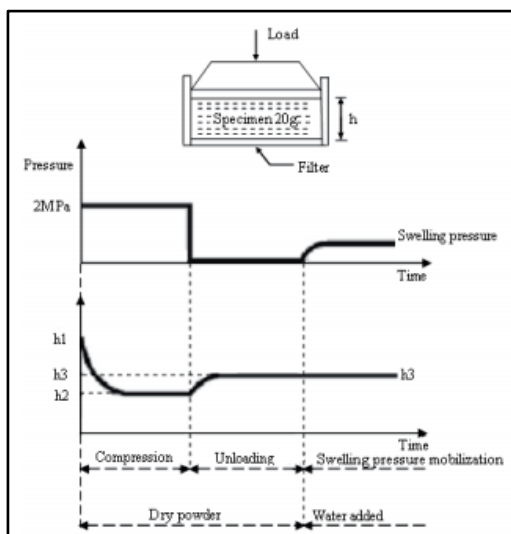
The manually operated wheel for worm gear adjustment is replaced by an automated step-motor

Figure 5-2: Photo of the updated Oedometer apparatus developed at the Norwegian University of Science and Technology, for swelling pressure measurements (Mao et.al, 2011).

The swelling pressure index is determined by the performing of 4 test stages, given in figure 5-3.

Test procedure:

The 20 cm<sup>2</sup> cylindrical test cell packed with 20 grams of the prepared milled powder, section 4.2, consisting of a brass filter at the top and a porous glass filter at the bottom is installed into the oedometer. The adjustment screw is used to align the balance lever to a position slightly above the horizontal line followed by the installation of the height transducer. Thereafter both the pressure ring and the pressure dial gauge are installed, before steel disc weights applied to the balance lever compresses the specimen at 2 MPa for 24 hours. Figure 5-3 gives a detailed photo of the test cell and the three stages in the test performance



- 0 Sample preparations
- 1 Compression
- 2 Unloading
- 3 Swelling

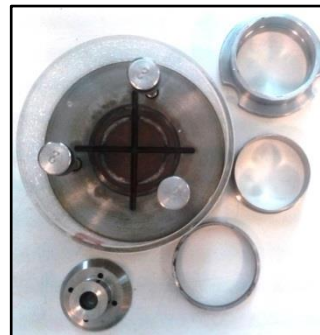


Figure 5-3: Sketch of the three stages in the swelling pressure measurements, left (Mao et.al, 2011) and photo of the test cell components, right.

In figure 5-3 the three stages of the test performance are shown. In the compression stage dry powder is used and the height of the sample is decreased. In the unloading stage dry powder is also used and the height of the sample increase to a certain level. Finally in the swelling stage water is added and the height of the sample remains stable.

Unloading of the specimen is done by removing the steel disc weights for a minimum of 2 hours until the height transducer no longer records any height changes. Distilled water with a depth of 10 mm is poured into the container and a continuous 24 hour registration of the one dimensional swelling pressure is performed. The automated step-motor adjusts continuously to avoid changes in the specimen volume and to compensate for the deformation of the apparatus. Figure 5-4 shows the oedometer setup for the compression stage and the swelling stage.



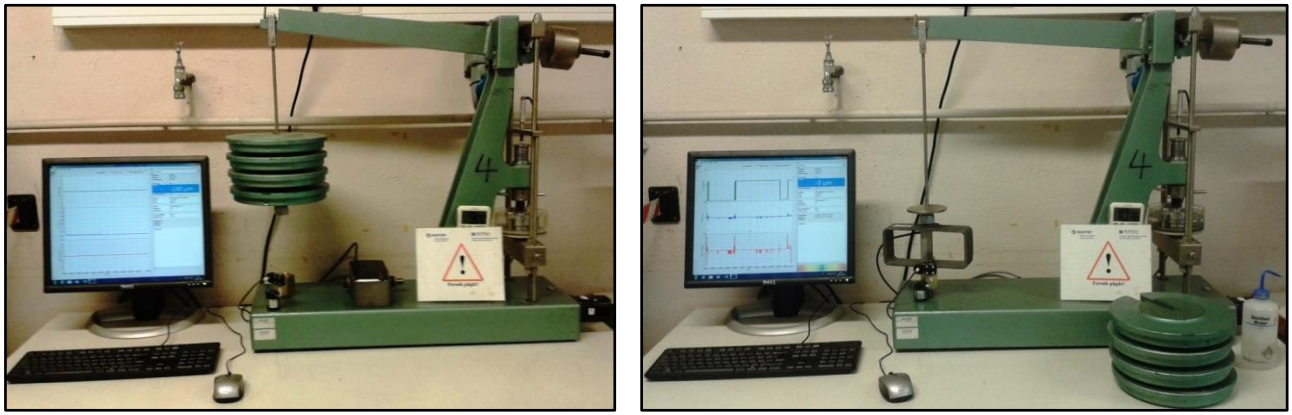


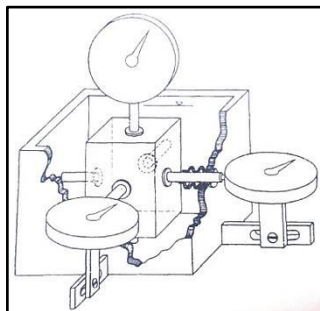
Figure 5-4: Oedometer setup for the compaction step, left, and the swelling stage, right.

For this master thesis free swelling tests were also performed. A measuring cylinder is filled with 45 ml of distilled water and 10 ml of loosely packed, carefully added, milled powder. After sedimentation the powder volume is recorded. The free swelling index number is the relation between this volume and the starting volume of the milled powder, where  $F_s = \frac{V_1}{V_0} \times 100\%$  (Mao et.al, 2011 and Dahl et.al, 2013).

### 5.1.2 The ISRM suggested method for determination of the swelling strain

The ISRM suggested method for determination of the swelling strain assumes an undisturbed and unconfined rock specimen, either prepared as a rectangular prism as the case for this laboratory testing or as a right cylinder and with duplicates (ISRM, 1977). For this thesis testing on rock cubes without duplicates have been carried out. Section 4.2.3 gives a description of the rock cube preparations.

The 3 dimensional expansion of the prepared rock cube is measured after it is submerged into water and digital distance gauges determinate the deformation of the rock specimen over time. This continuous electronic logging of the measurements includes the registration of water temperature by a digital thermometer, and the swelling displacement as a function of elapsed time is recorded (ISRM, 1977). Figure 5-5 shows the apparatus suggested by the ISRM and figure 5-6 shows the apparatus developed at SINTEF/NTNU in 2013.



#### Components of the test apparatus

- 1 Test cell with water level above the top of the specimen
- 2 Digital distance gauges on the central axis of the sample, reading to 0,0025 mm
- 3 Fixed plexiglass plates on the samples by adhesive

Figure 5-5: Sketch of the apparatus suggested by the ISRM and list of components for swelling strain measurements (ISRM, 1977).

Test procedure:

The rock specimen is marked with three gauge points that corresponds to the respectively axis of the cube. Measuring of the initial dimensions of the specimen, table 4-1, is registered and the plexiglass plates are fixed at each of the gauge point. The rock cube is placed into the apparatus and covered with distilled water. A continuous recording of the swelling displacement is performed until a constant level is reached or a peak is passed (ISRM, 1977).

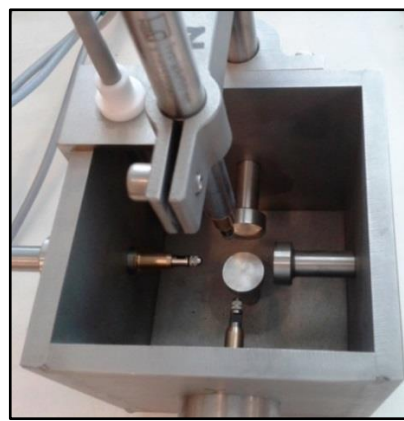
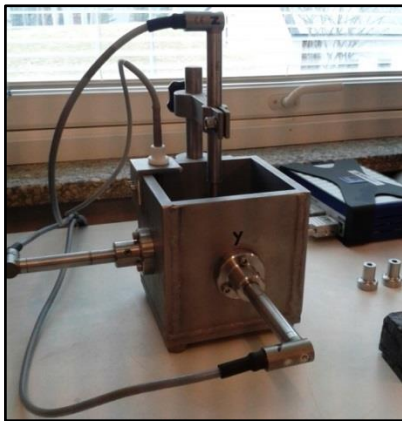


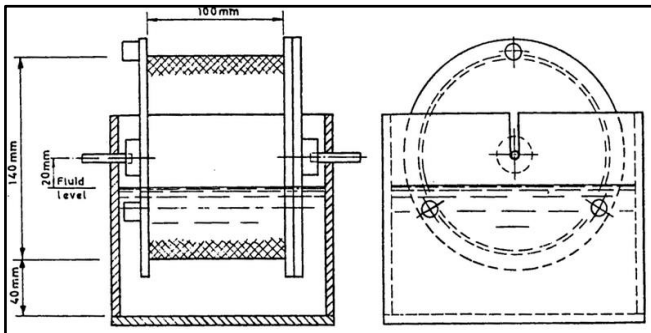
Figure 5-6: Photo of 3D measuring cell and apparatus for free swelling in 3 directions developed at SINTEF/NTNU in 2013.

The apparatus developed at SINTEF/NTNU in 2013 is given in figure 5-6 and it is quite similar to the one suggested by the ISRM except for the digital distance gauges and digital thermometer.

### 5.1.3 The ISRM suggested method for determination of the slake-durability index

The ISRM suggested method for determination of the slake-durability index is used for evaluating the ability the rock have to resist weakening and disintegration after two drying and wetting cycles (ISRM, 1977).

A selection of 10 rock pieces, prepared as in section 4.2.4, is used and the test apparatus is shown in figures 5-7 and 5-8. Figure 5-7 shows a sketch of the critical dimensions of the test equipment and a list of the components.



### Components of the test apparatus and equipment used for the testing

- 1 Test drum with a standard mesh cylinder
  - Thickness of mesh: 2.00 mm
  - Length of mesh: 100 mm
  - Diameter of mesh: 140 mm
  - Solid fixed base and solid removable lid
- 2 Trough
  - Support the drum with horizontal axis, allows free rotation
  - Slaking fluid: distilled water, water level 20 mm below the drum axis, 20°C
  - 40 mm clearance between trough and base of the mesh
- 3 Motor drive
  - Rotation of the drum: constant speed of 20 rpm
  - Time: 10 minutes
- 4 - Oven holding a constant temperature of 105°C
  - Weight for both drum and sample, accuracy of 0.5 g

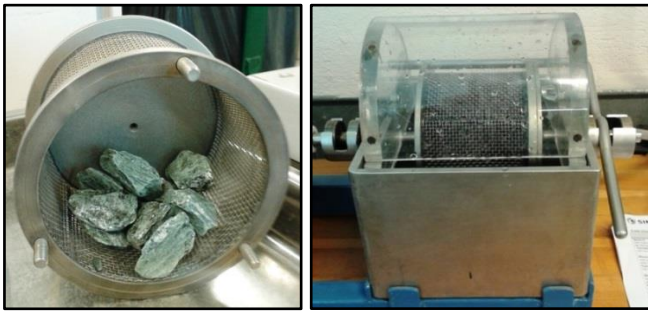


Figure 5-7: Sketch of the critical dimensions of slake-durability test equipment, upper left (ISRM, 1977) photo of test drum containing rock pieces from the green schist and test drum during testing, lower left and list of components, right (ISRM, 1977).

### Test procedure:

The total sample mass of 450-550 g, with rock pieces between 40 and 60 g, is placed in a clean drum and dried at 105°C (ISRM, 1977). The ISRM suggests drying from 2 to 6 hours, for this thesis the sample is dried for 24 hours. Mass A of cooled drum plus sample is recorded before the lid is replaced. The drum is then installed in the trough and connected to the motor, and the trough is filled with distilled water. The drum rotates for 200 revolutions before the drum is removed from the trough.

The lid is removed from the drum and the drum plus the sample is dried for 24 hours at 105°C. After cooling, mass B of drum plus the remains of the sample is recorded. The drum plus sample and lid is installed in the trough again and test cycle number 2 is conducted. The drum plus sample is dried for 24 hours before mass C, drum and the remains of the sample, is recorded. Finally the drum is cleaned and the mass D is recorded. Figure 5-8 shows the test apparatus during testing.



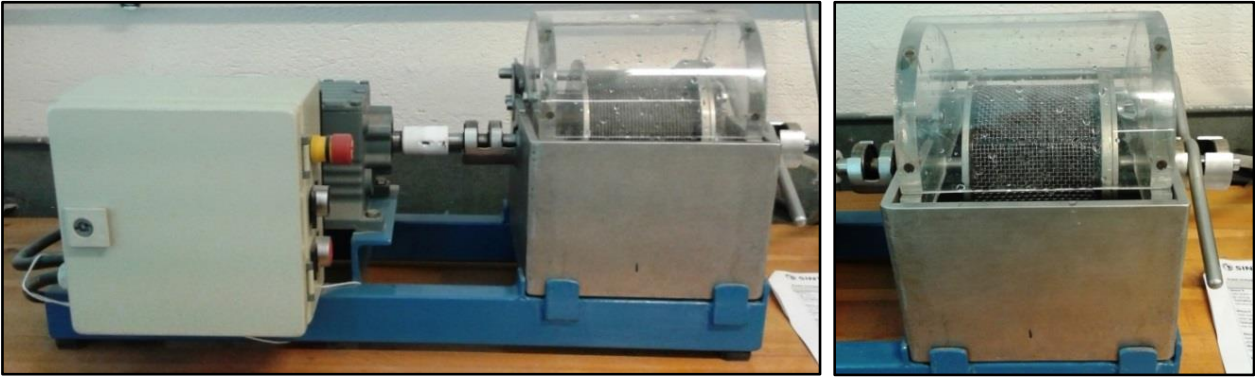


Figure 5-8: Photos showing the slake-durability test equipment (left) and a close-up of the test drum (right).

### 5.1.4 The ISRM suggested method for point load strength determination

The ISRM suggested method for point load strength determination is used as an index test for the strength classification of rock materials. Other strength parameters such as uniaxial tensile and compressive strength (ISRM, 1985) are computed from the point load strength index.

A selection of 10 irregular rock pieces, prepared as in section 4.2.4 and the requirements given in figure E-1 (Appendix E) is used. The test apparatus and its components are shown in figures 5-9 and 5-10.

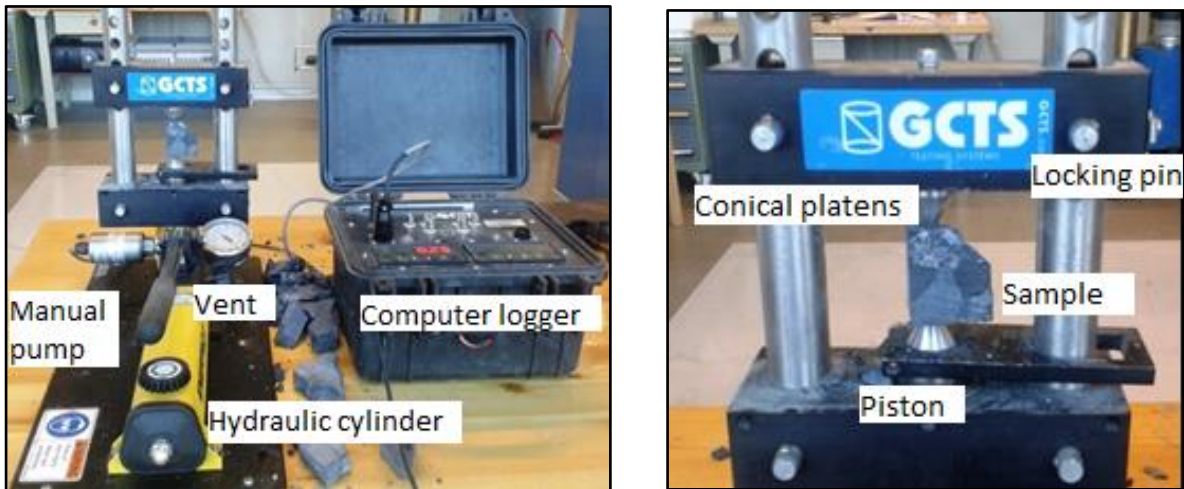
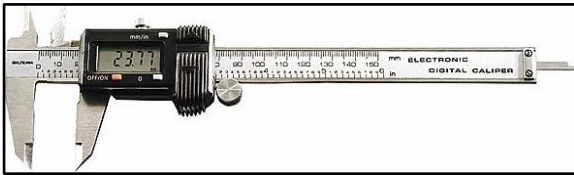
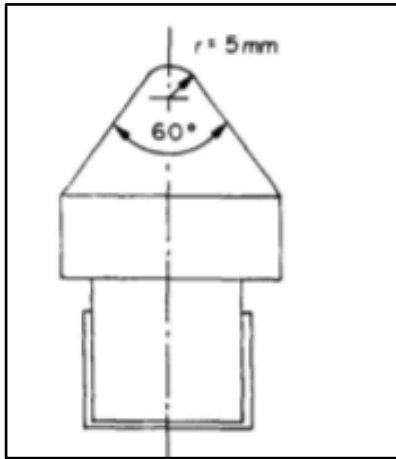
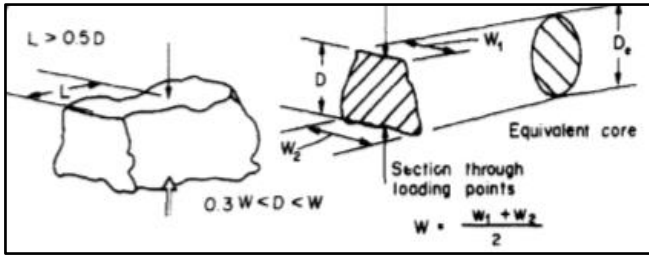


Figure 5-9: Photo of the test equipment, left, and a close up of the test rig, right.

In figure 5-9 the complete test apparatus, including a computer logger, a manual pump, a hydraulic cylinder and a vent, are shown. The close up of the test rig shows the conical platens, locking pins, a sample and a piston.



### Components of the test apparatus

- 1 Loading system: test rig
  - platen to platen clearance for rock specimens in the range 15-100 mm
  - enough loading capacity: break the strongest and largest rock piece
  - co-axial platens during testing:  $\pm 0.2 \text{ mm}$  distortion
  - rigid loading system to avoid slippage of the rock pieces
  - conical, spherically-truncated platens of hard material
- 2 Load measuring system: hydraulic pressure gauge and computer logging
  - measure the load  $P$  required to break the specimen, accuracy of  $\pm 5\%$   $P$  or better
  - resistant to vibration and hydraulic shock for an unaffected accuracy
  - maximum load indicating device to retain and record the failure load
- 3 Distance measuring system: computer logging and caliper
  - measure the distance  $D = D_e$  between the two platen contact points, accuracy of  $\pm 2\%$   $D$  or better
  - measure the width  $W_1$  and  $W_2$  of the rock piece by the caliper:  $W = \frac{W_1 + W_2}{2}$

Figure 5-10: Sketch of specimen shape requirements, upper left, shape of the conical platens, centre left and a caliper, lower left. A list of the apparatus components is shown to the right (ISRM, 1985).

Figure 5-10 shows a sketch of the specimen shape requirements, the shape of the conical platen, a caliper for measuring  $W$  and a list of the apparatus components.

### Test procedure:

The ISRM standard suggests rock pieces of size  $50 \pm 35 \text{ mm}$  (ISRM, 1985) and figure 5-10 shows the suggested shape of the irregular rock pieces. Due to difficulties in the preparing of the specimens varying sizes was obtained, some with smaller dimensions than the one suggested. The  $D/W$  ratio ought to be  $0.3 \geq D/W \leq 1.0$  and the distance  $L \geq 0.5W$  (ISRM, 1985).

The selected specimens are in turn positioned in the test apparatus allowing the conical platens having contact with the rock piece at its smallest dimension. The ISRM suggests that shaly, bedded or schistose rock samples should be tested both parallel and normal to the weakness planes. As it was not

possible to obtain enough samples, the specimens were only tested perpendicular to the planes (ISRM, 1985).

The distance  $D$  is registered and the width  $W$  is calculated from the formula:

$$W = \frac{W_1 + W_2}{2}$$

where  $W_1$  and  $W_2$  is measured using the caliper. The manual pump is used to gradually increase the pressure until fracture of the specimen is attained and the failure load  $P$  is registered. This procedure is repeated for all of the specimens.

## **5.2 Method for swelling pressure determination - constant volume, axial swelling**

The test procedure for swelling pressure determination of rock discs is fairly similar as the one for gauge material and rock powder, section 5.1.1, apart from some differences which are discussed in the following. The apparatus used is the same as for the suggested ISRM method and the cylindrical test cell has a dimension of  $10 \text{ cm}^2$ .

Test procedure:

The  $10 \text{ cm}^2$  cylindrical test cell, prepared as in section 4.2.2, consisting of a brass filter at the top and a porous glass filter at the bottom is installed into the oedometer. Figure 5-10 gives a detailed photo of the test cell. The adjustment screw is used to align the balance lever to a position slightly above the horizontal line followed by the installation of the height transducer. Thereafter both the pressure ring and the pressure dial gauge are installed, before steel disc weights applied to the balance lever compresses the specimen at 4 MPa for 24 hours.

Unloading of the specimen is done by removing the steel disc weights for a minimum of 2 hours until the height transducer no longer records any height changes. Distilled water with a depth of 10 mm is poured into the container and a continuous 24 hour registration of the swelling pressure is performed. The automated step-motor adjusts continuously to avoid changes in the specimen volume and to compensate for the deformation of the apparatus. Figure 5-4 shows the oedometer setup for the compression stage and the swelling stage.

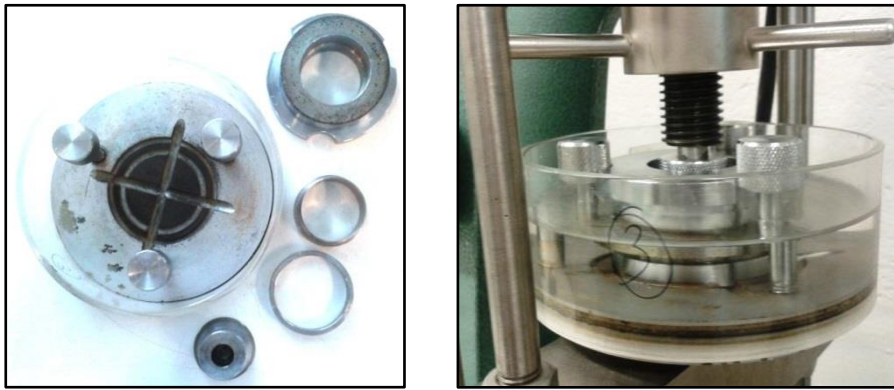


Figure 5-10: Photo of test cell components, left, and test cell in use, right.

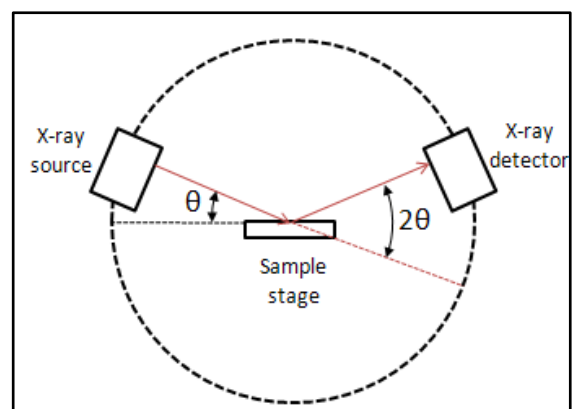
### 5.3 Petrographic and mineralogical test methods

Petrographic and mineralogical test methods such as XRD and thin section analysis are used to identify and classify the mineralogy and texture of the rock. A quantification of the minerals and a description of the texture and microstructure are done by performing thin section analyses, while the content and amount of the minerals is determined by X-ray diffraction.

#### 5.3.1 X-ray diffraction analysis

To identify the matrix minerals and to get a semi-quantitative analysis of the mineral content the X-ray diffraction analysis is used (Brattli and Broch, 1995). The sample material is prepared as in section 4.2.1 and the XRD analysis was performed at the chemical/mineralogical laboratory, NTNU.

For the performance of the XRD analysis a Bruker D8 ADVANCE with a DIFFRAC<sup>plus</sup> SEARCH software in combination with PDF-2 database is used. This is followed by a quantification of the minerals in the crystalline phases using the Bruker Rietveld (Topas 4) software. Figure 5-11 shows a photo of the instrument used for the XRD analysis.



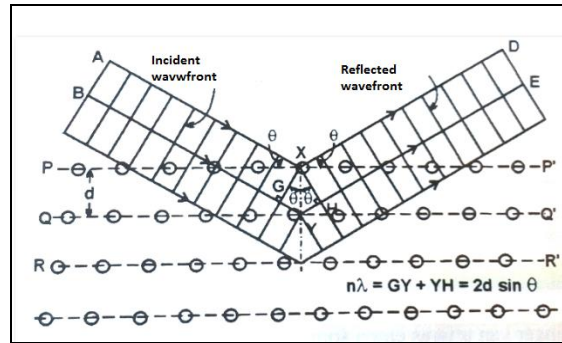


Figure 5-11: Photo of the XRD instrument used for X-ray diffraction analysis, left, a close up of the components of the XRD instrument, upper right (The Bruker Corporation, 2014) and the principal of XRD-analysis, lower right (Nilsen and Broch, 2009).

Test procedure:

The prepared sample material is placed in the sample stage and x-rays are submitted to the sample, figure 5-11. The incident x-rays hit the surface of the crystals and the reflected x-rays are related to the lattice structure of the crystals. The lattice spacing,  $d$ , is characteristics for each of the minerals and is calculated from the given integer  $n$  and wavelength  $\lambda$ , and measured angle  $\theta$ , from the formula (Nilsen and Broch, 2009):

$$n\lambda = 2d \sin\theta$$

A unique pattern, interference, is registered and compared to patterns for known minerals in the PDF-2 database (NGU, 2005 and Nilsen and Broch, 2009). The performed computation results in a suggestion of mineral phases and a percentage of each of the mineral, table 6-2, on the basis of the intensity of the peaks which is closely related to the amount of minerals in the sample (Brattli and Broch, 1995).

### 5.3.2 Thin section analysis

Thin section analysis is performed to characterize the mineralogy and the texture of the rock and to understand rock properties (Brattli and Broch, 1995). The thin sections, prepared as in section 4.2.5, are used in the petrographic analysis and are based on a microstructure examination using a Leica DM 2500 P microscope with transmitted, reflected and fluorescent light and a ProgRes CT3 software program. In figure 5-12 the microscope setup used for the thin section analysis is shown. The microscope is connected to a digital camera and a computer allowing direct transfer of the images taken.

Analysis of thin sections involve a determination of the mineral colour, pleochroism, relief, undulatory extinction and interference colour of the minerals (Brattli, 1991 and Prestvik, 2009). The colour of the minerals varies from colourless to strongly coloured, and is seen in plane polarized, parallel light. The colour reflects the minerals light absorption and anisotropic minerals change colour, have pleochroism, when rotated in plane polarized light. A minerals relief, also seen in plane polarized light, refers to the sharpness of the grain boundaries and how the mineral protrudes the other minerals in the matrix. Undulatory extinction is determined when cross polarized light is used and the stage is rotated. The minerals are alternating between their original colour and black resulting in an appearance variation as the extinction angle changes. Finally the interference colours, seen in crossed polarizers, vary from low to high order depending on the speed of the x-rays, figure D-1 (Appendix D).

Test procedure:

The petrographic microscope is adjusted to obtain the correct lighting, contrast and resolution capability and the right distance between the oculars is set, before studying of the thin sections (Brattli, 1991). The prepared thin section is positioned on to the rotating stage and the 2.5x objective lens is selected and focused using the focus knob. Adjustment and focusing of the microscope by changing the magnification of the objective lenses, up to 20x, continues until the optimum image is obtained. Adjustment of the computer settings is done and the selected image is taken and saved. For each of the



rock samples multiple images are taken to get a representative selection of the mineral content and the amount of them.

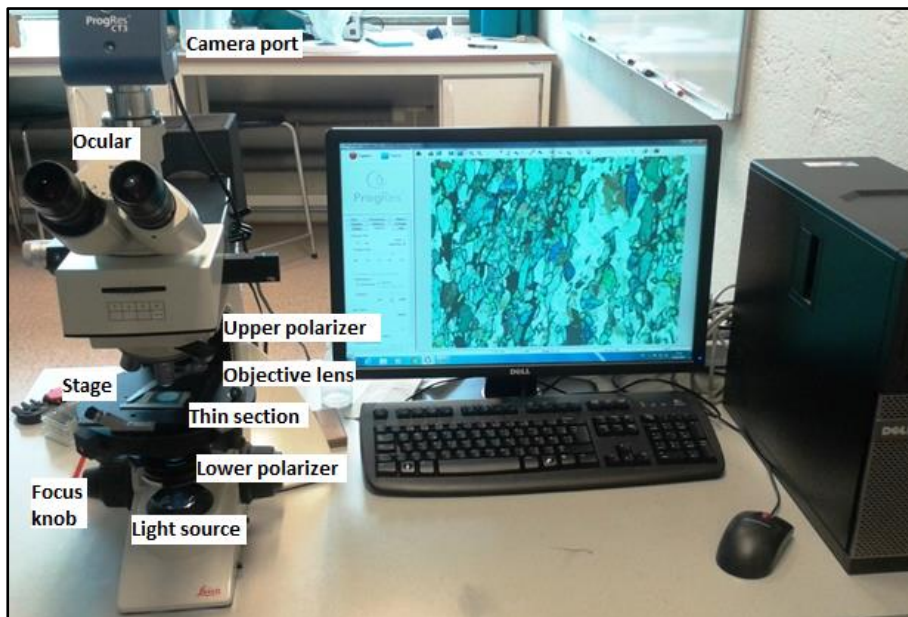


Figure 5-12: Photo of the microscope setup used for thin section analysis.

## 5.4 Rock mechanical test methods

For the determination of the mechanical properties of rock material a number of test methods are available. In addition to the point load test and slake-durability test performed for this specific master thesis, the density test was carried out.

### 5.4.1. Density test

The density of a rock mass is calculated as its mass divided by its volume and is a measurement of the compaction degree. The mineral content and amount of minerals and voids in the material affect the density resulting in various densities for the same rock type (Nilsen and Broch, 2009). The test material is prepared as in section 4.2.4 and the pycnometer is shown in figure 5-13.

Test procedure:

The pycnometer, a glass jar with a flat glass lid, is placed on the weight and the weight is then set to zero. The pycnometer is filled with the selected rock pieces and then weighed,  $W_s$ . After recording, the pycnometer is filled with tap water, and the lid is gently pushed over the glass jar to avoid air bubbles and weight  $W_1$  is recorded. The rock pieces are removed from the pycnometer and refilling of tap water and use of the glass lid is done. The weight  $W_2$  is recorded. Weight  $W_s$ ,  $W_1$  and  $W_2$  are used when determining the density, section 6.3.3.

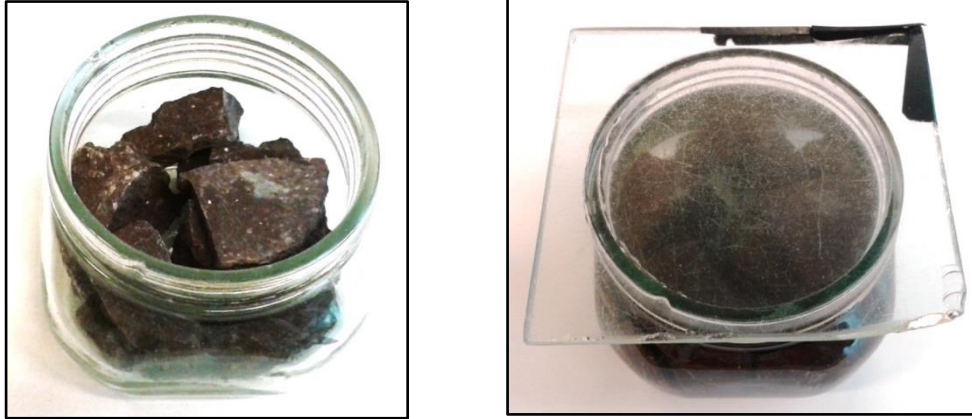


Figure 5-13: Photo of test equipment for density testing; sample without lid to the left and sample plus water with lid to the right.

The glass jar filled with rock pieces from the tuff is shown in figure 5-13, both without and with water and glass lid.



## 6 Results from laboratory work

In the following sections the results from the laboratory work are presented. Section 6.1 gives the results from the swelling test methods described in sections 5.1.1, 5.1.2 and 5.2. Section 6.2 gives the results from the mineralogical test methods described in section 5.3 and section 6.3 gives the results from the rock mechanical test methods described in sections 5.1.3, 5.1.3 and 5.4.

### 6.1 Swelling tests

#### 6.1.1 Swelling pressure index – bulk material and free swelling

The swelling pressure index is calculated from the formula:

$$\frac{F}{A}$$

where F is the maximum axial swelling force recorded and A is the cross sectional area of the specimen (ISRM, 1977).

The swelling pressure index is computed using a Microsoft Excel spreadsheet where the charts are created from the swelling log. In figures 6-1 the swelling pressure curves for the alum shale is shown.

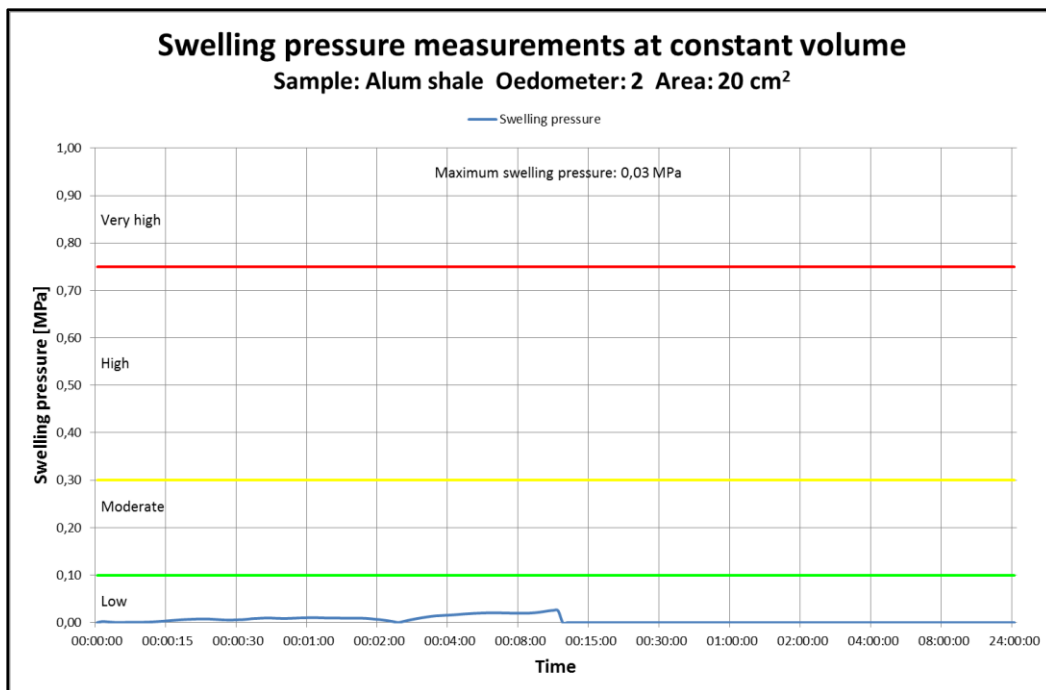


Figure 6-1: Swelling pressure chart for the alum shale showing the maximum swelling pressure measured.

The swelling pressure curve for the alum shale presented in figure 6-1 shows a very low to zero swelling pressure.

In figure 6-2 the swelling pressure curve for the greenschist is shown.

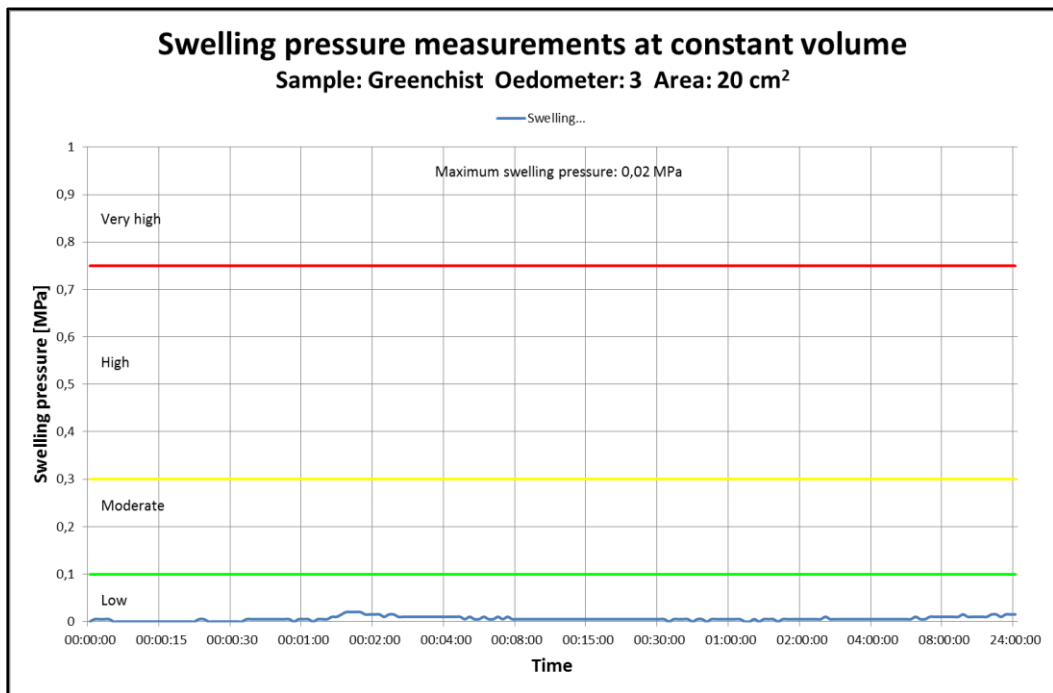


Figure 6-2: Swelling pressure chart for the green schist showing the maximum swelling pressure measured.

The swelling pressure curve for the greenschist presented in figure 6-2 shows a very low swelling pressure.

In figure 6-3 the swelling pressure curve for the tuff is shown.

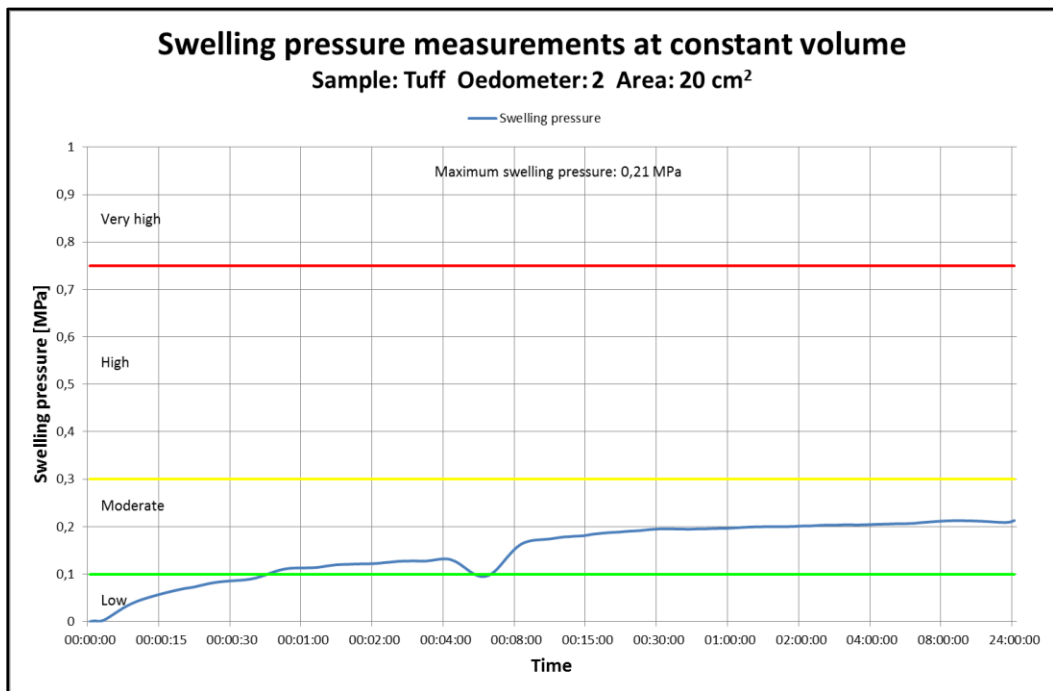


Figure 6-3: Swelling pressure chart for the tuff showing the maximum swelling pressure measured.

The swelling pressure curve for the tuff presented in figure 6-3 shows a low swelling pressure but the highest swelling pressure measured for all three rocks.

The free swelling index number,  $F_s$  is calculated from the formula:

$$\frac{V_1}{V_0} \cdot 100\%$$

where  $V_1$  is the volume of powder after sedimentation and  $V_0$  is the original volume of dry powder (Mao et.al, 2011).

The free swelling index is computed using the same Microsoft Excel spreadsheet as above and parts of the spreadsheet is shown in figure C-1 (Appendix C). Figure 6-4 shows the measuring cylinder where the free expansion of the sample is determined.

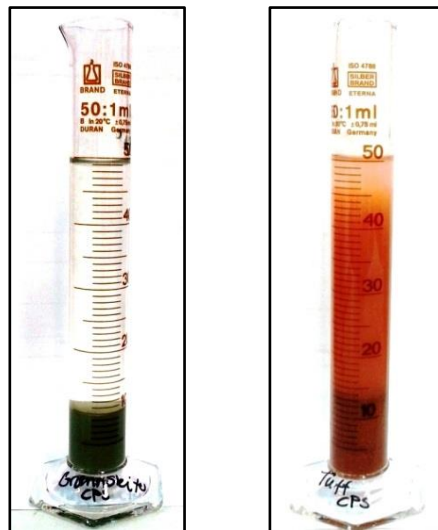


Figure 6-4: Determination of free swelling using a measuring cylinder, showing the green schist to the left and the tuff, not fully settled, to the right. Photo of the alum shale is not included due to poor quality of the photo (Private photos).

Table 6-1 gives the classification of the swelling pressure index and the free swelling for all three rock samples on the basis of the classification in table C-1 (Appendix).

Table 6-1: Classification of the free swelling and the swelling pressure index of the rock samples.

Sample	Free swelling		Swelling pressure	
	[%]	Classification	[MPa]	Classification
Alum shale	130	Moderate	0,03	Low
Greenschist	100	Moderate	0,02	Low
Tuff	135	Moderate	0,21	Moderate

For all three rock samples the free swelling is determined as moderate and the swelling pressure ranges from low to moderate.

For this master thesis no duplicate tests are performed and only three rock samples have been tested, making it difficult to confirm a correlation between the free swelling and the swelling pressure for other rock types.

In figure 6-5 the correlation between the free swelling and swelling pressure index values are shown.

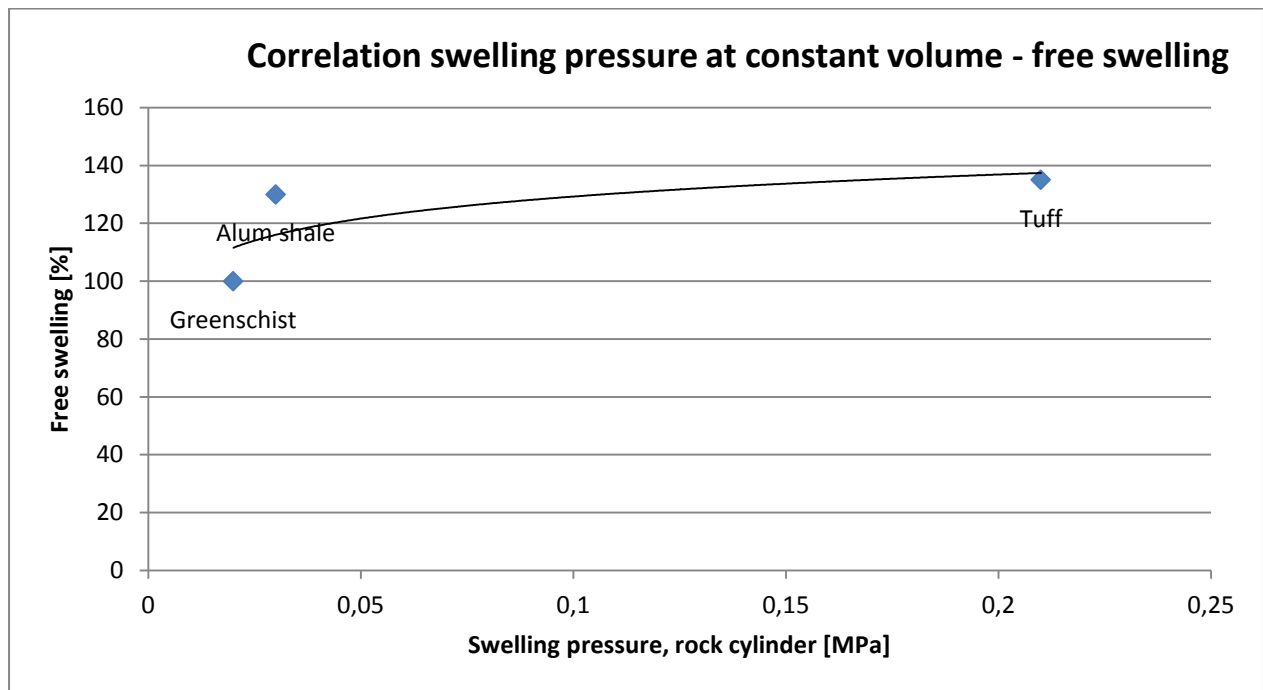


Figure 6-5: Correlation between the free swelling and the swelling pressure at constant volume (Modified after Dahl et.al, 2013 and Mao et.al, 2011).

The rock sample with the highest free swelling value, the tuff, has the highest value for swelling pressure and the rock sample with the lowest free swelling value, the greenschist, has the lowest value for swelling pressure. This corresponds well to fact that both test methods are used in the quantification and classification of swelling properties and the relative swelling potential of gauge and bulk material (Dahl et.al, 2013).

### 6.1.2 Swelling pressure - rock cylinders

The swelling pressure for rock discs is computed using the Microsoft Excel spreadsheet, section 6.1.1, where the charts are created from the swelling log.

In figure 6-6 the swelling pressure curve for alum shale is shown.

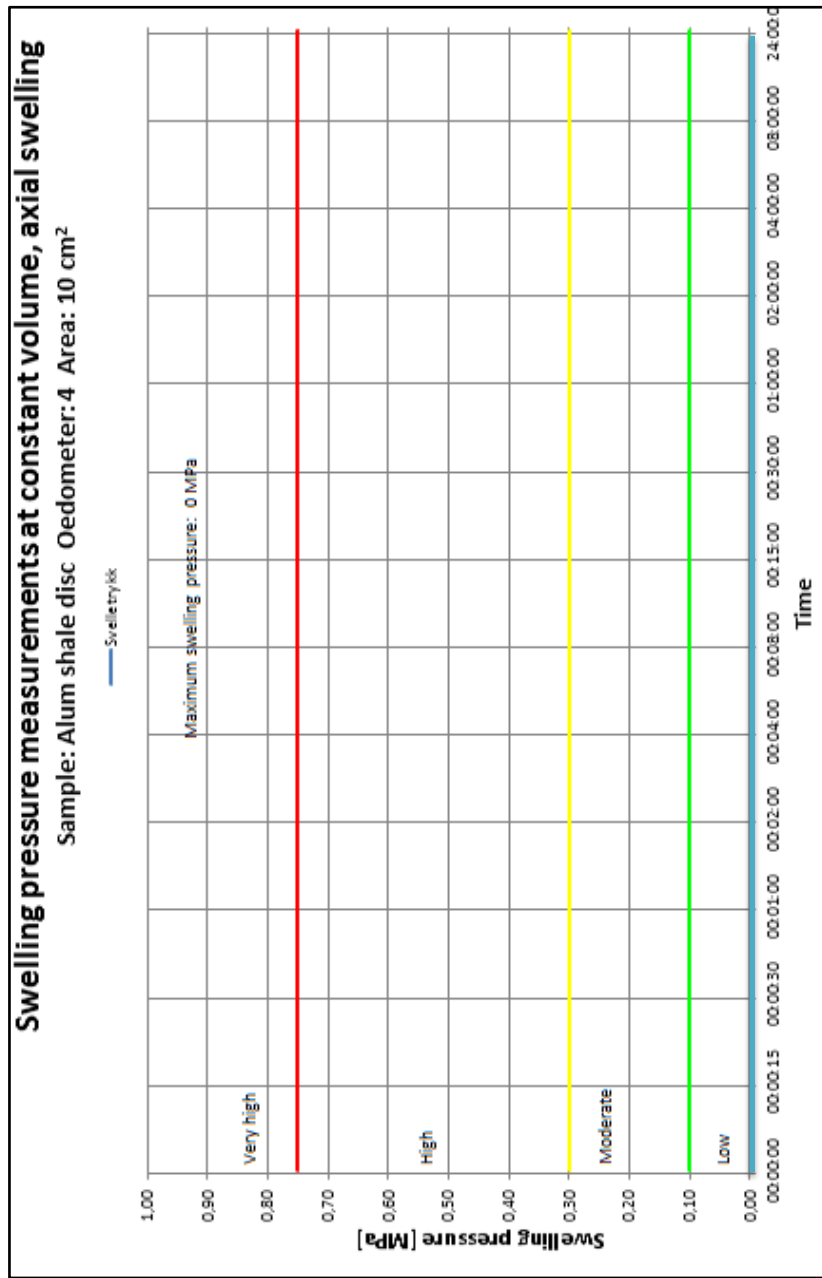


Figure 6-6: Swelling pressure chart for the alum shale showing the maximum swelling pressure measured.

The alum shale is showing zero swelling pressure, indicating an inactive rock material, table C-1 and C-2 (Appendix C).

In figure 6-7 the swelling pressure curve for the greenschist is shown.

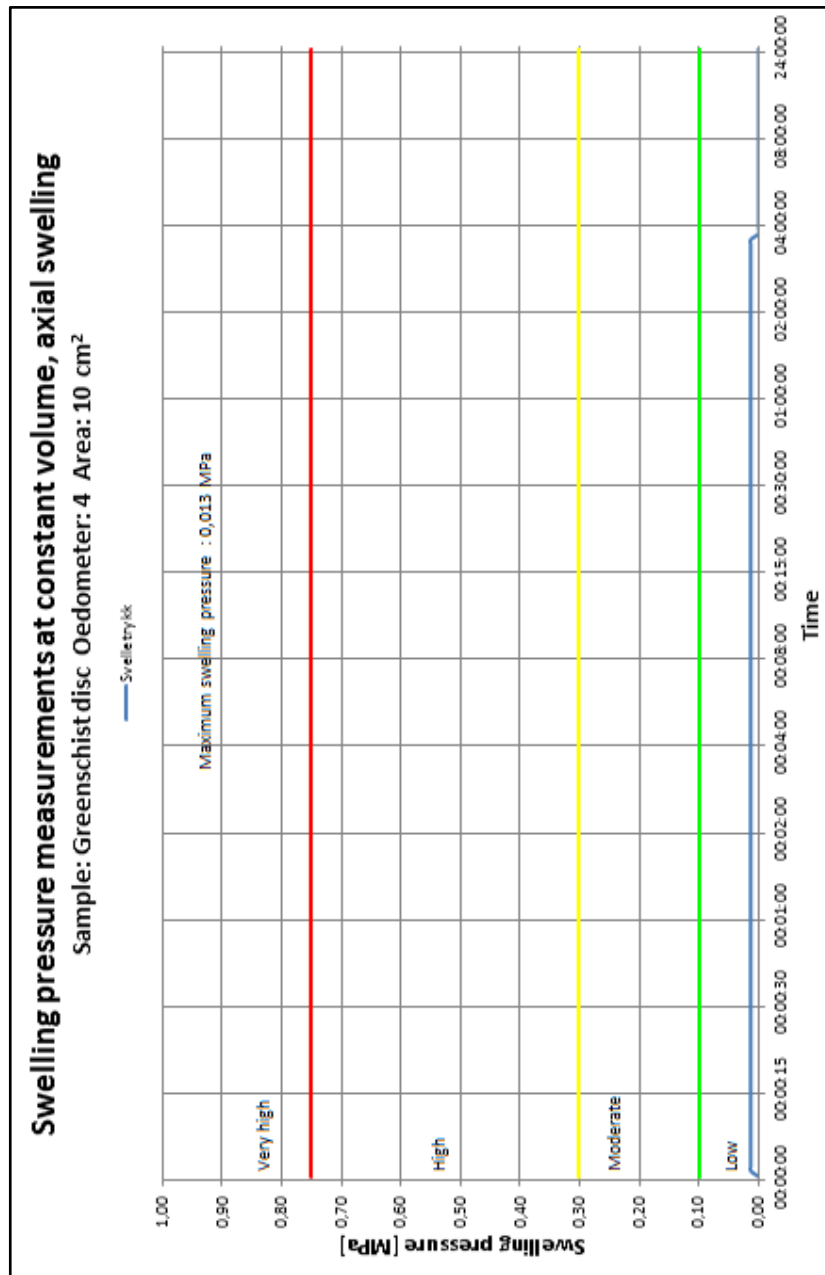


Figure 6-7: Swelling pressure chart for the greenschist showing the maximum swelling pressure measured.

The greenschist has a maximum swelling pressure of 0,013 MPa and is classified with low swelling potential, table C-1 and C-2 (Appendix C).

In figure 6-8 the swelling pressure curve for the tuff is shown.

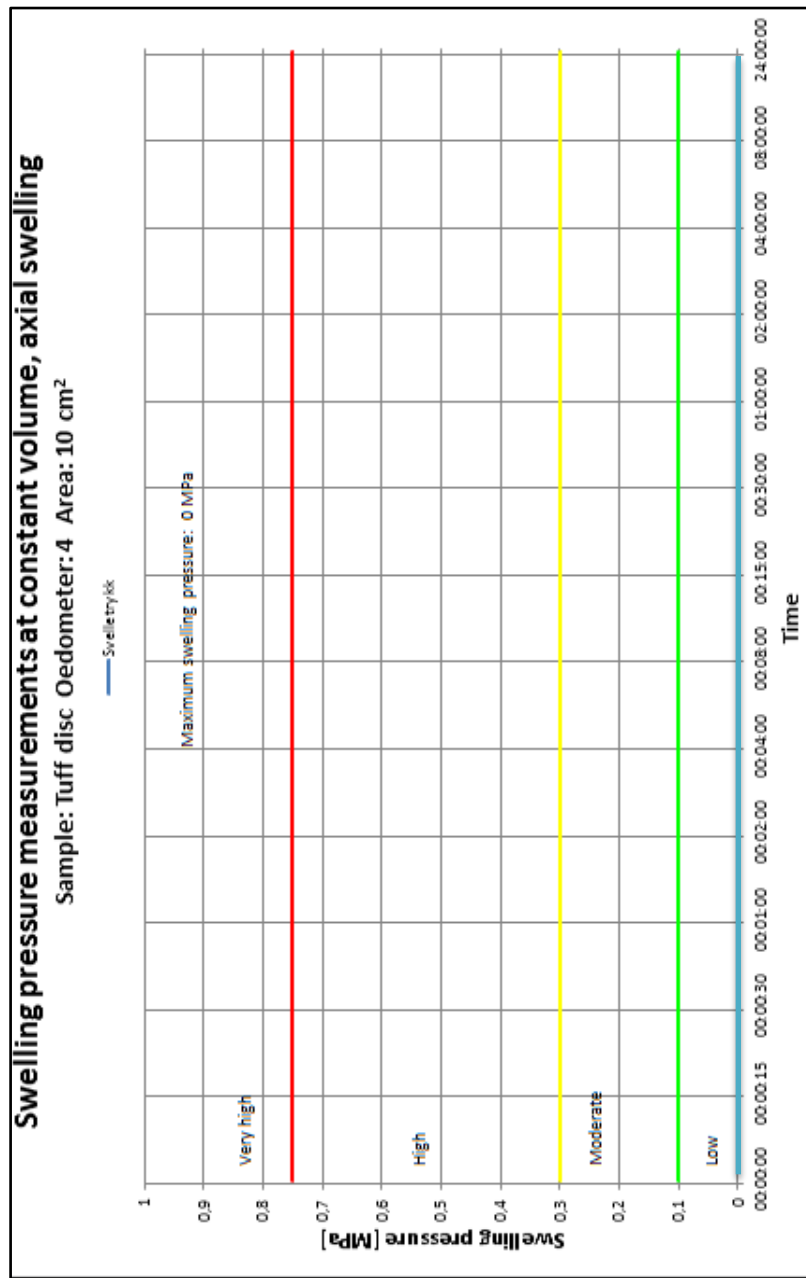


Figure 6-8: Swelling pressure chart for the tuff showing the maximum swelling pressure measured.

The tuff is showing zero swelling pressure, indicating an inactive rock material, table C-1 and C-2 (Appendix C).

Table 6-2 gives the classification of the swelling pressure for all three rock samples on the basis of the test results and the gauge material classification in Appendix C.

Table 6-2: Swelling pressure results of the three rock samples.

<b>Sample</b>	<b>Swelling pressure</b>	
	<b>[MPa]</b>	<b>Classification</b>
Alum shale	0,00	Inactive
Greenschist	0,01	Low
Tuff	0,00	Inactive

Both alum shale and tuff is showing zero swelling pressure, indicating an inactive rock material. The greenschist shows the greatest swelling pressure of the three rocks. The test values of rock discs correlate to the test values of bulk material expect for the greenschist that is showing a significant deviation between the two values.



### 6.1.3 Swelling strain - undisturbed and unconfined rock cubes

The swelling strain is calculated for three directions, x, y and z and the measurement in direction x is equal to the formula:

$$\frac{d}{L} \times 100\%$$

where x is a direction relative to the bedding or foliation, d is the maximum swelling displacement recorded in direction x during test and L is the initial distance between gauge points in direction x, see table 4-1 (ISRM, 1977).

The swelling strain of undisturbed and unconfined rock cubes are computed using a Microsoft Excel spreadsheet where the charts are created from the swelling strain log. In figures 6-9, 6-10 and 6-11 the swelling strain charts for the three rock samples are shown.

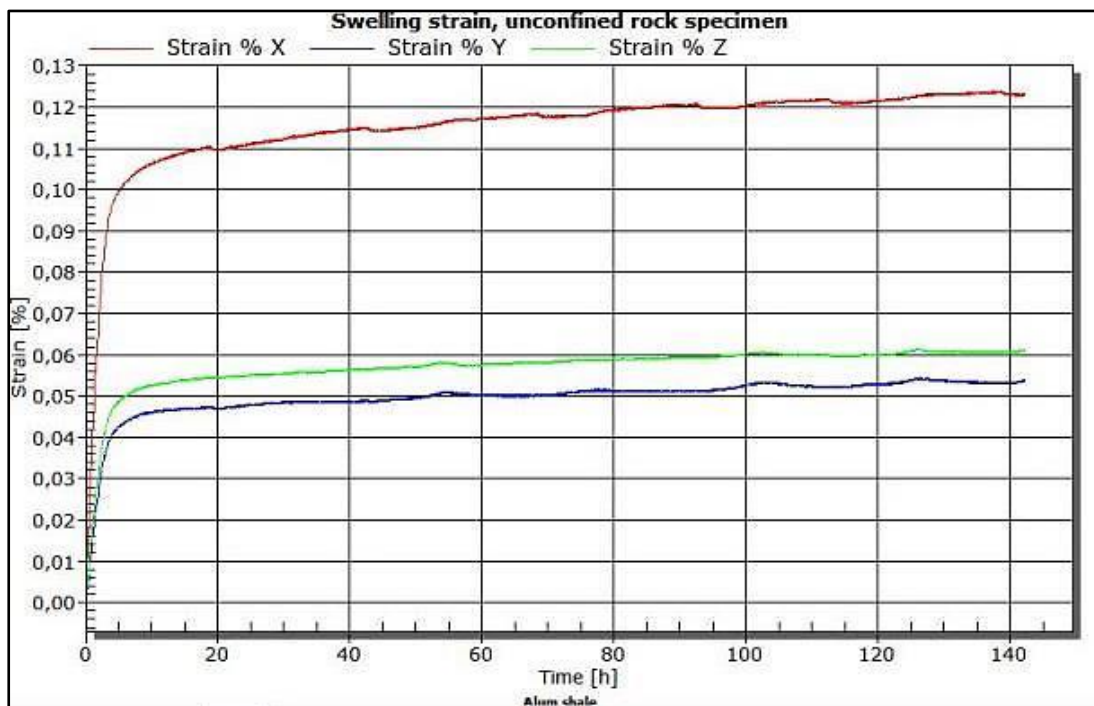


Figure 6-9: Unconfined swelling strain chart for the alum shale.

The alum shale shows the greatest swelling strain in the x-direction, red curve.

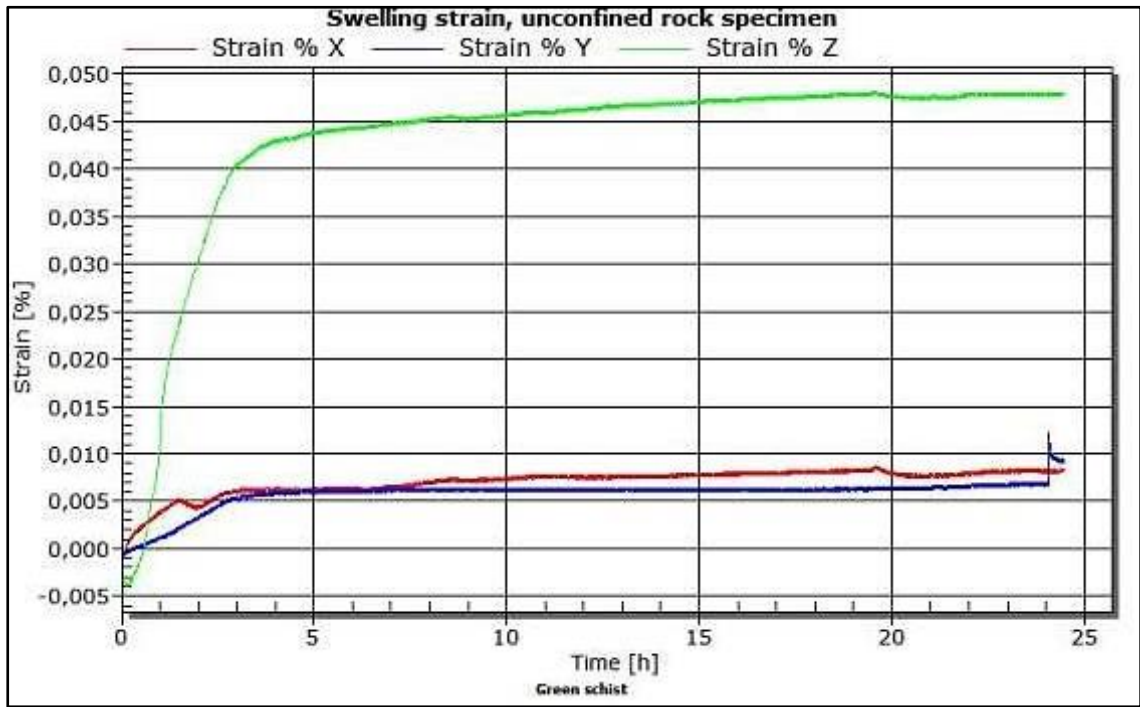


Figure 6-10: Unconfined swelling strain chart for the greenschist.

The greenschist shows the greatest swelling strain in the z-direction, green curve.

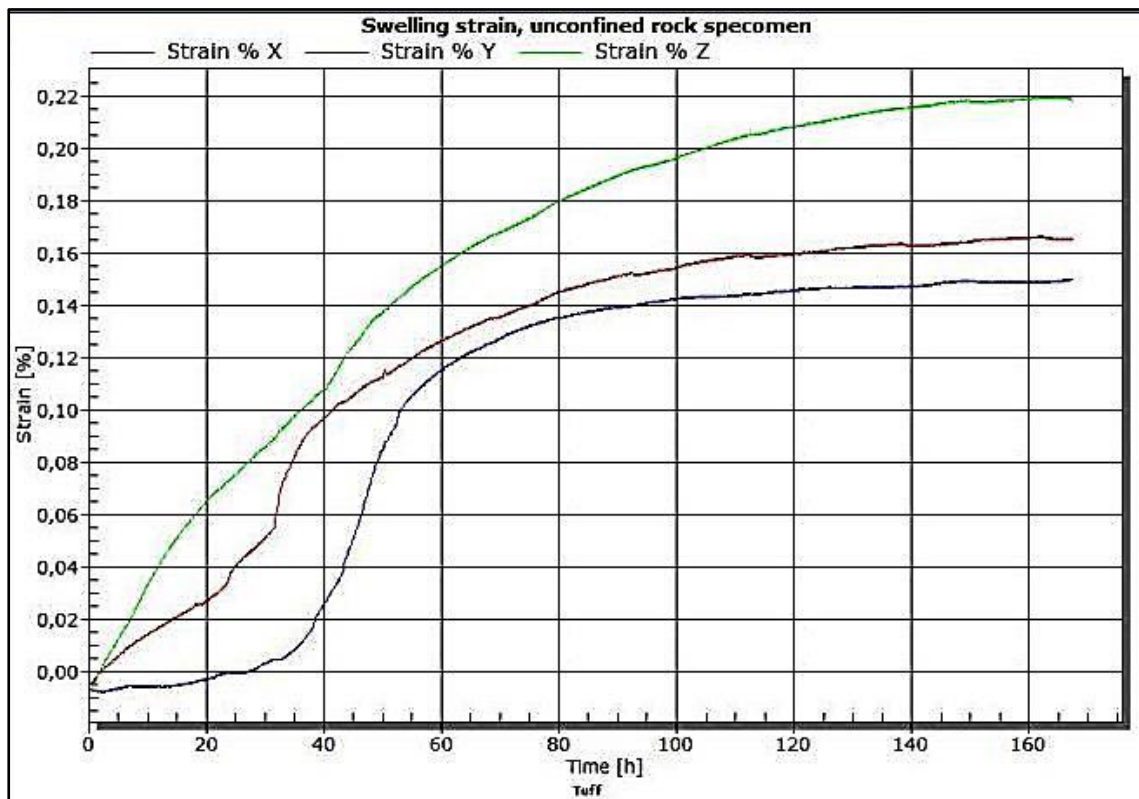


Figure 6-11: Unconfined swelling strain chart for the tuff.

The tuff shows the greatest swelling strain in the z-direction, green curve.

In table 6-3 the highest measured swelling strain in x-, y- and z-direction is given both swelling strain in percentage and in mm.

Table 6-3: Swelling strain results of the three rock samples.

Sample	Swelling strain x-direction		Swelling strain y-direction		Swelling strain z-direction	
	[%]	[mm]	[%]	[mm]	[%]	[mm]
Alum shale	0,125	0,0602	0,055	0,0241	0,060	0,0295
Greenschist	0,008	0,0035	0,006	0,0026	0,048	0,0209
Tuff	0,165	0,0826	0,145	0,0770	0,220	0,1122

The alum shale shows greatest swelling strain in the x-direction, as opposed to the green schist and tuff with the greatest swelling strain in the z-direction. The tuff also shows significant swelling strain in the x- and y-direction and these values correspond to values calculated for the free swelling and the swelling pressure index in section 6.1.1.

## 6.2 Mineralogical tests

### 6.2.1 X-ray diffraction – bulk material

Figures 6-12, 6-13 and 6-14 show the X-ray diffractograms with the suggested mineral phases and the percentage distribution of minerals for each of the rock sample. All mica, plagioclase and feldspar within the same mineral group are considered together due to the equal peaks in the XRD charts.

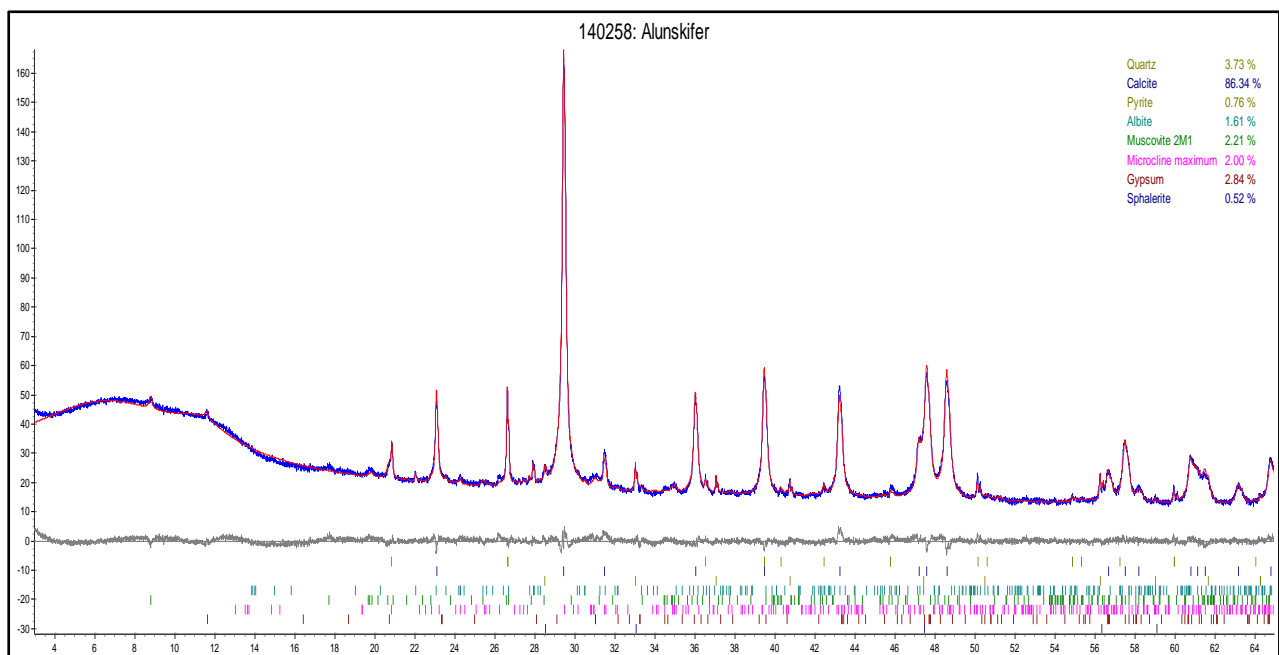


Figure 6-12: X-ray diffractogram (Brattli and Broch, 1995) for the alum shale showing the mineral phases and percentage distribution.

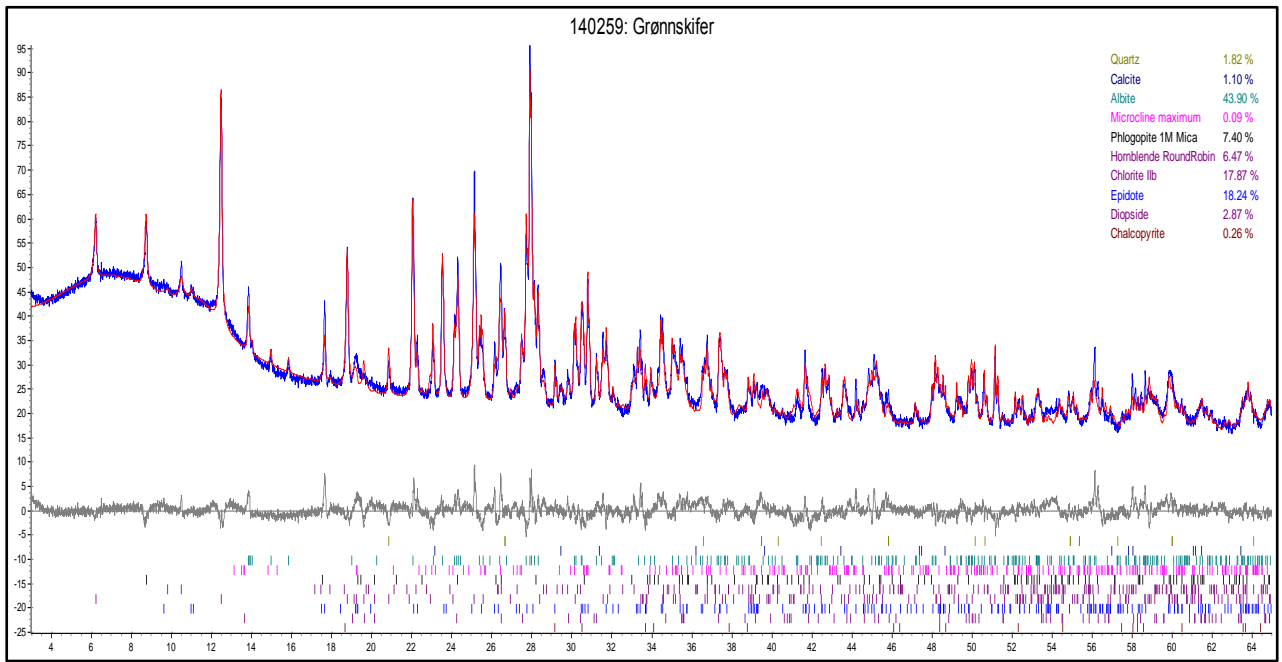


Figure 6-13: X-ray diffractogram (Brattli and Broch, 1995) for the greenschist showing the mineral phases and percentage distribution.

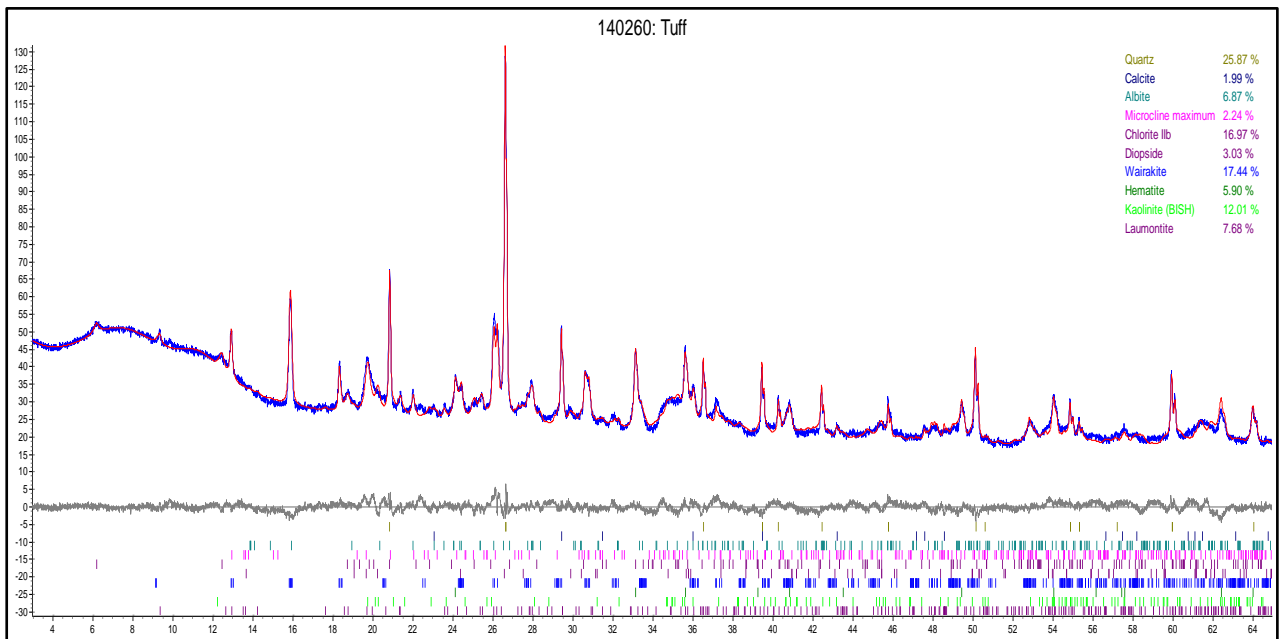


Figure 6-14: X-ray diffractogram (Brattli and Broch, 1995) for the tuff showing the mineral phases and percentage distribution.

Table 6-4 gives the complete list of mineral phases based on the diffractograms.

Table 6-4: Presentation of mineral phases from the XRD analysis for all three rock specimens is given.

Mineral	Sample		
	Alum shale	Greenschist	Tuff
Quartz	4 %	2 %	26 %
Calcite	86 %	1 %	2 %
Pyrite	< 1 %		
K-feldspar	2 %	44 %	7 %
Mica	2 %	7 %	
Plagioclase	2 %	< 1 %	2 %
Gypsum	3 %		
Sphalerite	< 1 %		
Amphibole		6 %	
Chlorite		18 %	17 %
Epidote		18 %	
Pyroxene		3 %	3 %
Chalcopyrite		< 1 %	
Wairakite (zeolite)			17 %
Hematite			6 %
Kaolinite			12 %
Laumontite (zeolite)			8 %

Based on table 6-4 the minerals of greatest interest are listed:

- Alum shale:
  - Calcite, 86 %
  - Other minerals of significance are gypsum, two types of sulphides; pyrite and sphalerite and mica.
- Green schist:
  - Albite (feldspar-group), 44 %
  - Other minerals of interest are chlorite, epidote, mica and sulphide; chalcopyrite.
- Tuff:
  - Quartz, 26 %
  - Other minerals are chlorite, kaolinite and wairakite.

The minerals listed and their importance to swelling potential is discussed in detail in section 8.2.

## 6.2.2 Thin sections – customized rock cores

Figures 6-15, 6-17 and 6-19 show the thin sections in their entirety and figures 6-16, 6-18 and 6-20 show the microscope images of the three selected rock samples. Optical properties to be discussed are mineral colour, pleochroism, relief, undulatory extinction and interference colour, section 5.3.2 (Brattli, 1991) and the mineral properties (Prestvik, 2005). In the following the minerals with the highest percentage are to be discussed. For a complete list of percentage distribution of the minerals for all three rock samples see table 6.2.1. Classification of mineral arrangement, sorting and orientation of the mineral grains and classification of silicate minerals is according to Appendix D.

### Alum shale:

Figure 6-15 shows the thin section image and figures 6-16 A-F show microscope images of the alum shale. The alum shale has a moderately to poorly sorting of the minerals and a heterogeneous mineral composition and the blackish grey coloured matrix is dominated by colourless to grey calcite minerals and calcite veins of varying sizes and white to grey quartz minerals. Mineral arrangement for the alum shale is classified as partly veined, due to the observed calcite veins, and partly unoriented. The opaque colouring of the sample makes it difficult to distinguish the rest of the minerals from one another.

Calcite minerals with chemical formula  $\text{CaCO}_3$  are greyish-brown and show low pleochroism in plane polarized light. The minerals have very high relief and are showing distinct twinning, both simple and lamellar. Using cross polarized light the calcite minerals show undulatory extinction in shades of blue and appear with high order interference colours like pink, blue and yellow. Anhedral and angular quartz minerals, tectosilicates, have low relief and show no cleavage. The quartz minerals show white to grey colours and pleochroism in plane polarized light and appear black with undulatory extinction in cross polarized light.

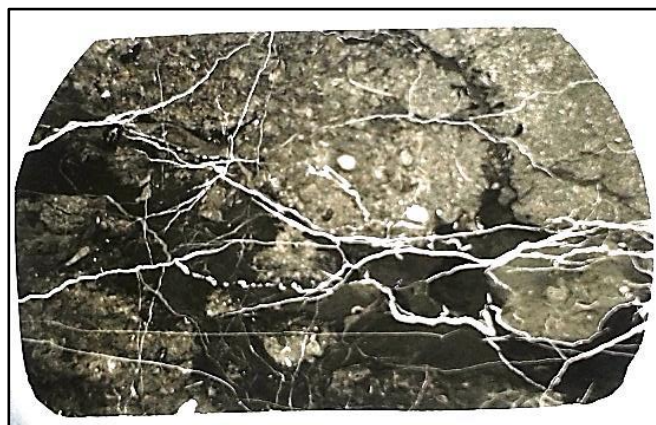


Figure 6-15: Thin section image of alum shale.

In figure 6-16 A and B relatively large calcite veins in cross polarized light are shown. In figure A the bright interference colour of the calcite and the distinct twinning of the minerals are also shown. Figure 6-16 C show some organic matter surrounded by calcite minerals, cross polarized light. An image of the pale brown colours of the matrix and calcite veins, plane polarized light, are shown in



figure 6-16 D. It is also possible to see small brown spherulite minerals and mineral coating on the calcite minerals that cements the grains together. Figures E and F show bright interference colours of the gypsum mineral, cross polarized light. Figure F also shows calcite minerals and organic matter.

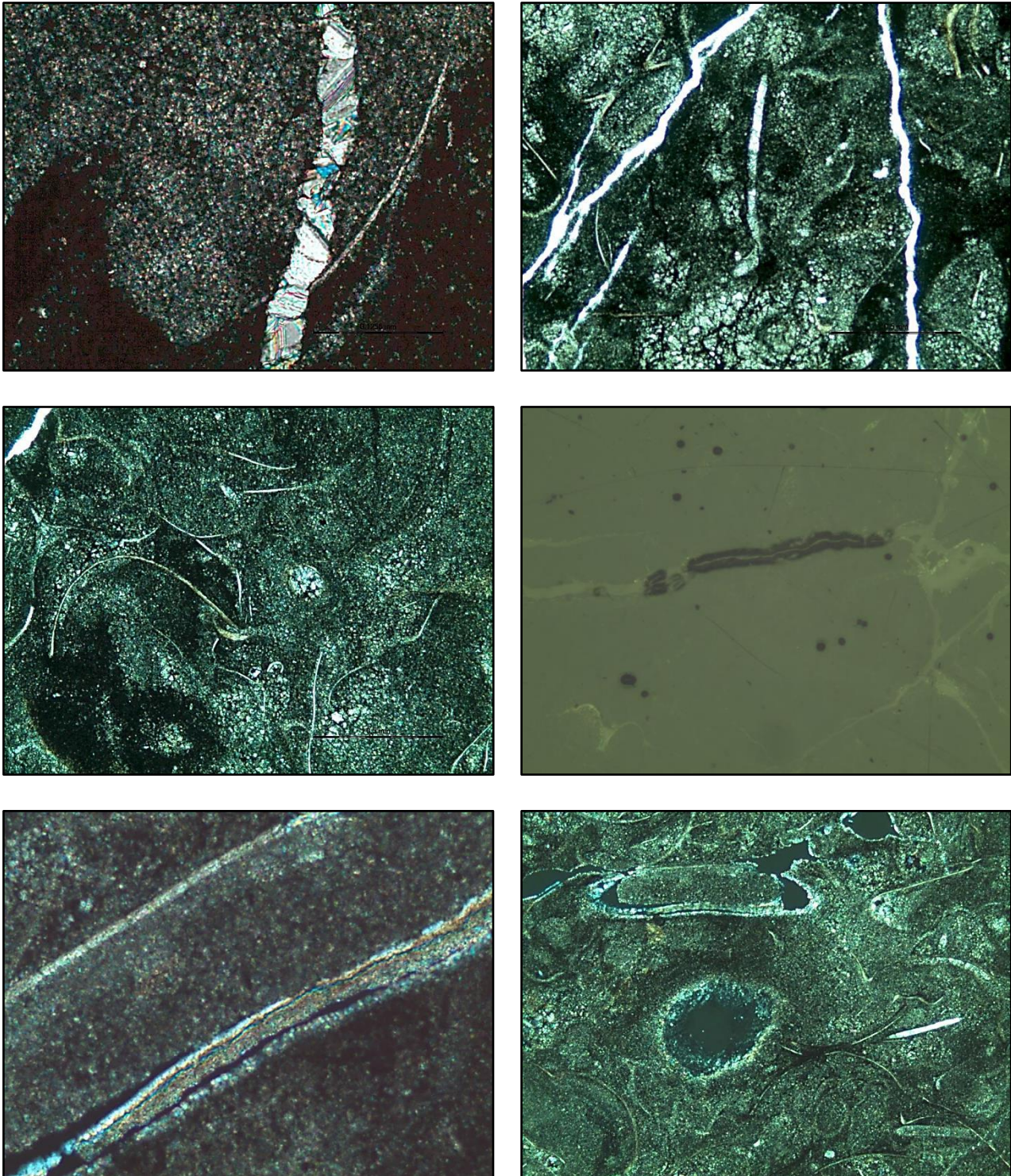


Figure 6-16: Microscope images of alum shale. A) Cross polarized light; a relatively large calcite vein with distinct twinning and quartz minerals. B) Cross polarized light; calcite veins. C) Cross polarized light; organic matter and calcite veins with coating. D) Plane polarized light; pale brownish matrix consisting of calcite veins with mineral coating and small spherulite minerals. E) Cross polarized light; close-up of a gypsum mineral. F) Cross polarized light; calcite minerals, organic material and gypsum mineral.



## Greenschist:

Figure 6-17 shows the thin section image and figures 6-18 A-F show microscope images of the greenschist. The greenschist have moderately sorting of the minerals and a heterogeneous mineral composition. The matrix is mainly green and dominated by colourless and green minerals such as albite (feldspar-group), chlorite and epidote, see table 6-4. The greenschist has an unoriented mineral arrangement and the minerals vary in size and shape.



Figure 6-17: Thin section image of greenschist.

White to grey albite minerals, tectosilicates, show both single twinning and cross-hatched twinning with pink, blue and green colours in plane polarized light. The tabular and elongated shaped albite minerals show pleochroism and have high relief and cleavage, figure 6-18 B. In cross polarized light the albite minerals show undulatory extinction in white to grey colours.

Flaky chlorite minerals, phyllosilicates, are colourless to brownish-green and have pleochroism. The minerals show dark green to black undulatory extinction colours and a greenish grey interference colour in cross polarized light.

Epidote minerals, sorosilicates, show high relief with sharp boundaries and a yellowish green colour in plane polarized light. High order interference colours like sharp pink and blue are seen in cross polarized light and the epidote minerals have a prismatic shape with distinct stripes and show pleochroism.

A small amount of brownish-green hornblende (amphibole-group) minerals, double chain inosilicates, with low relief are found in the thin section. The angular shaped hornblende minerals show a bluish-turquoise interference colour in cross polarized light.



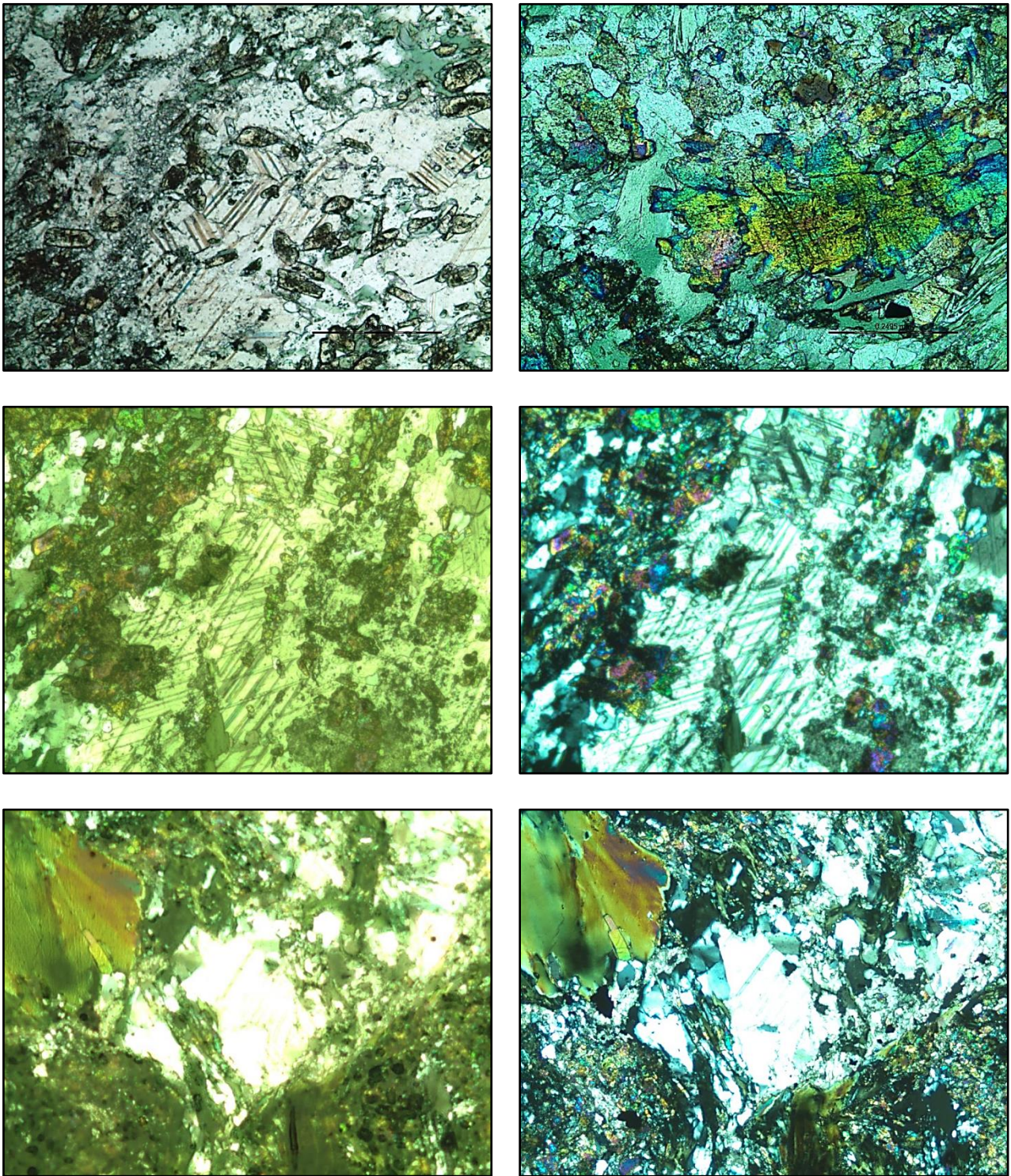


Figure 6-18: Microscope images of the greenschist. A) Plane polarized light; colourless albite with twinning, brown elongated chlorite minerals and colourless epidote minerals. B) Cross polarized light; green chlorite matrix with high interference coloured epidote and hornblende minerals and some small phlogopite minerals, lower right. C) Plane polarized light; albite minerals with twinning. D) Cross polarized light; albite minerals with twinning and high interference order colours of epidote minerals. E) Plane polarized light; brownish-green phlogopite mineral, yellowish-green epidote minerals, albite mineral with twinning and greenish-brown hornblende minerals. F) Cross polarized light; high interference coloured phlogopite mineral, albite minerals and hornblende minerals.

Figure 6-18 A shows colourless albite minerals with twinning, brown elongated chlorite minerals and colourless epidote minerals. In figure 6-18 B, in addition to the mentioned albite minerals above, some brown and elongated chlorite minerals are shown. The microscope images in figure 6-18 C and D are in cross polarized light and show high order interference colours of the epidote minerals and the hornblende minerals

In figure 6-18 B, cross polarized light, a green chlorite matrix with high interference coloured epidote and hornblende minerals are shown. Also seen are some small phlogopite minerals.

Figure 6-18 C and D show albite minerals with twinning, greenish-brown in plane polarized light and grey in cross polarized light. Also seen are high interference order colours of epidote minerals.

In figure 6-18 E and F a relatively large phlogopite minerals is seen, yellowish-brown in plane polarized light and with high interference colours in cross polarized light. Also seen are green epidote minerals, albite minerals with twinning, in figure E, and high interference coloured hornblende minerals, in figure F.



## Tuff:

Figure 6-19 shows an image of the thin section and figure 6-20 A-F show microscope images of the tuff. The tuff shows a poorly sorted and heterogeneous mineral composition and the reddish-brown microcrystalline matrix is dominated by well crystallized colourless, white, brown and reddish-brown rock fragments and irregular shaped volcanic glass. The mineral arrangement for the tuff is classified as slightly oriented and the minerals are of varying shape and size, showing a range from very fine grained to grain diameters up to 5-6 mm. This range in mineral size and percentage, from ash-size (< 2mm) to lapilli-size (2-64 mm) classifies the tuff as lapilli-tuff, see figure D-4, Appendix D.

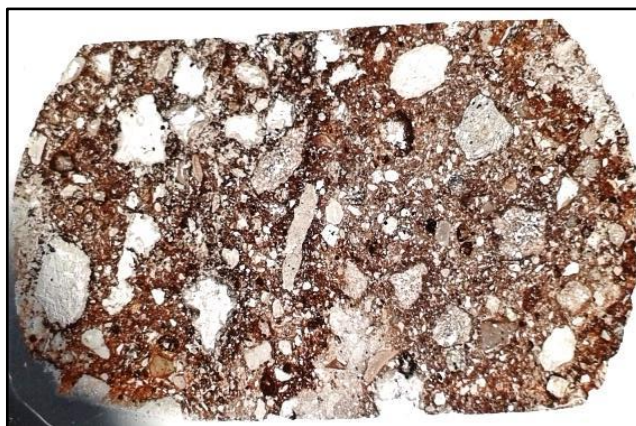


Figure 6-19: Thin section image of the tuff.

Phenocrystals of clear to white euhedral quartz, tectosilicates, with low relief were found in the thin section. The angular shaped crystals show no cleavage. Flaky and angular chlorite minerals, phyllosilicates, are colourless to brown and show pleochroism. The minerals show dark green to black undulatory extinction colours and a greenish grey interference colour in cross polarized light.

A number of relatively large zeolites, wairakite and laumontite, were found in the thin section. Subhedral and massive wairakite crystals, tectosilicates, are showing a dull white to brownish-grey colour and nearly opaque appearance in plane polarized light. The minerals show high relief and no pleochroism. A greyish-black colour is shown in cross polarized light and no undulatory extinction.

The white to light brown and opaque kaolinite minerals, phyllosilicates, have a pearly speckled appearance and show a moderate relief with aggregated plates of minerals.

Reddish-brown to metallic grey, plan polarized light, hematite minerals are opaque, have a platy shape and show no cleavage or pleochroism. The greyish hematite minerals show distinct lamellar twinning, figure 6-20 and have an earthy appearance. In cross polarized light the hematite minerals appear black and shown no undulatory extinction.

The volcanic glass is a fine grained and amorph material formed by rapid cooling of lava. The light brown glass fragments are elongated and irregular shaped, figure 6-20 B.

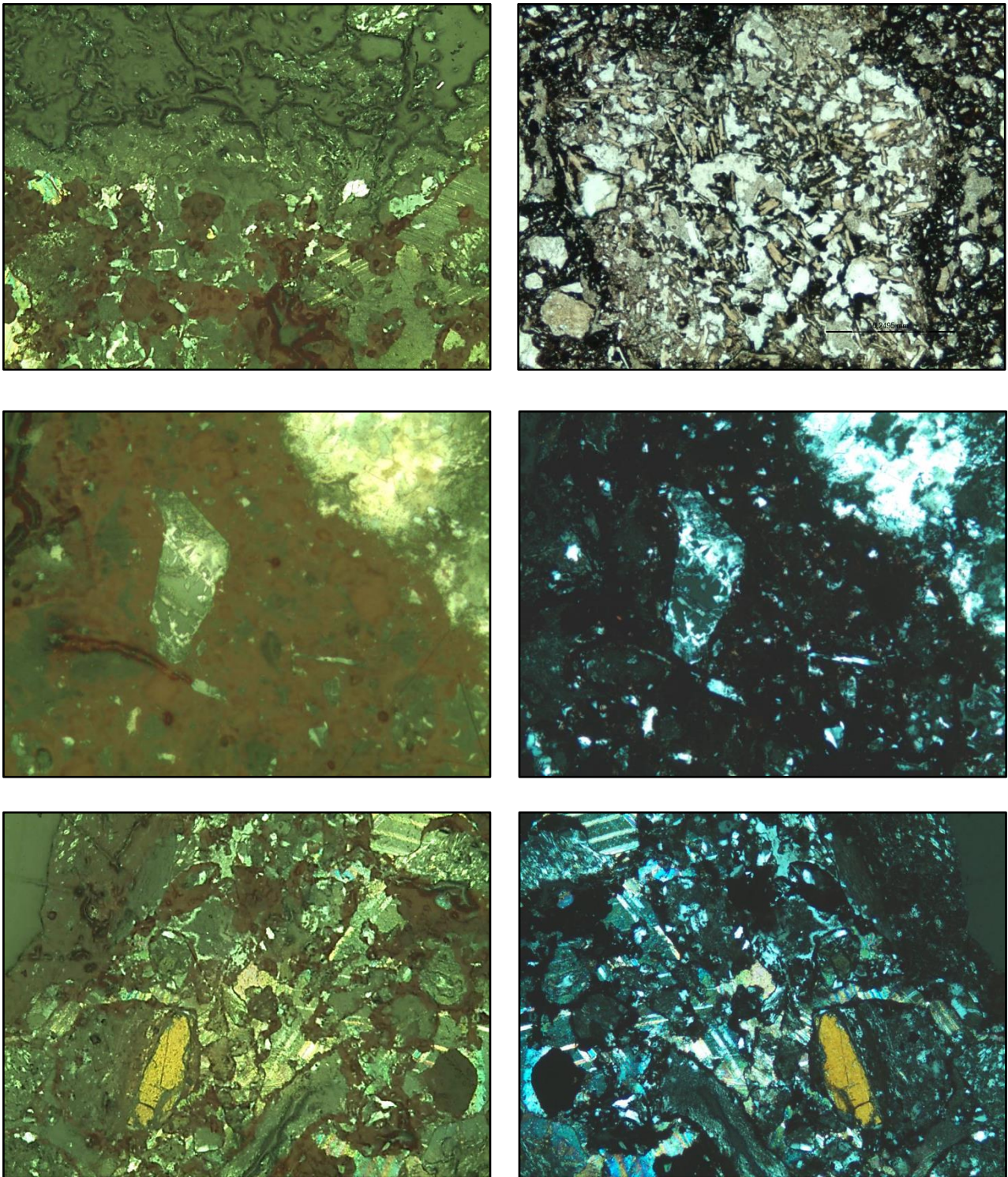


Figure 6-20: Microscope images of the tuff. A) Plane polarized light; a light brown wairakite mineral with black edge around the mineral, upper left, albite minerals with twinning, middle and brownish-red hematite, lower left. B) Cross polarized light; calcite mineral containing volcanic elongated glass fragments and black hematite minerals. C) Plane polarized light; an angular laumontite mineral (zeolite) surrounded by brownish-red hematite minerals and a yellowish-white kaolinite mineral, upper right. D) Cross polarized light; an angular laumontite mineral (zeolite) surrounded by black hematite minerals and a white kaolinite minerals, upper right. E) Plane polarized light; brownish-red hematite minerals, a yellowish pyroxene mineral, lower left, and greyish striped feldspar minerals, upper right. F) Cross polarized light; black hematite minerals, a yellowish pyroxene mineral, lower left and striped feldspar minerals, upper right.



Figure 6-20 A shows a light brown wairakite mineral with black edges, brownish-grey albite minerals with twinning and brownish-red hematite minerals. The microscope image is seen in plane polarized light.

In figure 6-20 B a calcite mineral containing elongated and irregular shaped volcanic glass fragments is shown. Also seen are black hematite minerals, greyish quartz minerals and smaller hematite minerals, cross polarized light.

Figure 6-20 C and D, respectively plane and cross polarized light, an angular laumontite minerals surrounded by hematite minerals is seen. The hematite minerals are brownish-red in plane polarized light and appear black in cross polarized light. Also seen is a kaolinite mineral is seen, the colour ranges from yellowish-white to white depending of the polarized light.

Presented in figure 6-20 E and F is brownish-red to black, respectively plane and cross polarized light, hematite minerals, a yellowish pyroxene mineral and greyish striped feldspar minerals.

## 6.3 Rock mechanical testing

### 6.3.1 Point load strength – rock pieces

The point load strength index is calculated from the formula:

$$I_s = \frac{P}{D_e^2}, \quad D_e = \frac{4A}{\pi}$$

where P is the measured load at failure (kN),  $D_e$  is the equivalent sample diameter (mm) and A is the minimum cross sectional area between the two contact points (NBG, 2000).

The point load index is computed using Microsoft Excel spreadsheets, Appendix E, figures E-3 to E-6. In figure 6- 18 the point load strength chart for the three samples is shown.

Using the same spreadsheets, the uniaxial compressive strength and the tensile strength can be calculated. The formulas are (NBG, 2000):

$$\text{Uniaxial compressive strength } \sigma_c = k_{50} \cdot I_{s\ 50}$$

$$\text{Uniaxial tensile strength } \sigma_t = I_{s\ 50} \cdot 0.8$$

where the factor k increases with the rock strength

Determination of the  $I_{s50}$  assumes standard 50 mm samples. In cases where the samples differ from the standard, like here, an adjustment of the  $I_{s50}$  is done;

$$I_{s\ 50} = F \cdot I_s, \quad F = \left(\frac{D_e}{50}\right)^{0.45}$$

In figure 6-18 the point load strength for the alum shale, the green schist and the tuff is plotted.

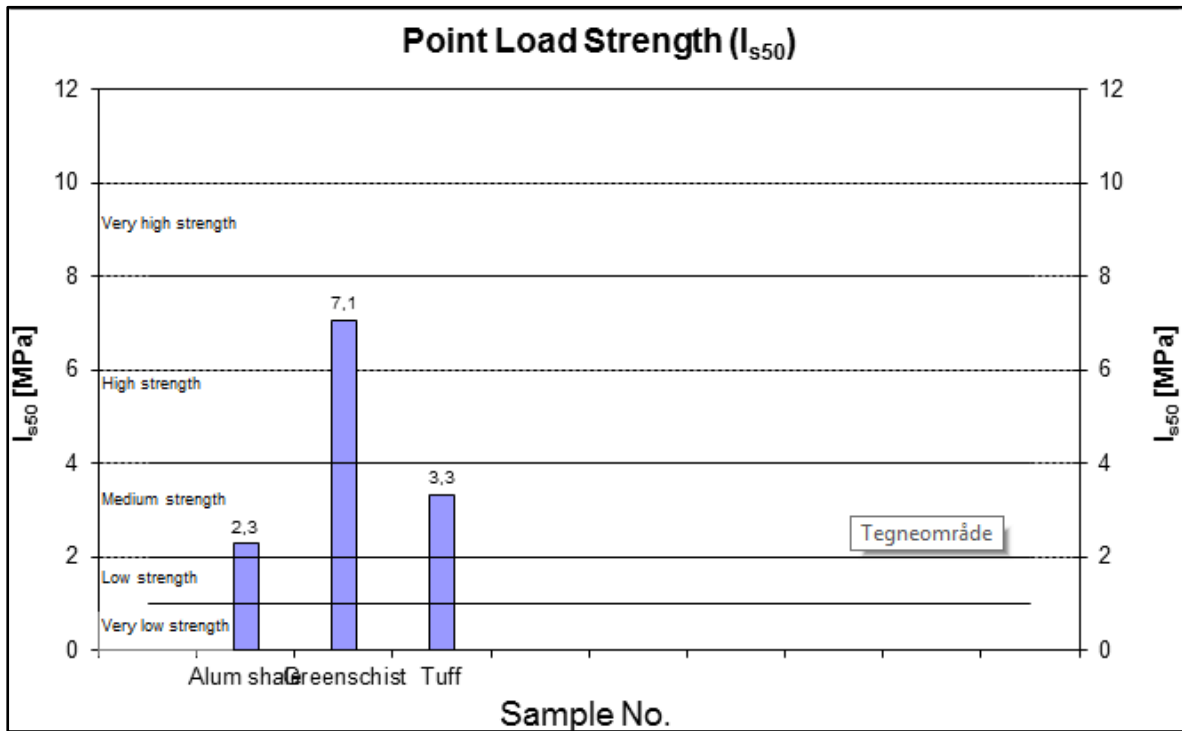


Figure 6-18: Point load strength chart for the alum shale, the greenschist and the tuff.

Table 6-5 gives the calculated mean values for the point load strength, the uniaxial compressive strength and tensile strength.

Table 6-5: Calculated mean values for the point load strength, uniaxial compressive strength and the tensile strength.

Sample	$I_s$ [MPa]	$I_{s50}$ [MPa]	$\sigma_c$ [MPa]	$\sigma_t$ [MPa]
Alum shale	2,9	2,3	31,7	1,8
Greenschist	8,0	7,1	141,1	5,6
Tuff	4,3	3,3	46,4	2,7

From the chart in figure 6-18 and according to table E-1 (Appendix E) the alum shale and tuff is classified with medium point load strength, and the greenschist with high point load strength, table 6-5.

The suggested value of the factor  $k$  in table E-2 (Appendix E) presupposes a uniaxial compressive strength greater than 25 MPa and a point load strength index greater than 1.8 MPa and that is the case for all three rock samples. The suggested value of  $k_{50}$  is 14 for the alum shale and tuff and 20 for the greenschist.

### 6.3.2 Slake-durability index – rock pieces

The slake-durability index is calculated from the formula:

$$I_{d2} = \frac{C - D}{A - D} \times 100\%$$

where A-D is the initial sample mass and C-D is the final sample mass, see section 5.1.3.

Figure 6-19 to 6-21 show the test material before testing, left, the appearance of fragments retained in the drum after testing, middle, and the material which has passed through the drum, right.



Figure 6-19: Photo of the material before testing, left, retained alum shale fragments after the testing, centre and material which has passed through the drum, right.

Figure 6-19, middle, shows the alum shale after slaking and there has been some fragmenting of the initial sample material. The material which has passed the drum, right, is greatest for the alum shale.



Figure 6-20: Photo of the retained green schist fragments after the testing, left and material which has passed through the drum, right.

In figure 6-20 the greenschist after slaking is shown, middle and right. A small amount of the initial rock material is fragmented and the corners are slightly rounded.





Figure 6-21: Photo of the retained tuff fragments after the testing, left and material which has passed through the drum, right.

Figure 6-12 presents the tuff after slaking, middle and right. Minor fragmenting of the initial material is seen and the material is slightly rounded. The amount of material that has passed the drum is minimal.

The percentage ratio of final to initial dry sample masses is determined, figure 6-22.

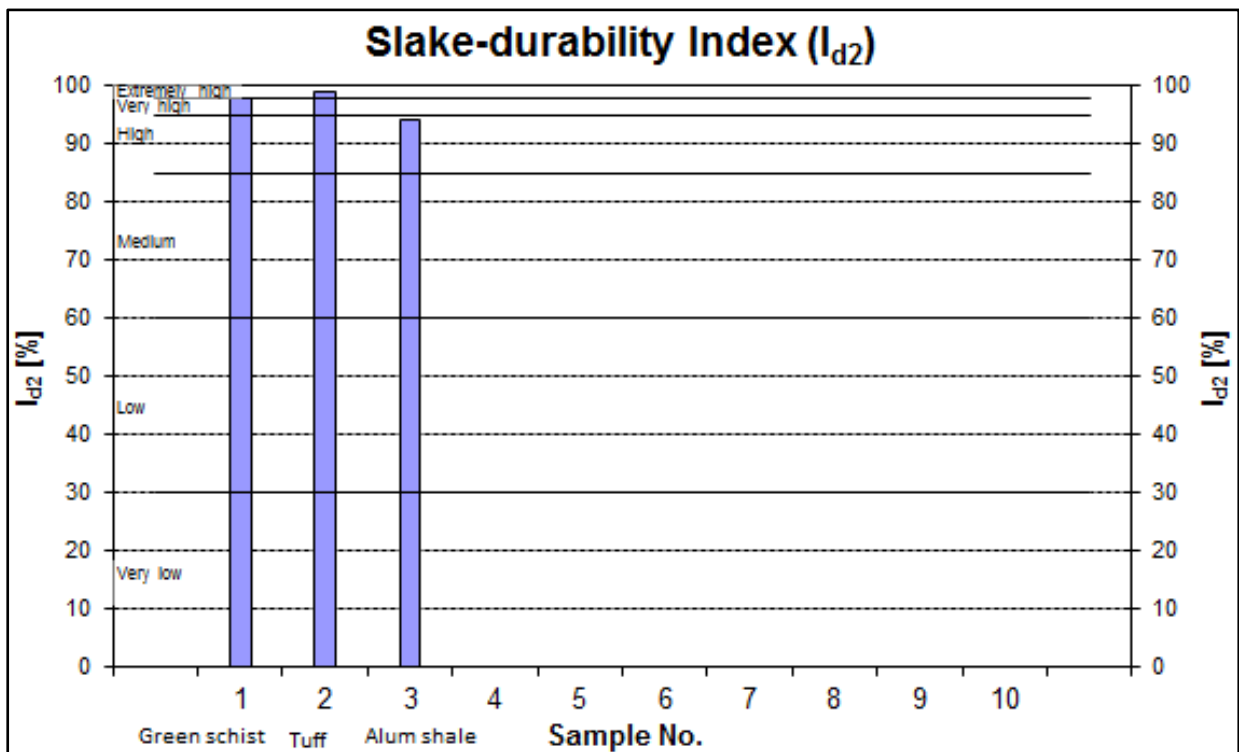


Figure 6-22: Calculated slake durability index for the three rock samples using the excel spreadsheets in Appendix F, figure F-1.

A classification of the slake durability index is done, table 6-6 (ISRM, 1977).

Table 6-6: Results from the slake-durability testing and a classification of the slake-durability index based on Appendix F, table F-1.

Sample	I <sub>d1</sub> [%]	I <sub>d2</sub> [%]	Classification
Alum shale	96,0	94,3	High
Greenschist	98,8	98,1	Very high
Tuff	99,4	99,0	Very high

The slake-durability index for the alum shale is determined to be 94.3 and thus classified as high according to table F-1 (Appendix F). This implies a high resistance to repeated weakening and disintegration cycles. The material retained in the drum after testing shows minor fragmentation which agrees well with the calculated slake-durability index for the alum shale.

The slake durability index for the greenschist and the tuff is respectively 98.1 and 99.0 and thus classified as very high according to table F-1 (Appendix F). A very high slake-durability index implies a very high resistance to the repeated weakening and disintegration cycles and the index values correspond well to the extent of fragmentation of the rock material.

In figure 6-20 and 6-21 the green schist and the tuff is shown and the rock sample with the highest slake-durability index, the tuff, has the lowest fragmentation of the material.

### 6.3.3 Density – irregular rock pieces

The density is calculated from the formula:

$$\rho = \frac{W_s \cdot \rho_w}{W_s - W_1 + W_2}$$

where  $W_s$  is weight of rock sample,  $W_1$  is weight of pycnometer, water and sample,  $W_2$  is weight of pycnometer and water and  $\rho_w$  is the specific weight of water;  $1\text{g/m}^3$  (Nilsen and Broch, 2009).

Table 6-7 gives the calculated density for each of the three rock samples.

Table 6-7: Density of the tested rock samples.

Sample	Density [ $\text{g/m}^3$ ]
Alum shale	2,59
Greenschist	2,86
Tuff	2,62

Calculated density for the alum shale is  $2.59\text{ g/m}^3$ , for the greenschist  $2.86\text{ g/m}^3$  and for the tuff  $2.62\text{ g/m}^3$ . All three values correspond to the values given in table G-1 (Appendix G).

## 7 Evaluations and comparisons

Finding correlations between the results of the various test methods is essential to better understand the swelling mechanisms that can cause instabilities in tunnels, slopes and foundations.

Sections 7.1 gives an evaluation of the test results for the mechanical properties and the swelling characteristics of the tested rocks are presented in section 7.2. The mechanical properties of the tested rocks are compared with competent crystalline rocks, section 7.1.2., and the comparisons in relation to the different sample material and comparison with swelling clay, are discussed in section 7.2.2 and 7.2.3. Finally, the applicability of the two test methods for rock cylinders and rock cubes are discussed and compared, section 7.3.

### 7.1 Mechanical properties of the tested rocks

The test results for the mechanical properties are given in section 6.3. Table 7-1 gives a compilation of the results from the performed rock mechanical test methods and a classification of point load strength and slake-durability index.

#### 7.1.1 Evaluation of the test results

In table 7-1 the values for point load strength, compressive strength, tensile strength, slake-durability index and density are given. Included are also classifications of the point load strength and slake durability index of the rocks.

Table 7-1: Compilation of rock mechanical test results for point load strength, slake-durability index and density.

Rock type	Test method							Density [g/m <sup>3</sup> ]
	Point load strength [MPa]			Compressive strength [MPa]	Tensile strength [MPa]	Slake-durability index [%]		
	I <sub>s</sub>	I <sub>s50</sub>	Classification	σ <sub>c</sub>	σ <sub>t</sub>	I <sub>d2</sub>	Classification	
Alum shale	2,9	2,3	Medium	31,7	1,8	94,3	High	2,59
Green schist	8,0	7,1	High	142,1	5,6	98,1	Very high	2,86
Tuff	4,3	3,3	Medium	46,4	2,7	99,0	Very high	2,65

The greenschist shows the highest values for point load strength, compressive strength and tensile strength. These values correspond well to the slake-durability value. For the greenschist the slake durability value is determined 98.1 % which is classified as very high resistance to repeated cycles of wetting and drying, section 5.1.3. Compared to the density value the greenschist is classified as a very strong rock due to the high values for strength and durability, table G-2 in Appendix G.

A classification of the alum shale and tuff as medium rocks, Appendix G, is due to the medium strength values although the density values are low. The tuff has a slightly higher density value than the alum shale and show the highest slake-durability value of all three samples.

Values given in table 7-1 show a good correlation between the various test methods regarding rock mass strength and properties regardless of any deviations found. Increasing rock mass strength indicates high values for both slake-durability and density.

### **7.1.2 Comparisons with competent crystalline rocks**

As shown in table 7-1 the values for point load strength varies for the different rocks. The alum shale and the tuff are classified with medium point load strength and the greenschist with high point load strength. These values are compared to determined values for point load for some Norwegian schistose rocks (NBG, 2000).

The black shale (Slemmestad) has a value of 8.8 MN/m<sup>2</sup> (MPa), the gneiss (Fosen) a value of 7.8 MN/m<sup>2</sup> (MPa) and the mica schist (Tydalen) a value of 2,0 MN/m<sup>2</sup> (MPa). The point load value for the alum shale corresponds well to the value for the mica schist due to good cleavage properties for both rocks. There is a deviation between the point load values for the alum shale and the black shale which could be explained due to different localities of the shales. The point load value for the greenschist corresponds to the value listed for the gneiss which agrees well with regard to the structure of the rocks.

The uniaxial compressive strength values listed in table 7-1 are ranging from 31.7 MPa for the alum shale to 142.1 MPa for the greenschist with a suggested value of  $k = 14$  and 20, table E-2 (Appendix E). Comparing these values to the listed values for some typical rocks (NBG, 2000) a great deviation between the values are seen.

The greenschist shows a value of 93 MPa, which is considerably lower than for the tested greenschist listed in table 7-1. Other rocks to be mentioned are greenstone, quartzite and granite with the values 105 MPa, 172 MPa and 169 MPa which correlate well to the strong and hard rocks. The alum shale, with the lowest values for compressive strength in table 7-1, correlates to the clay schist/ clay stone with a compressive value of 40 MPa. The similarities between the latter and the alum shale in both formation and structure emphasise a reliable value of the determined compressive strength given in table 7-1.

Determination of the slake-durability index for tested volcanic rocks shows a range from 25.7 to 99.5 % remaining material > 2 mm after two drying and wetting cycles (Dahl et.al, 2013). The index values for the tested rocks in table 7-1 are classified as high to very high and are thus in the upper range of the listed values for the volcanic rocks. The slaking-durability for some sedimentary rocks (Panthi, 2006) is given in figure 7-1.

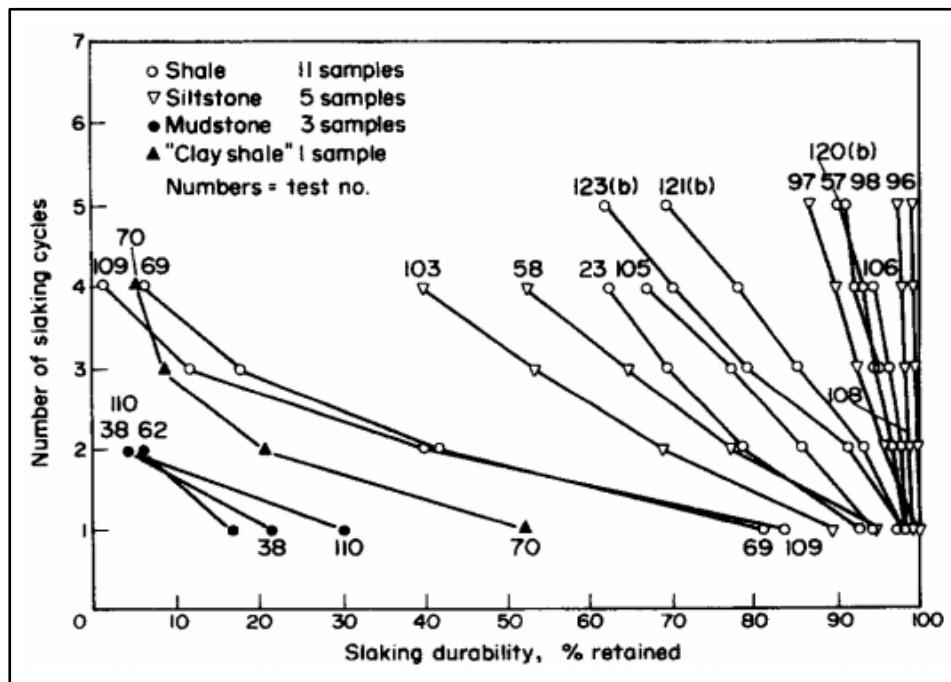


Figure 7-1: Influence of the number of slaking cycles on slake-durability (Panthi, 2006).

Influence of the number of slaking cycles on slake durability is shown in figure 7-1. There is a correlation between the number of slaking cycles and the slake-durability of the sedimentary rocks. An increasing number of slaking cycles indicates a decrease in the resistance against weakening and disintegration caused by repeated drying and wetting cycles.

Figure 7-2 presents slake-durability versus cycle of drying and wetting (Panthi, 2006).

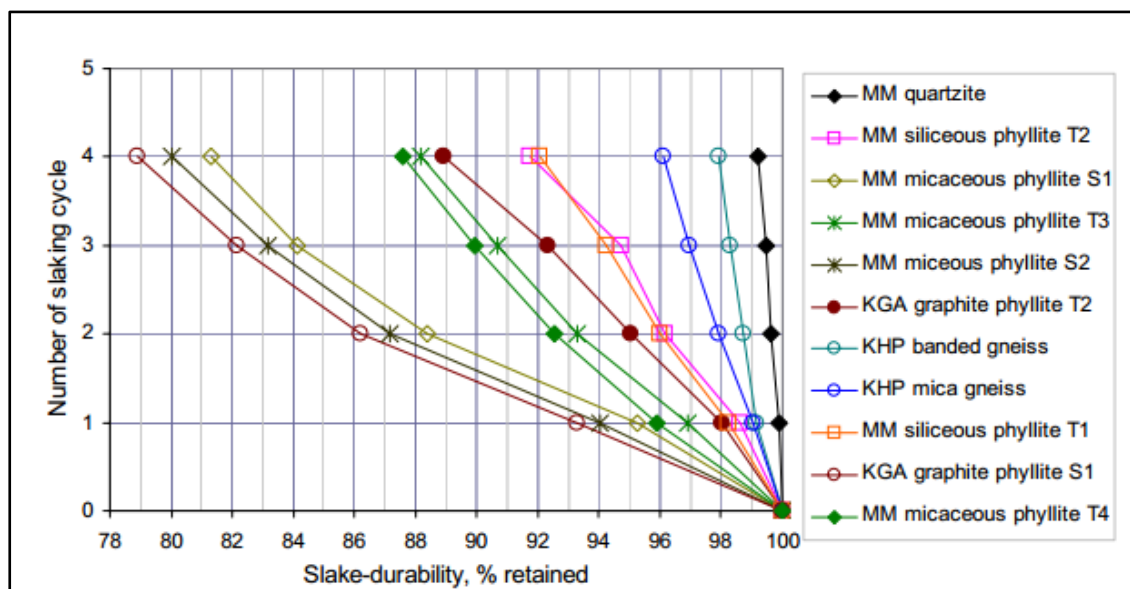


Figure 7-2: Slake-durability versus cycle of drying and wetting (Panthi, 2006).

Slake-durability is influenced by the number of slaking cycles as shown in figure 7-2. The rock mass diminishes with repeated cycles of drying and wetting and this is indicated by decreasing percentage of retained material.

Calculated values for rock density in table 7-1 are compared to the values given in table G-1 (Appendix G). The alum shale has a density lower than granite and quartzite;  $2.65 \text{ g/cm}^3$ , and the tuff has the same density as the given rocks. Granite and quartzite are hard and massive rocks with no distinct mineral structure and medium to coarse grained. It was expected to place the density value for the alum shale below the value for the granite and quartzite due to the mineral arrangement and hardness of the rocks. The anticipated density value for the tuff was higher than the one determined, which is quite surprisingly as it was believed that the tuff has greater porosity than the value implies. The greenschist has a density value slightly higher than the value listed for greenstone and these values correspond well considering the hardness and the mineral structure within the rock types.

## 7.2 Swelling characteristics of the tested rocks

The test results for the swelling characteristics are given in section 6.1. Table 7-2 gives a compilation of the results from the performed swelling test methods and classifications of the swelling pressure for both dust powder and rock cylinders are included. A classification of the free swelling and swelling strain for rock cubes are also given. Correlations between the various test methods are given figure 7-3 to 7-8.

### 7.2.1 Evaluation of the test results

In table 7-2 the values for swelling pressure, free swelling and swelling strain are given. Also included is the classification of swelling pressure and free swelling of the rocks.

Table 7-2: Compilation of the swelling test results for dust powder, rock cylinder and rock cube.

Rock type	Test method								
	Swelling pressure Dust powder		Free swelling Dust powder		Swelling pressure Rock cylinder		Swelling strain Rock cube		
	MPa	Classification	%	Classification	MPa	Classification	Direction	[%]	[mm]
Alum shale	0,03	Low	130	Moderate	0,00	Inactive	x	0,125	0,0602
							y	0,055	0,0241
							z	0,060	0,0295
Greenschist	0,02	Low	100	Moderate	0,01	Low	x	0,008	0,0035
							y	0,006	0,0026
							z	0,048	0,0209
Tuff	0,21	Moderate	135	Moderate	0,00	Inactive	x	0,165	0,0826
							y	0,145	0,0770
							z	0,220	0,1122

The alum shale shows higher values for swelling pressure performed on dust powder and free swelling compared to the greenschist, but is classified as inactive according to the value for swelling pressure performed on rock cylinder. Measured swelling strain on the rock cube, is greatest for the alum shale compared to the greenschist. Compared to results from tests performed on alum shale in Oslo, with swelling pressure values ranging from 0.00 to 1.00 MPa (Dahl et.al, 2013) the value for swelling pressure on rock disc in table 7-2 is placed in the bottom of the range. The measured value is low but reliable when compared to the values for the alum shale in Oslo.

The greenschist is classified with an inactive swelling pressure on rock cylinder and show higher swelling strain on the rock cube compared to the alum shale and lower value compared to the tuff. Compared to tests performed on greenstone and phyllite in 2012 with values ranging from 0.01 to 0.03 MPa for the greenstone and < 0.01 MPa for the phyllite (Dahl et.al, 2013) the value for swelling pressure in table 7-2 lies within the listed range.

The tuff shows the highest values for swelling pressure on the dust powder, free swelling and swelling strain on rock cube. Measured value for swelling pressure on rock cylinder is classified as inactive. Recorded swelling pressures for dust powder from red tuff, South America, ranges from 0.15 to 1.12 MPa and this value correlates well to the measured value for the tuff in table 7-2.

### 7.2.2 Comparison in relation with dust powder, rock cylinders and rock cubes

In the following correlations and comparisons of the various swelling test methods are given. Also included is the correlation between free swelling and the various test methods.

Figure 7-3 shows the correlation between measured swelling pressure for dust powder and free swelling.

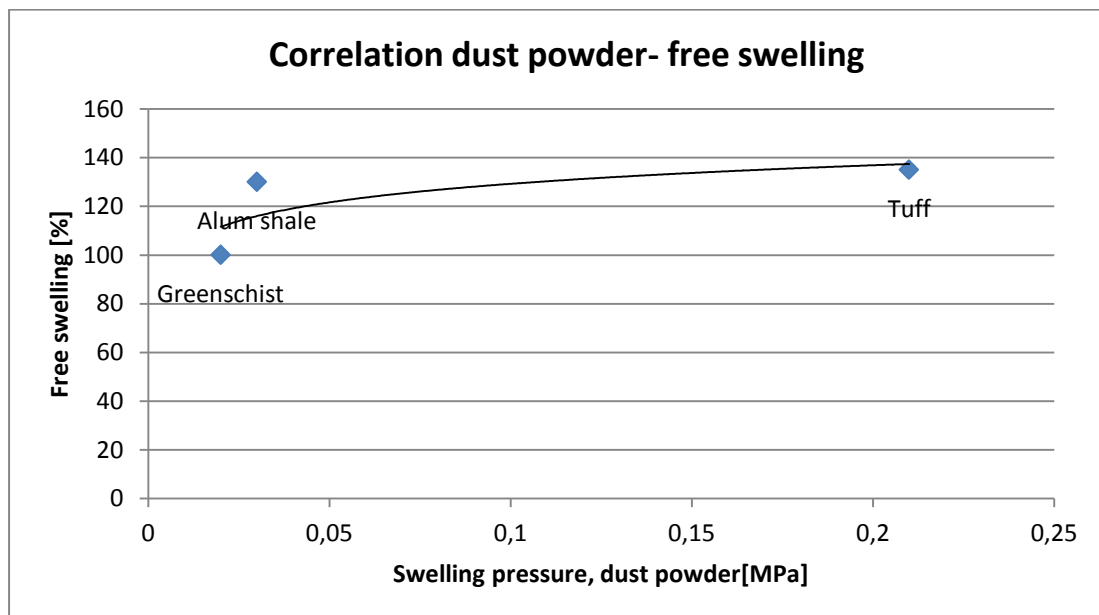


Figure 7-3: Correlation between swelling pressure for dust powder and free swelling.

For these specific rock samples an increase in the swelling pressure indicates an increase in the free swelling value and it is possible to make a correlation between the test methods. Since there have been performed tests on only three rock samples with no duplicates, more testing have to be carried out to get a trustworthy correlation and to specify a conversion factor (Dahl et.al, 2013) between the test methods.

In figure 7-4 the correlation between measured swelling pressure of dust powder and rock cylinders is given.

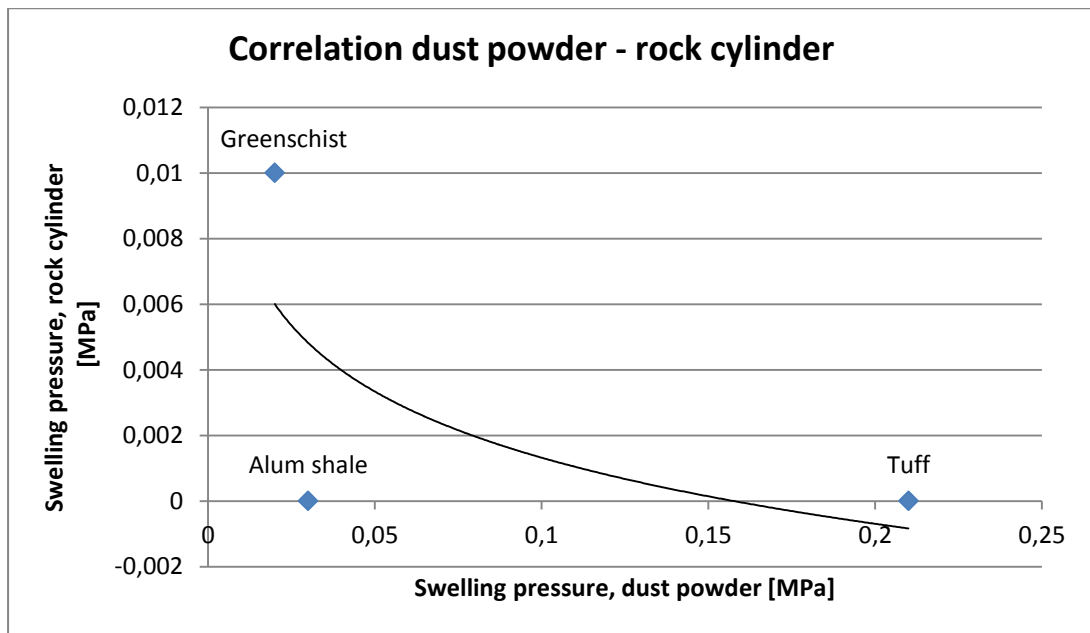


Figure 7-4: Correlation between swelling pressure for dust powder and swelling pressure for rock cylinder.

For the alum shale there is a nearly good correlation between the two values, with low swelling pressure for both dust powder and rock cylinder which are classified as low and inactive. The greenschist shows an even better correlation between the two values which are classified as low. The measured values for the tuff differs somewhat, making it difficult to draw any correlations between swelling pressure for dust powder and free swelling.



Figure 7-5 shows the correlation between measured swelling pressure for dust powder and swelling strain for rock cubes in three directions.

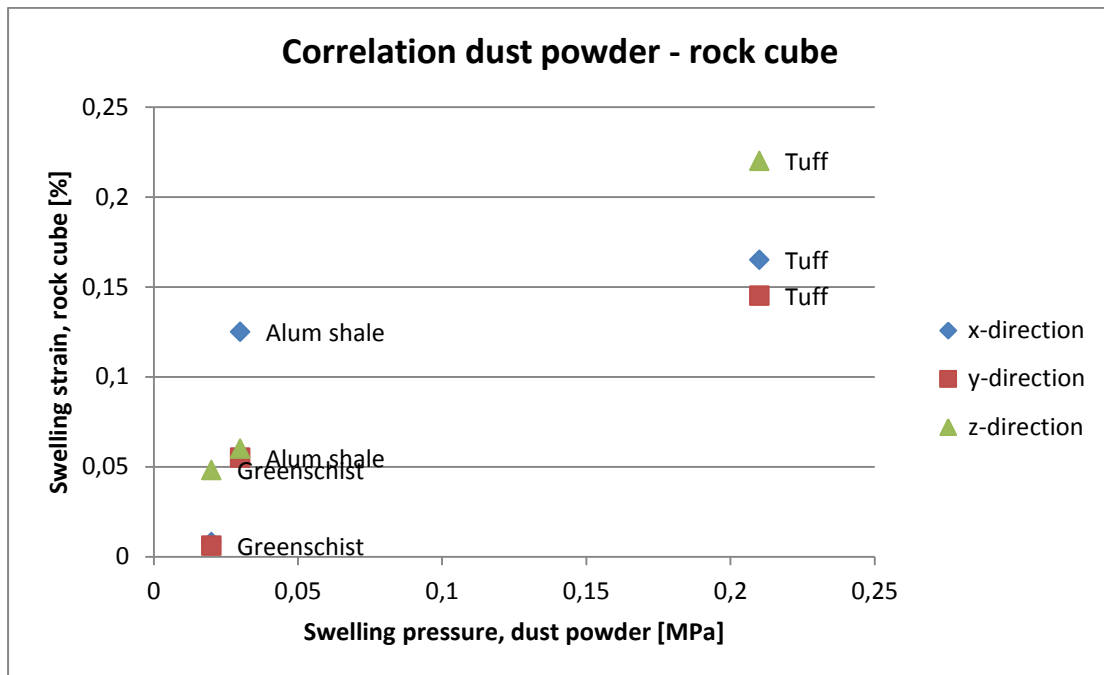


Figure 7-5: Correlation between swelling pressure for dust powder and swelling strain for rock cube.

For the alum shale there is a good correlation between the low classified swelling pressure and the swelling strain, and the highest expansion is in the x-direction. The greenschist shows the lowest values for both swelling pressure, classified as low, and the swelling strain. The measured expansion is slightly higher in the z-direction compared to the x- and y-direction. A good correlation between the two test methods for the tuff is found, due to the values for both swelling pressure and swelling strain. The tuff shows the greatest expansion of all three rock samples and the highest expansion is in the z-direction. A correlation between the swelling pressure for dust powder and swelling strain for rock cube are seen, the higher the swelling pressure the higher the swelling strain.

In figure 7-6 the correlation between measured swelling pressure for rock cylinders and swelling strain for rock cubes in three directions is given. A deviation in the values for swelling pressure and swelling strain for the alum shale is found.

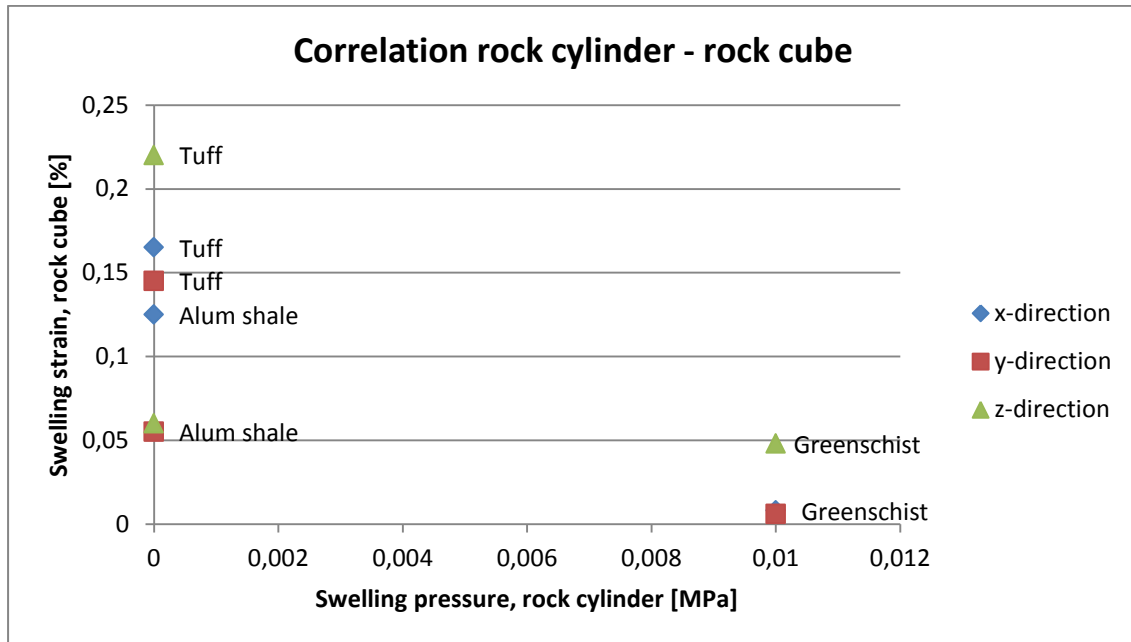


Figure 7-6: Correlation between swelling pressure for rock disc and swelling strain for rock cube.

The swelling pressure is, as mentioned previously, classified as inactive even though expansion in all three directions has been measured. The greenschist shows low values for both measurements in contrast to the tuff which show significant swelling strain in all three directions and no swelling pressure for the rock cylinder. Deviations in the values for the tests imply difficulties in finding correlation between the methods; nevertheless the determination of swelling strain for rock cubes is a very good indication on the swelling characteristic of intact rocks. The determination of swelling pressure and swelling strain appear thus as two independent test methods.

Figure 7-7 shows the correlation between swelling pressure for rock cylinders and free swelling.

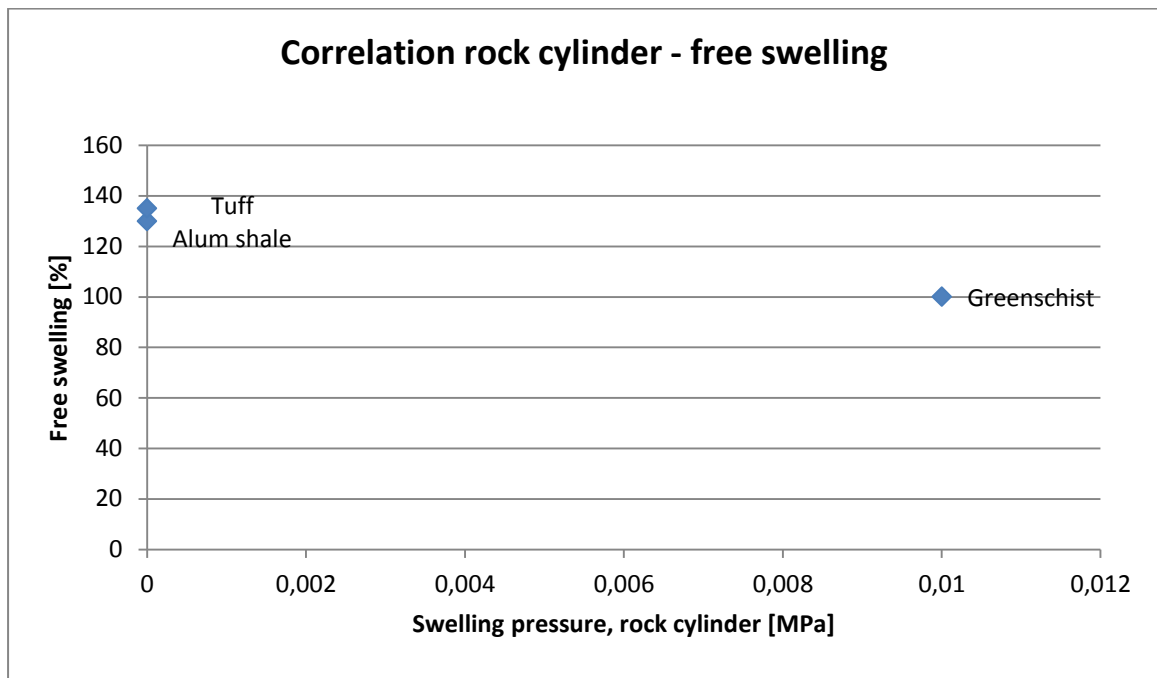


Figure 7-7: Correlation between swelling pressure for rock cylinder and free swelling.

The alum shale and tuff show moderate free swelling and no swelling pressure. The greenschist show low swelling pressure and close to within a moderate free swelling. No specific correlations between the test methods are found other than the possibility to obtain good values for free swelling regardless of the swelling pressure values.

In figure 7-8 the correlation between free swelling and swelling strain for rock cubes are shown.

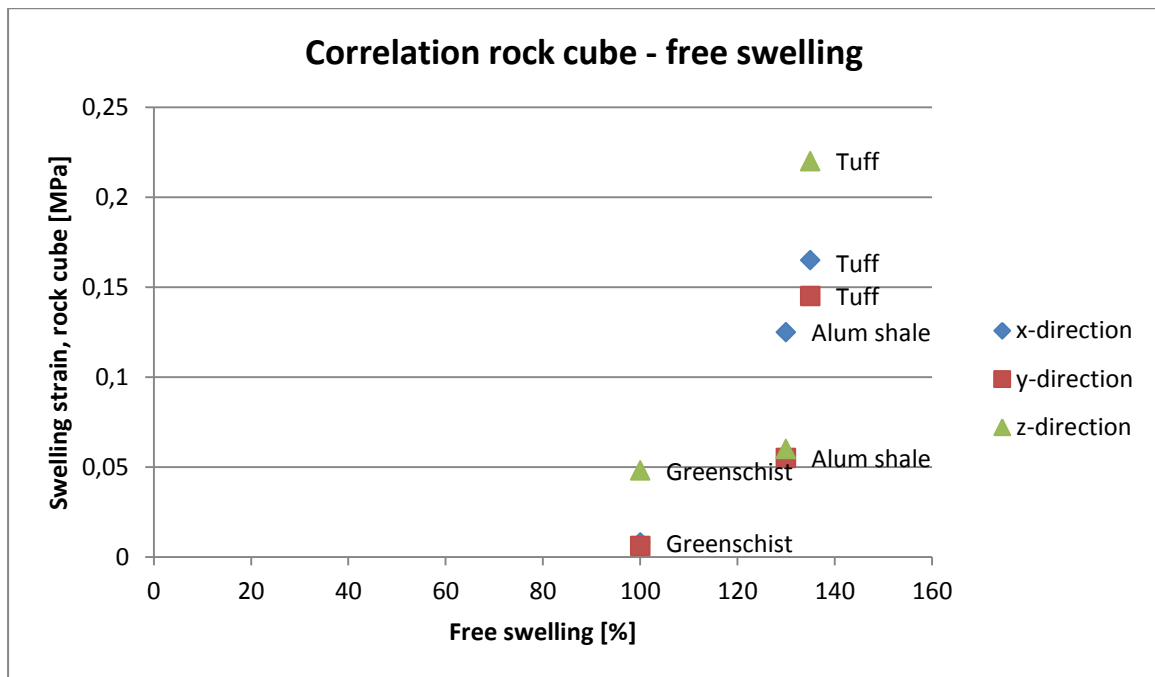


Figure 7-8: Correlation between swelling strain for rock cube and free swelling.

All three rock samples show moderate free swelling and various expansions in x-, y- and z-direction. There is an evident correlation between the two test methods; an increase in the free swelling indicates an increase in the swelling strain.

### 7.2.3 Comparison with swelling clays

In comparison with swelling clays the test methods discussed are free swelling and swelling pressure. Determination of swelling pressure and free swelling for swelling clays involves the preparation of fine material < 20 µm and the method is quite similar to one described in section 4.2.1; swelling pressure of bulk material. The performance of the test methods are the same as for bulk material, section 5.1.

Figure 7-9 presents the number of samples in each category of swelling pressure tested at the NTNU/SINTEF laboratory (Mao et.al, 2011; based on NBG, 1985).

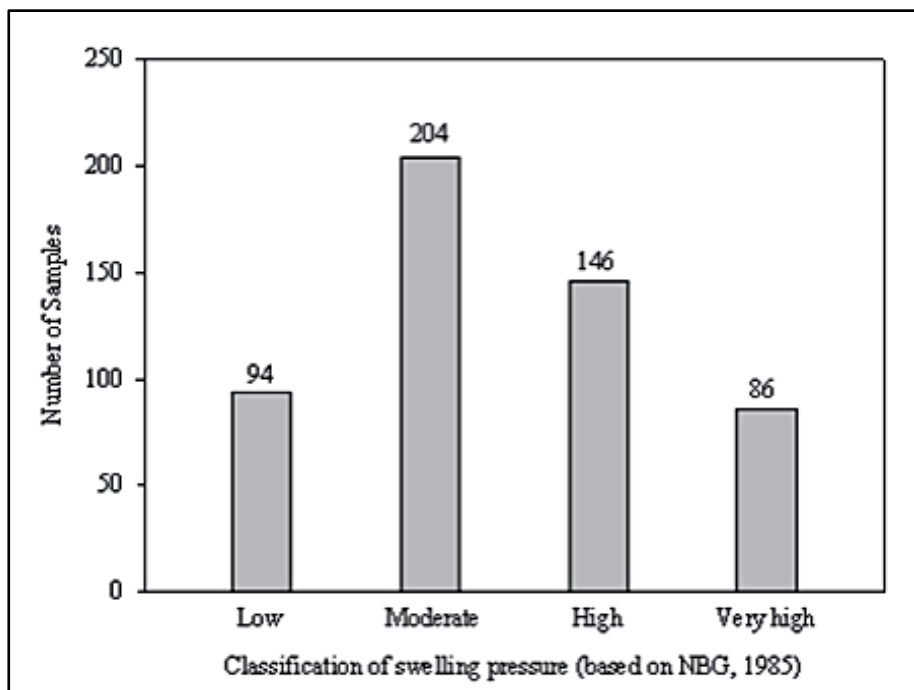


Figure 7-9: Numbers of tested samples in each category of swelling pressure (Mao et.al, 2011; based on NBG, 1985).

The majority of the 530 tested samples are classified with a moderate to high swelling pressure according to table C-1 (Appendix C). A swelling pressure greater than 4 MPa is the highest measured value of the tested samples.

Figure 7-10 shows the accumulative curve of the test results for swelling pressure (Mao et.al, 2011; based on NBG, 1985).

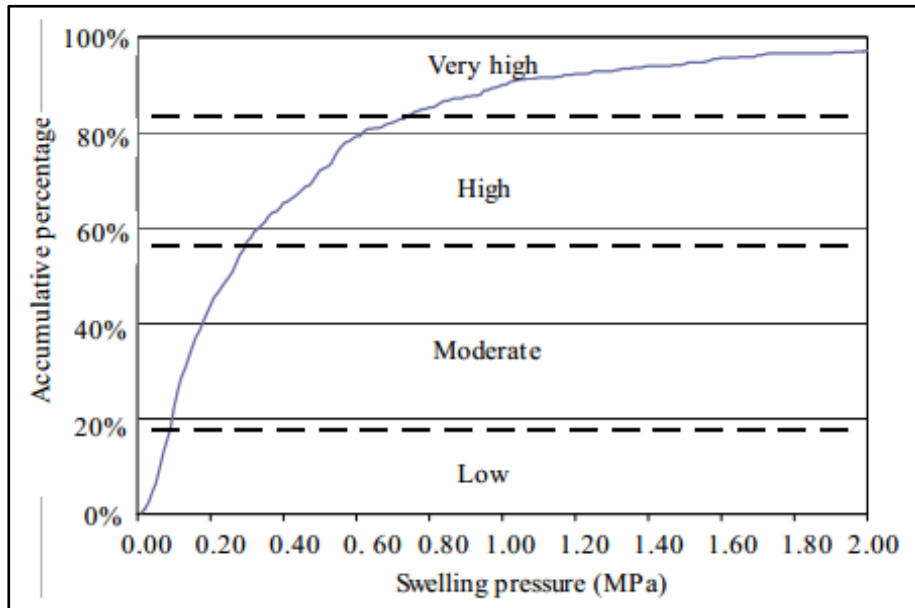


Figure 7-10: Accumulative curve of the test results for swelling pressure (Mao et.al, 2011; based on NBG, 1985).

The accumulative percentage of each category for swelling pressure, figure 7-10, are; 17.7 %, 38.5 %, 27.2 % and 16.6 %.

Figure 7-11 presents the number of samples in each category of free swelling tested at the NTNU/SINTEF laboratory (Mao et.al, 2011; based on NBG, 1985).

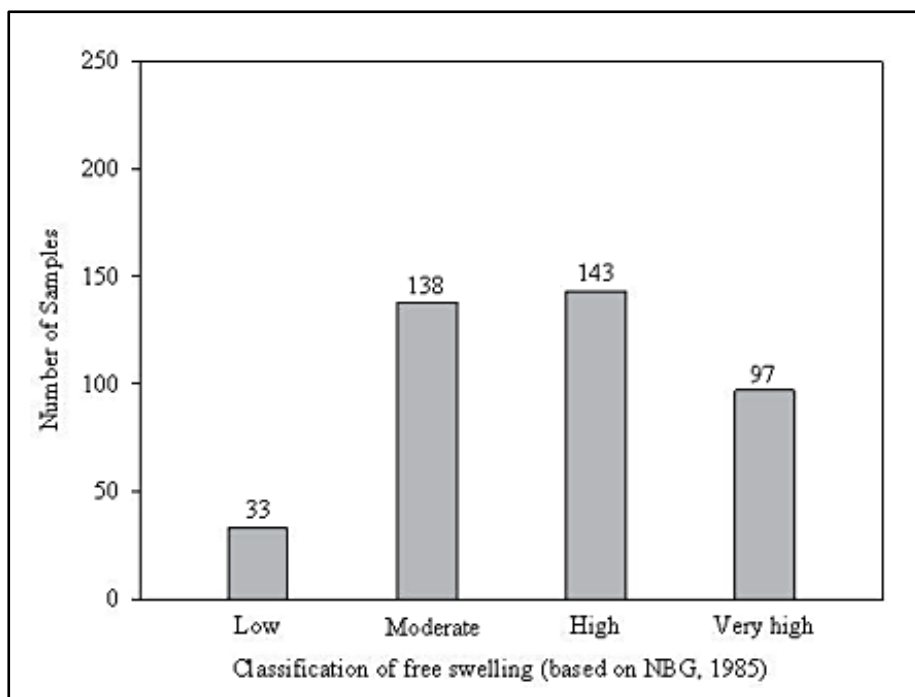


Figure 7-11: Number of samples in each category of free swelling (Mao et.al, 2011; based on NBG, 1985).

The majority of the 411 tested samples are classified with high to moderate free swelling according to table C-1 (Appendix C).

Figure 7-11 shows the accumulative curve of the test results for free swelling (Mao et.al, 2011; based on NBG, 1985).

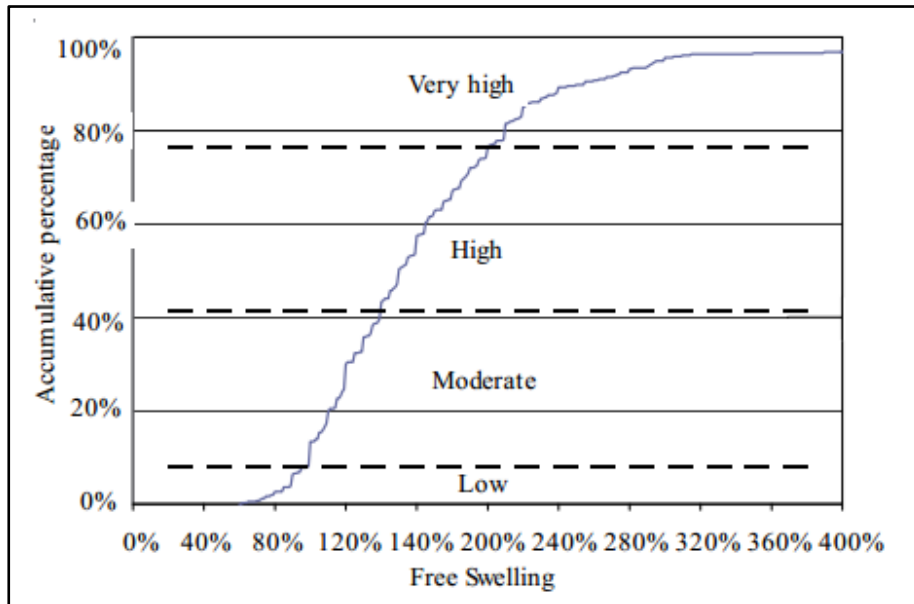


Figure 7-12: Accumulative curve of the test results for free swelling (Mao et.al, 2011; based on NBG, 1985).

The accumulative percentage of each category for free swelling, figure 7-12, are; 8.0 %, 33.6 %, 34.8 % and 23.6 %.

Table 7-2 gives the values for the tested rocks; the free swelling is classified as moderate for all three samples and the swelling pressure is classified as low for the alum shale and the greenschist and moderate for the tuff.

There is greatest deviation between swelling clays and intact rocks in the values for swelling pressure and due to the limited number of samples tested for this thesis it is difficult to find a good correlation between the test results. More tests should be carried out to get a representative distribution of the test results and further a correlation between the values for free swelling and swelling pressure.

## **7.3 Applicability of the testing methods for rock cylinders and rock cubes**

The testing methods for rock cylinders and rock cubes involve different sample preparations and test performances. The presentation and classification of the test results also differs. In the following the differences between the testing methods and the applicability of them are to be discussed.

### **7.3.1 Evaluation and discussion of the sample preparation**

Section 4.2.2 and 4.2.3 give a thorough review of the sample preparation for the rock cylinders and rock cubes.

Cores from the rock specimens were drilled using a drilling machine and further sliced into rock cylinders/discs by the Sliplaboratorium at NTNU. The rock cubes were sawn out from the specimens using the cutter machine.

There were some difficulties in the preparation of the samples due to the risk for fracturing of the rock specimens. The greatest concern was on the preparation of the alum shale which apparently seemed very fragile. All three rock specimens were successfully prepared as both rock cylinders and rock cubes.

### **7.3.2 Evaluation and discussion of the performance and results of the testing**

The test method for rock cylinders involves three stages; compaction, unloading and swelling, see section 5.2. All stages are conducted during a specific time, compared to the test method for the rock cubes which continuous the recording of the swelling displacement until a constant level is reached or a peak is passed, section 5.1.2. The swelling pressure measured for rock cylinders are given in MPa and classification tables make it possible to compare different rocks with respect to the swelling characteristics, section 6.1.2.

In terms of swelling strain the testing on rock cubes, section 6.1.3, provide a measurement unit in percentage which easily is converted to mm displacement;

$$\text{Initial dimension}_{x,y,z} \text{ (mm)} \times \text{Swelling strain (\%)} = \text{Swelling displacement (mm)}$$

Determination of the swelling displacement in situ is done by changing the initial dimension in the spreadsheet in order to obtain a realistic approach to the actual swelling characteristics of the rock mass. Tables for classification of the swelling strain measurements are not yet established and more research and testing have to be carried out to achieve a better understanding of the swelling behaviour of rocks.



### 7.3.3 Comparison of the applicability for the two testing methods

Table 7-3 gives a compilation of the advantages and disadvantages of the two test methods. A comparison of the stages in the testing process is made to decide which method is the most applicable.

Table 7-3: Comparison of the applicability for the two testing methods; rock cylinder and rock cube.

	Rock cylinder		Rock cube	
<b>Preparation of the samples</b>	Have to order preparations from an external laboratory	-	Preparations done by qualified laboratory technician at the laboratory	+
	May be challenging if difficult rock material → cracking, fracturing	-	May be challenging if difficult rock material → cracking, fracturing	-
	Additional grinding of the cylinders to fit the cylindrical test cell	-	Difficult to obtain correctly cubic form, may differ in length	-
<b>Test performance</b>	Three stages, keep track of every element	-	One stage, simple	+
	Fixed time	+	Not finished until stabilization of the strain → time consuming	-
<b>Test results</b>	Swelling pressure, MPa → easy to classify by existing tables	+	Swelling strain, % → easy to convert to mm	+
			No classification table	-
	Swelling only in one direction; dust powder, and axial swelling; rock cylinder	-	Swelling in three directions → Measurement of expansion in all three directions	+
	Potential swelling pressure, index test differ from in situ conditions	-	Actual swelling strain Relate to in situ conditions	+

In the preparation of the samples most disadvantages are found for the rock cylinders. The slicing of the rock cores into cylinders has to be performed by an external laboratory and there might be problems with fracturing of the rock specimens and additional grinding of the discs to fit the test cell. The rock cubes are sawn out by the technicians at the laboratory but challenging rock mass conditions might cause problems getting the right cubical shape and dimensions of the cubes.

The testing of the rock cylinders involves the performance of three stages, compared to the testing of the rock cubes which only entails the swelling stage. A disadvantage of the rock cube testing is the time aspect of it since a continuing record of the displacement has to be carried out until there is a stabilization of the swelling strain.

Test results for the testing of rock cylinders are given in MPa and on the basis of classification tables the swelling characteristics of the rocks is compared and evaluated. For the testing of rock cubes no such tables exists, nevertheless the percentage swelling strain in three directions can easily be converted into mm giving a realistic view on the in situ swelling conditions of rocks and the stability problems caused by swelling.

Applicability of the testing method for rock cubes is the greatest, due to easier sample preparations, an effortlessly test performance and the presentation of the test results. A comparison of the swelling displacement and the swelling pressure show the former one as the most tangible regarding criterias and behaviour of expansive rocks.

## 8 Discussion

---

The research topic for this master thesis is “*Study on the swelling potential of some selected rocks*”. Research of the swelling potential of intact rocks that have an expansive character has been carried out by extensive laboratory work. This research is compared to more comprehensive and traditional research of swelling potential for clays and gouge material. The swelling potential may cause stability problems and threats to tunnels, slopes and foundation if mobilized, and to better understand the mechanisms causing these instabilities a number of tests are performed. The results from the various tests might contribute in finding correlations and thus increase the understanding of factors influencing on the stability.

This section addresses main features of the swelling characteristics for clays and rocks, and an evaluation of the swelling potential for the selected rocks based on the test results. The strengths and limitations of the laboratory work are also discussed. For more detailed discussion it is referred to section 2: Swelling characteristics of clay minerals; 5: Methodology and standards; 6: Results from laboratory work and 7: Evaluations and comparisons.

### 8.1 Swelling characteristics

Stability problems caused by expandable minerals and rocks occur if certain factors and assumptions are fulfilled. There need to be a potential for swelling and the swelling potential has to be mobilized in order to influence on the stability of tunnels, slopes and foundation. In most cases a number of factors interacts and enabling for a swelling potential to arise, see section 2 for a more detailed discussion.

For gouge material and swelling clays the presence of montmorillonite might be the triggering factor which allows for a swelling potential to occur. The type, amount and structure of the clay minerals are of great significance regarding the degree of swelling and the swelling characteristics.

- Clay minerals have a distinct structure consisting of sheets assembles in unit layers of SiO<sub>4</sub>-tetrahedrons and Al(OH)<sub>3</sub>-octahedrons with interlayers capable of holding water molecules and exchangeable cations. The 2:1 ratio between the tetrahedrons and octahedrons is the most common for expandable clay minerals and this ratio and the length of the interlayers determines the swelling potential and the degree of expansion. The greater spacing of the unit layers, the greater shrink and swell behaviour.
- Different types of positively charged cations have attractive forces acting on the exchangeable positions on the surface of the clay minerals and the concentration and valence of the cations reflect the magnitude of the mobilized swelling pressure in the order of ;  $Li^+ < Na^+ < Mg^{2+} < Ca^{2+} < H^+$
- Initial water content, dry density of the swelling clay and the particle bonding influence on the swelling degree due to an interacting between repulsive and attractive forces. The greater the

repulsive forces between the particles and the average surface of the clay minerals, the greater volume change and consequently an increase in the swelling pressure.

- Average swelling pressure and free swelling values measured at the NTNU/SINTEF laboratory is respectively moderate and high. Testing performed on the selected rocks show swelling pressure values from low to moderate and moderate free swelling values for all three rocks.

Swelling potential of rocks with an expansive character is influenced by a variety of factors, and as for clay minerals there need to be a mobilization of the swelling potential for stability issues to occur and to get a better understanding of the mechanisms causing these instabilities a number of tests have been carried out. The test methods have been performed on three different rocks; alum shale, greenschist and tuff and the specimens have been prepared as; dust powder, rock cylinders, rock cubes, rock pieces and thin section.

The results from the rock mechanical testing are also included in this section due to possible correlations between rock strength and swelling behaviour. Values for point load strength, uniaxial compressive and tensile strength, slake-durability index and density have been determined, see table 7-1. Values for free swelling, swelling pressure and swelling strain are given in table 7-2 and mineralogical properties of the rocks are presented in section 6.2.

Interpretations and analysis of the results for swelling testing and rock mechanical testing are given in the following:

- Alum shale:
  - Swelling test results show moderate free swelling, insignificant swelling pressure, both dust powder and rock cylinder, and greatest swelling strain in the x-direction;  $x > z > y$ .
  - Rock mechanical test results show medium point load strength, high slake-durability index, values for  $\sigma_c$  and  $\sigma_t$  indicating a medium strong rock (table G-2 in Appendix G) and the lowest density value of the tested rocks.
- Greenschist:
  - Swelling test results show moderate free swelling, insignificant swelling pressure, both dust powder and rock cylinder, and greatest swelling strain in the z-direction;  $z > x > y$ .
  - Rock mechanical test results show high point load strength, very high slake-durability index, values for  $\sigma_c$  and  $\sigma_t$  indicating a very strong rock (table G-2 in Appendix G) and the highest density value of the tested rocks.

- Tuff:
  - Swelling test results show moderate free swelling, moderate swelling pressure on dust powder, insignificant swelling pressure on rock cylinder and greatest swelling strain in the z-direction;  $z > x > y$ .
  - Rock mechanical test results show medium point load strength, very high slake-durability index, values for  $\sigma_c$  and  $\sigma_t$  indicating a medium strong rock (table G-2 in Appendix G) and a density value in between the one for the alum shale and the greenschist.
- The tuff shows the greatest values for swelling in all tests except for the swelling pressure on rock cylinder where the greenschist is determined with the highest value. The recorded swelling strain for the tuff in the z-direction is considerably larger than the recorded swelling strain in the other directions and compared to the alum shale and the greenschist. The alum shale shows the second highest values for swelling and the greenschist
- The greenschist shows the greatest values for rock mechanical properties in all tests except for the slake-durability index where the tuff is determined with a slightly higher value.

## 8.2 Swelling potential based on test results

This section provides a qualitative analyses and interpretation of the results from the laboratory work in conjunction with the main features listed in section 8.1. Section 7.1 and 7.2 give evaluations and comparisons of the results and the various methods from the laboratory testing. Included in this section is an interpretation of the mineralogical properties of the rocks in correlation of the swelling potential.

- Alum shale:
  - The very fine grained rock shows a distinct foliation and schistosity which may be a reason for swelling due to capillarity. The test results show limited values for both swelling pressure and swelling strain but nonetheless a potential for swelling. The highest value for swelling strain was recorded in the x-direction and this might be inconsistent with the assumptions of capillarity.
  - The XRD analysis show a content of 86 % calcite and this is confirmed by the thin section analysis. Relatively large calcite veins, some with mineral coating, were observed parallel to the foliation. This mineral coating might fill the fractures in the alum shale and the swelling normal to the foliation is decreased. In order to compensate

for the swelling pressure build up a volume increase parallel to the foliation might occur and thus greatest swelling strain in the x-direction.

- Small amounts of two types of iron sulphides were found; sphalerite and pyrite. The quantity of the sulphides indicates a low impact on the swelling potential.
- Small amounts of mica and gypsum were also found. For the same reason mentioned above the effect on the swelling potential is insignificant.

- Greenschist:

- The rock shows a distinct foliation and schistosity which may be a reason for swelling due to capillarity, as for the alum shale.
- The XRD analysis shows a high content of numerous sheet silicates and this is confirmed by the thin section analysis. The structure of the distinct sheet silicates may be a reason for swelling due to the various lengths of interlayers and the capability of holding exchangeable cations and water molecules. The silicate minerals are as follows:
  - Albite is a tectosilicates consisting of  $\text{SiO}_4$ -tetrahedrons in a three dimensional framework with a 1:2 ratio between silicon and oxygen elements.
  - Chlorite and phlogopite are phyllosilicates where the  $\text{SiO}_4$ -tetrahedrons are bonded together in a parallel sheet structure with a 1:2.5 ratio between the silicon and oxygen elements.
  - Amphibole is inosilicate meaning the  $\text{SiO}_4$ -tetrahedrons are bonded together in a double chains structure. The ratio between the silicon and oxygen elements is 1:2.75.
  - Epidote is a sorosilicate where isolated  $\text{SiO}_4$ -tetrahedrons are bonded together and the ratio between the silicon and oxygen elements is 2:7.

The structure of the tectosilicates, phyllosilicates and double chained inosilicates enable for a volume increase due to the interlayer spacing between the unit layers. The swelling potential is mobilized provided the other factor influencing on the swelling are fulfilled.

- Small amounts of mica and sulphide; chalcopyrite were found. The quantity of the minerals indicates a low impact on the swelling potential.

- Tuff:
  - The rock is compact and fine grained with a certain degree of porosity and no distinct layering is observed.
  - The XRD analysis shows a high content of numerous sheet silicates and this is confirmed by the thin section analysis. The structure of the distinct sheet silicates may be a reason for swelling, as above, due to the various lengths of interlayers and the capability of holding exchangeable cations and water molecules. The silicate minerals are as follows:
    - Quartz and zeolites like wairakite and laumontite are tectosilicates consisting of  $\text{SiO}_4$ -tetrahedrons in a three dimensional framework with a 1:2 ratio between silicon and oxygen elements. The three dimensional framework of the zeolites consist of  $(\text{Al,Si})\text{O}_4$ -tetrahedrons arranged in an open ring structure providing an easy flow of water molecules and cations in and out of the silicates (Prestvik, 2005). Changes in the volume due to water content changes will affect the swell and shrink behaviour and thus be a significant contributor to swelling potential of the greenschist.
    - Chlorite and kaolinite are phyllosilicates where the  $\text{SiO}_4$ -tetrahedrons are bonded together in a parallel sheet structure with a 1:2.5 ratio between the silicon and oxygen elements. The kaolinite mineral is a nonexpansive clay mineral and will thus not affect the swelling potential.

The structure of the tectosilicates and phyllosilicates enable for a volume increase due to the interlayer spacing between the unit layers. The swelling potential is mobilized provided the other factor influencing on the swelling are fulfilled.

- No sulphides were found by the XRD-analysis.

When comparing the three tested rocks in terms of swelling characteristics and rock mechanical properties the greenschist is determined as the strongest rock with the lowest swelling potential. The weakest rock is the alum shale which has a moderate swelling potential. The rock with the highest swelling potential is the tuff, which is classified as a medium strong rock.

This indicates correlations between swelling characteristics, mineralogical properties and rock mechanical properties of the rock but also seen are some deviations between the various test results.



### **8.3 Strength and limitations of the laboratory work**

The aim of the extensive laboratory work for this master thesis has been to study the swelling potential of some selected rocks. Strength and limitations of the laboratory work are discussed in the following:

#### Strength:

- The results from the laboratory work provide a good understanding and knowledge of the properties and characteristics of the rocks and thus the mechanisms influencing on the swelling potential
- The laboratory work provides test results that allows for comparisons and correlations between different rock types and test methods.

#### Limitations:

- The performed test methods are used as index tests which means that the laboratory measured values not always correlate to the in situ measured values. Reasons for this difference are due to the sampling and preparations of the specimens and the small quantities and dimensions of the tested material.
- Determination of actual in situ rock conditions for rock support and security measurements involve the need for comprehensive field investigations and geological survey.
- For this particular laboratory work only three rock types were tested and no duplicate tests were performed. The test results obtained for this laboratory work might not be adequate for determining swelling potential of intact rock.

## 9 Conclusions and recommendations

---

### 9.1 Conclusions

On the basis of obtained test results following conclusions can be drawn:

- All three rocks show swelling potential of varying degree and some correlations between swelling potential and rock mechanical properties are found.
  - Alum shale: is classified as a medium strong rock and show moderate swelling pressure and highest swelling strain in the x-direction. Swelling of the alum shale might be explained by various factors and the main reasons are related to the distinct foliation and schistosity of the rock and the presence of a great amount of calcite minerals. Calcite veins with mineral coating fill up the fractures in the rock and the swelling pressure built up in the z-direction is compensated by a swelling strain in the x-direction thus greatest swelling parallel to the foliation.
  - Greenschist: is classified as a very strong rock and show low swelling pressure and highest swelling strain in the z-direction. Swelling of the greenschist might be explained by the distinct foliation and schistosity of the rock and the presence of a great amount of various sheet silicates. The silicate minerals influencing mostly on the swelling potential are the tectosilicates, the phyllosilicates and the double chained inosilicates due to their distinct structure which enable for water molecules and exchangeable cation to enter the interlayers of the silicates and causing a volume increase in the unit layers. This corresponds well to the recorded swelling strain in the z-direction.
  - Tuff: is classified as a medium strong rock and show moderate swelling pressure and the highest swelling strain in the z-direction of all three rocks tested. The rock shows no distinct layering and a great amount of various sheet silicates are found. Tectosilicates and phyllosilicates are the sheet silicates that have the greatest impact on the swelling potential. As for the greenschist these silicate minerals will influence on the swelling degree and the huge difference in the recorded swelling strains for the rocks must be explained by the distinct structure of the zeolites wairakite and laumontite. These tectosilicates consist of a three dimensional framework of  $(Al,Si)O_4$ -tetrahedrons which are arranged in an open structure. This allows for a free flow of water molecules and cations in and out of the interlayers in the silicates providing a change in the water content. An increase in the water content entails an increase in the swelling strain and thus contributes to greatest swelling in the z-direction.

- The testing methods for rock cylinders and rock cubes vary in both methodology and presentation of the test result. The differences are greatest concerning the test performances and the presentation of the test results.
  - Rock cylinder: the test is performed in three stages; compaction, unloading and swelling and the time is specified. This test method allows for measuring of swelling pressure in one direction only. Tables for swelling pressure classification are available enabling for comparisons of the test results and the various rocks.
  - Rock cube: the test is performed in one stage; swelling and continues until the swelling strain is stabilized or has reached a peak. This test method allows for measuring of the swelling strain in three directions and the percentage displacement is easily converted into millimetre displacement. No classifications tables for swelling strain are available

The testing method for rock cube is by far the best in terms of execution and presentation. This method is the most tangible regarding criterias and behaviour of expansive rocks as it results in values for actual displacement of the rock mass.

## 9.2 Recommendations

On the basis of this research following recommendations has been made for future researches:

- Compare two or three rock types in each category of sedimentary, metamorphic and igneous and perform a minimum of three tests for each rock type to get a realistic approach on the swelling potential.
- Replace the testing method on rock cylinders with the testing method for rock cube due to very low values for swelling pressure and high values for swelling strain.
  - Perform testing on rock cubes both parallel and normal to the layering.
  - Perform repeated drying and rewetting cycles to observe shrinkage and swelling behaviour.
- Include SEM and DTA analysis, to confirm the XRD results, in order to distinguish between the various sheet silicates and study the mineral coating on the calcite minerals.
- Include more rock mechanical testing such as Poisson's ratio, young's modulus, UCS, sonic velocity and Brazilian tensile strength to get an even better understanding of the correlations between rock mechanical properties and swelling potential.

## References

---

Bollingmo, P., Nilsen, B. and Nordgulen, Ø. 2007. *The cave-in at the Hanekleiv tunnel, 25 December 2006*. Report from investigation panel established by the Norwegian Department of Transportation, 14 February 2007.

**URL:**<http://www.regjeringen.no/upload/SD/Vedlegg/Veg%20og%20vegtrafikk/Manus070213.pdf>

Brattli, B. 1991. *Polarisasjonsmikroskopi – En introduksjon. Kompendium, Norwegian University of Science and Technology (NTNU)*, 37p. In Norwegian

Brattli, B. and Broch, E. 1995. *Stability problems in water tunnels caused by expandable minerals. Swelling pressure measurements and mineralogical analysis*. Elsevier, Engineering Geology, 39: pp.151-169

Brekke, T. L. and Selmer-Olsen, R. 1965. *Stability problems in underground constructions caused by montmorillonite-carrying joints and faults*. Elsevier, Engineering Geology: p 17.

Cecil, O. 1971. *Correlation of Seismic Refraction Velocities and Rock Support Requirements in Swedish Tunnels, Stability and Strengthening of Rock Tunnels in Scandinavia*, Särtryck och Preliminära rapporter, Statens Geotekniska Institut, pp.1-4

Chen, F. H. 1988. *Foundations on expansive soils*, Developments in geotechnical engineering Vol. 54.

Dahl, F., Hagen, S. and Holmøy, K. H. 2013: *Utvikling innenfor testing av svelleegenskaper-testapparaturer og metodikk-svelleleirer og bergarter. Fjellsprengeingsteknikk/Bergmekanikk/Geoteknikk*, p17. In Norwegian.

EARTHNERD's NOTES ON GEOLOGY, website: *Physical Geology, Earth as a System, Rocks and Minerals* (2014.06.30).

**URL:** <http://www.earthnerd.eu/notes/?p=149>

International Union of Geological Science (IUGI), International Commission on Stratigraphy. 2013. *International chronostratigraphic chart*.

**URL:** <http://www.stratigraphy.org/index.php/ics-chart-timescale>

ISRM Commission on Swelling Rocks. 1977. *Part 2: Suggested methods for determining swelling and slake-durability index properties*. International Journal of Rock Mechanics and Mining Science & Geomechanics. Abstracts: pp.151-156.

ISRM Commission on Testing Methods. 1985. *Suggested method for determining point load strength*. International Journal of Rock Mechanics, Mining Science & Geomechanics. Abstracts, Vol.22, No. 2: pp.51-60.

Jensen, E. S. 2006. Damms Naturhåndbøker - *Bergarter og mineraler*, 220p. In Norwegian

Mao, D., Nilsen, B. and Dahl, F. 2011. *Laboratory Testing of Swelling Gouge from Weakness Zone - Principle and Recent Update*. ARMA 11-152, 45<sup>th</sup> US Rock Mechanics/Geomechanics Symposium, San Francisco, CA, June 26-29: 6p.

Mineralogy Database, official website: *Mineral Data* (2014.06.18)

**URL:** <http://www.webmineral.com/data>

Mørk, M. B. 2008. *Geologi innføring. Lecture notes, Norwegian University of Science and Technology (NTNU)*. In Norwegian.

NGI (Norwegian Geotechnical Institute). 2010. *Alunskifer byr på utfordringer*. In Norwegian.

**URL:**<http://www.ngi.no/no/Arkiv/Aktualiteter---ARKIV/Alunskifer-Et-voksende-problem/>

NGI (Norwegian Geotechnical Institute). 2014. *Black shale*.

**URL:** <http://www.ngi.no/en/Project-pages/Blackshale/Background/>

NGU (Geological Survey of Norway). 2005. *NGU-lab; XRD-analysis*. In Norwegian.

**URL:** [http://www.ngu.no/upload/Norges%20geologi/NGU-lab/NGU\\_LAB\\_XRD\\_analyser.pdf](http://www.ngu.no/upload/Norges%20geologi/NGU-lab/NGU_LAB_XRD_analyser.pdf)

NGU (Geological Survey of Norway). 2014. *Navn på vulkansk glass*. In Norwegian.

**URL:**<http://www.ngu.no/no/tm/Vare-tjenester/Spor-en-geolog/Tidligere-stilte-spor-smal/Navn-pa-vulkansk-glass/>

Nilsen, B. 2013. *Hard rock subsea tunnels-investigation, planning, excavation and rock support*.

NTU-JTC, Industrial Infrastructure Innovation centre, Seminar 20.02.2013, Singapore.

**URL:** <http://ntu-jtc->

[centre.ntu.edu.sg/News\\_Events/Seminars/Documents/NTU\\_Singapore20\\_02\\_13\\_SubseaTunnels.pdf](http://ntu-jtc-centre.ntu.edu.sg/News_Events/Seminars/Documents/NTU_Singapore20_02_13_SubseaTunnels.pdf)

Nilsen, B. and Palmstrøm, A. 2013. *Methodology for predicting and handling challenging rock mass conditions in hard rock subsea tunnels*. Proc. 6<sup>th</sup> Int. Symp. on Strait Crossings, Bergen June 2013, Statens vegvesen, Tekna

**URL:** <http://www.tekna.no/ressurs/filer/sc2013/032%20Bjorn%20Nilsen%20-%20Methology%20for%20predicting%20and%20handling%20challenging%20rock%20mass%20conditions.pdf>

Nilsen, B. 2012. *Ingeniørgeologi – Berg. Kompendium - Videregående kurs, Norwegian University of Science and Technology (NTNU)*. In Norwegian.

Nilsen, B. 2012. *Ingeniørgeologi – Berg. Lecture notes - Videregående kurs, Norwegian University of Science and Technology (NTNU)*. In Norwegian.

- Nilsen, B. 2010. *Ingeniørgeologi. Lecture notes - Grunnkurs, Norwegian University of Science and Technology (NTNU)*. In Norwegian.
- Nilsen, B. and Broch, E. 2009. *Ingeniørgeologi – Berg. Kompendium – Grunnkurs, Norwegian University of Science and Technology (NTNU)*. In Norwegian
- Nilsen, B. 2010. *Cases of instability caused by weakness zones in Norwegian tunnels*. Bull. Eng. Geol. Environ. 70: pp.7-13.
- NGU (Geological Survey of Norway). 2014. *Kart og data – Berggrunn*. In Norwegian.  
**URL:** <http://www.ngu.no/no/hm/Kart-og-data/Berggrunn/>
- NBG (Norwegian Group for Rock Mechanics). 2000. *Engineering Geology and Rock Engineering, Handbook No. 2*. Oslo, Norway, 192p.
- NBG (Norwegian Group for Rock Mechanics). 1985. *Handbook in Engineering Geology – Rock*. Trondheim, Norway, 140. In Norwegian.
- Palmström, A., Stille, H. and Nilsen, B. 2000. *The Frøya tunnel – a sub-sea road tunnel in complex ground conditions*. Fjellsprengeteknikk/Bergmekanikk/Geoteknikk, pp. 19-30.
- Panthi, K. K. 2008. *Analysis of Engineering Geological Uncertainties Related to Tunnelling in Himalayan Rock Mass Conditions. Doctoral theses, Norwegian University of Science and Technology (NTNU)*. Faculty of Engineering Science and Technology, Chapters 3 and 4.
- Prestvik, T. 2001. *Petrologi og geokjemi*, pp.170-178. In Norwegian
- Prestvik, T. 2005. *MINERALOGI, En innføring i krystallografi og mineralogi, p 138*. In Norwegian.
- Prestvik, T. 2009. *Mineralogi/Petrografi. Lecture notes, Norwegian University of Science and Technology (NTNU)*. In Norwegian
- Pusch, R. 2012. *Environmental Soil Properties and Behaviour, Swelling Clays, chapter 4*. CRC Press, Taylor & Francis Group, LLC: pp.133-161.
- Rogers, J. D., Olshansky, R. and Rogers, R. B. 2014. *Damage to foundations from expansive soils*.  
**URL:**  
[http://web.mst.edu/~rogersda/expansive\\_soils/DAMAGE%20TO%20FOUNDATIONS%20FROM%20EXPANSIVE%20SOILS.pdf](http://web.mst.edu/~rogersda/expansive_soils/DAMAGE%20TO%20FOUNDATIONS%20FROM%20EXPANSIVE%20SOILS.pdf)
- Rønning, J. S., Ganerød, G. V., Dalsegg, E. and Reiser, F. 2013. *Resistivity mapping as a tool for identification and characterisation of weakness zones in crystalline bedrock: definition and testing of an interpretational model*. Bull. Eng. Geol. Environ: 20p.  
**URL:** [http://download.springer.com/static/pdf/436/art%253A10.1007%252Fs10064-013-0555-7.pdf?auth66=1400668130\\_8df2b95c629474cfbdf9f67b087f6c&ext=.pdf](http://download.springer.com/static/pdf/436/art%253A10.1007%252Fs10064-013-0555-7.pdf?auth66=1400668130_8df2b95c629474cfbdf9f67b087f6c&ext=.pdf)

Selmer-Olsen, R. and Palmstrøm, A. 1989. *Tunnel collapses in swelling clay zones*. Tunnels & Tunnelling, Nov., 1989: pp. 49-51.

Statens Vegvesen. 2010. *Håndbok 021 - Vegtunneler*, Statens Vegvesen Vegdirektoratet, pp. 29-39. In Norwegian.

**URL:** <http://www.vegvesen.no/Fag/Publikasjoner/Handboker>

Statens Vegvesen. 1992. *Håndbok 021 – Vegtunneler: normaler*, Tidligere utgaver, Statens Vegvesen Vegdirektoratet, pp. 9-13. In Norwegian.

**URL:** <http://www.vegvesen.no/Fag/Publikasjoner/Handboker>

Sæther, O. M., Xie, R., Aagaard, P., Endre, E., Løken, T. and Rudolph-Lund, K. 2010. *Report 2009.063, Main and trace element content of shales from Ankerskogen (Hamar) and Øvre Slottsgt. (Oslo), Norway* (NGU): 128p.

The Bruker Corporation, website: *Products - X-ray Diffraction, D8 ADVANCE*. (2014.06.02)

**URL:** <http://www.bruker.com/products/x-ray-diffraction-and-elemental-analysis/x-ray-diffraction/d8-advance/overview.html>

The Cooperative Soil Survey, website: *Soil tutorial, Soil texture-Physical Properties, Clay Minerals and Related Properties*. (2014.05.06)

**URL:** <http://soils.missouri.edu/tutorial/page8.asp>

Wallis, S. 2010. *Links across the waters – Strait Crossings Conference Report*. 5<sup>th</sup> Int. Symp. on Strait Crossings, Trondheim June 21-14.

**URL:** <http://www.tunneltalk.com/Strait-Crossings-Jan10-Conference-report.php>



## Appendix A: Tunnel profile

The Norwegian Public Roads Authorities (2006) classifies Norwegian road tunnels in six classes which range from A to F. The classification is based on the total length of the tunnel, in km, and the AADT (20), expected value 20 years after opening. On the basis of the tunnel classes A-F, the tunnel profile, number of tunnel tubes etc. are then determined, figure A-1 (Statens Vegvesen, 2010).

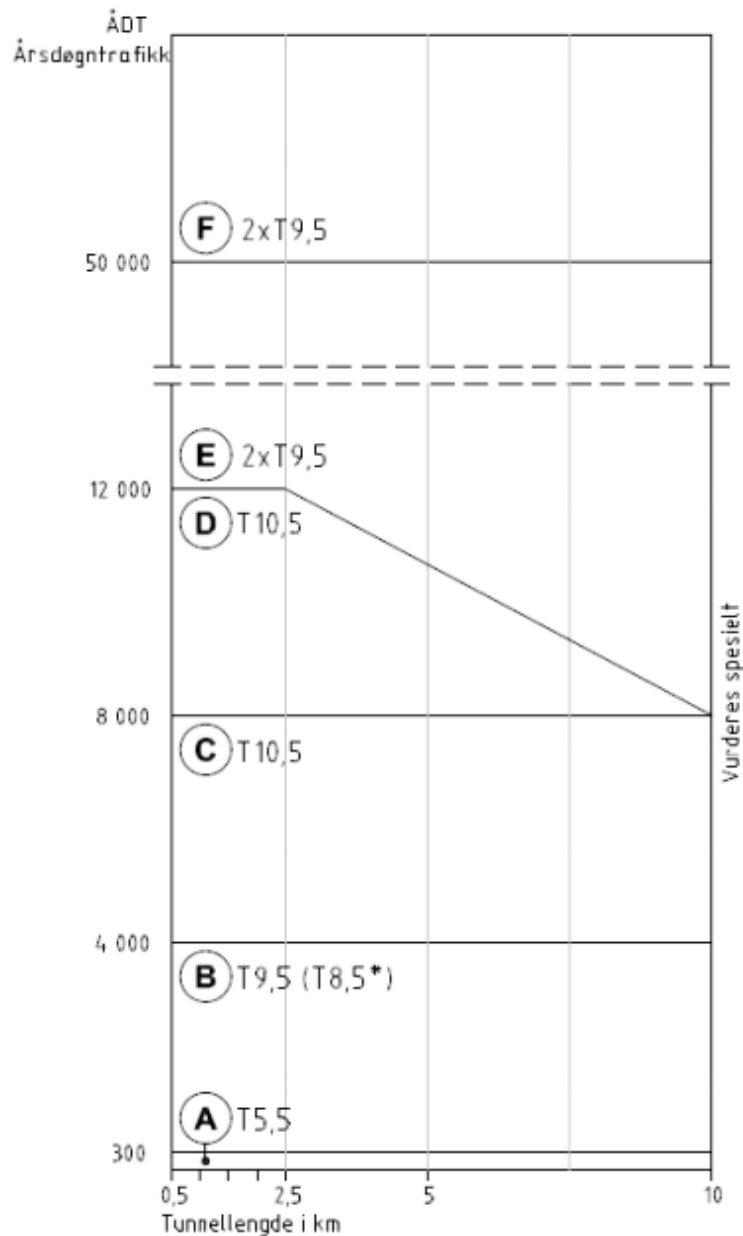


Figure A-1: Tunnel classes A-F based on total tunnel length and AADT (Statens Vegvesen, 2010).

Figure A-2 shows the designation of the tunnel profile by total width in the roadway level.

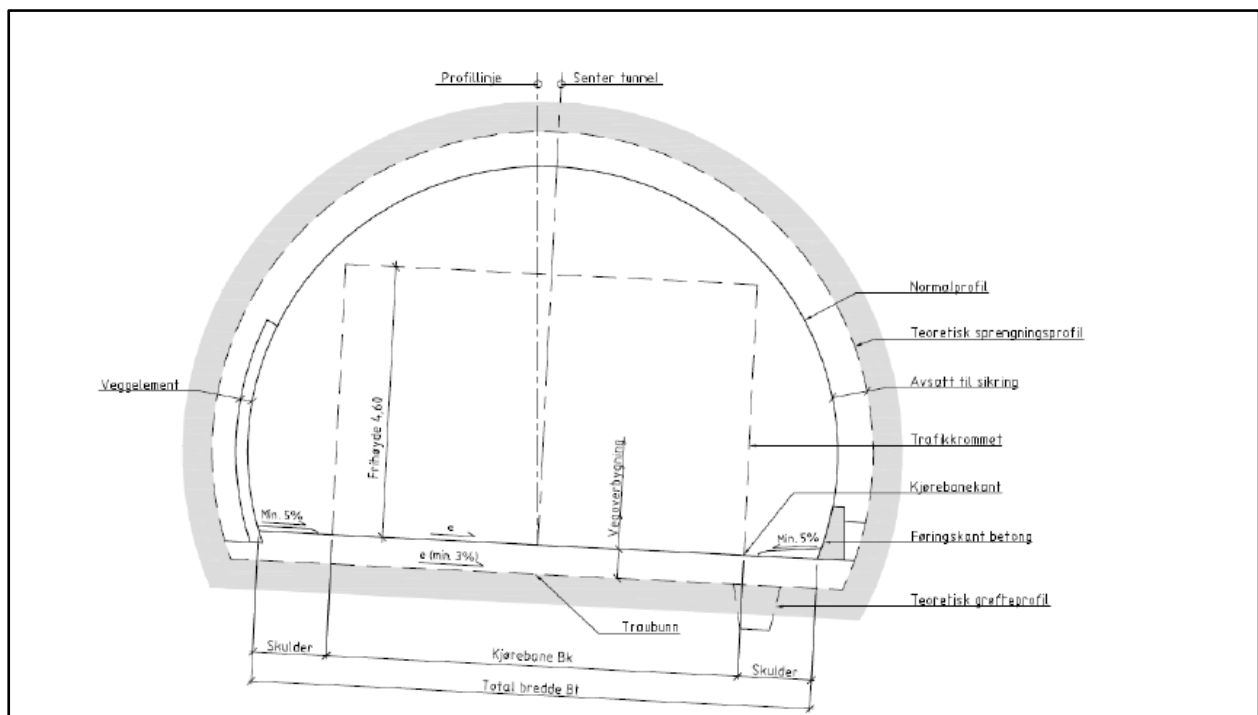


Figure A-2: Schematic tunnel profile of a road tunnel (Statens Vegvesen, 2010).

Figures A-3 and A-4 shows the geometrical measures and the cross section data for the different tunnel profiles.

Profil	Total bredde <b>B<sub>T</sub></b>	Kjørebane- bredde <b>B<sub>K</sub></b>	Senterhøyde veggradier <b>Y<sub>V</sub></b>	Veggradius <b>R<sub>V</sub></b>	Senteravstand veggradier <b>X</b>	Senterhøyde hengradius <b>Y<sub>H</sub></b>	Hengradius <b>R<sub>H</sub></b>
<b>T4</b>	4,00	3,00	-	-	-	1,330	2,400
<b>T5,5</b>	5,50	3,50	1,770	4,790	3,402	3,171	2,587
<b>T8,5</b>	8,50	6,50	1,770	4,790	0,402	1,981	4,500
<b>T11,5</b>	11,50	9,50	1,770	4,790	2,598	-0,258	7,199
<b>T7,5</b>	7,50	5,00	1,570	4,790	1,550	2,481	3,594
<b>T9,5</b>	9,50	7,00	1,570	4,790	0,450	1,213	5,212
<b>T10,5</b>	10,50	8,00	1,570	4,790	1,450	0,664	5,950
<b>T12,5</b>	12,50	10,00	1,570	4,790	3,450	-0,466	7,458
<b>T13,0</b>	13,00	10,50	1,570	4,790	3,950	-0,735	7,825
<b>T13,5</b>	13,50	11,00	1,570	4,790	4,450	-0,817	8,053
<b>T14,0</b>	14,00	11,50	1,570	4,790	4,950	-1,294	8,575

Figure A-3: Geometrical measures for the different tunnel profiles, in meters (Statens Vegvesen, 2010).

Profil	Teoretisk sprengningsprofil		Normalprofil	
	Areal, $A_S$ $m^2$	Buelengde, $B_S$ m	Areal, $A_N$ $m^2$	Buelengde, $B_N$ m
T4	22,84	12,94	13,65	10,04
T5,5	42,59	17,73	29,72	14,79
T8,5	66,08	21,18	49,65	18,23
T11,5	90,72	24,36	70,87	21,42
T7,5	55,39	19,50	40,39	16,56
T9,5	70,89	21,66	53,60	18,72
T10,5	78,83	22,71	60,40	19,78
T12,5	96,24	24,93	75,48	22,00
T13,0	100,71	25,48	79,37	22,54
T13,5	105,66	26,08	83,72	23,14
T14,0	109,83	26,58	87,33	23,64

Figure A-4: Cross section data for the different tunnel profiles (Statens Vegvesen, 2010).

Figures A-5 and A-6 shows the tunnel profiles, respectively T8 and T9.

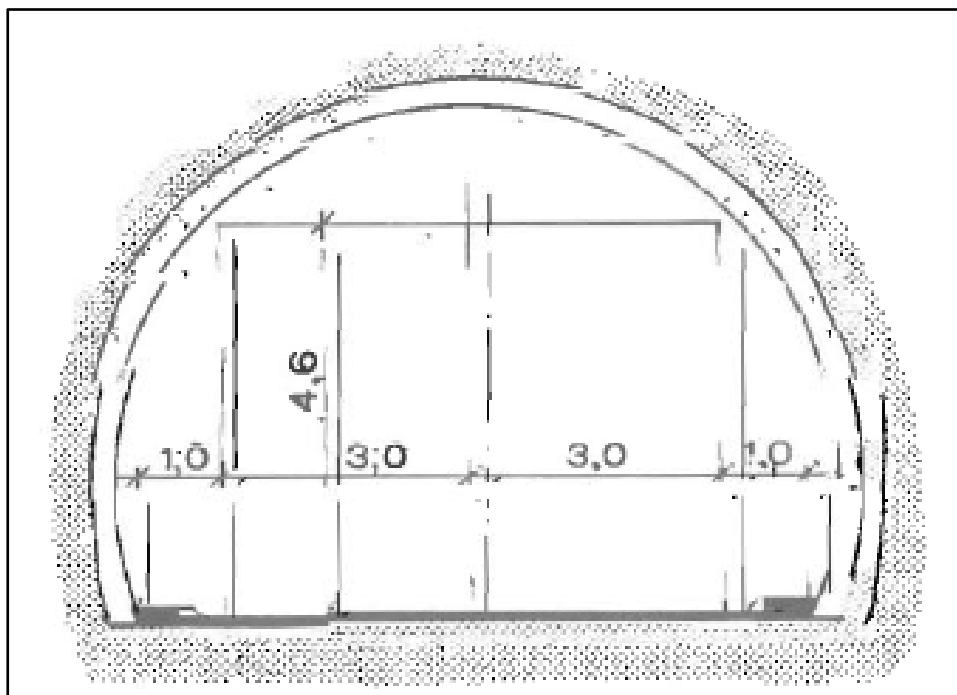


Figure A-5: Geometrical measures for tunnel profile T8 (Statens Vegvesen, 1992).

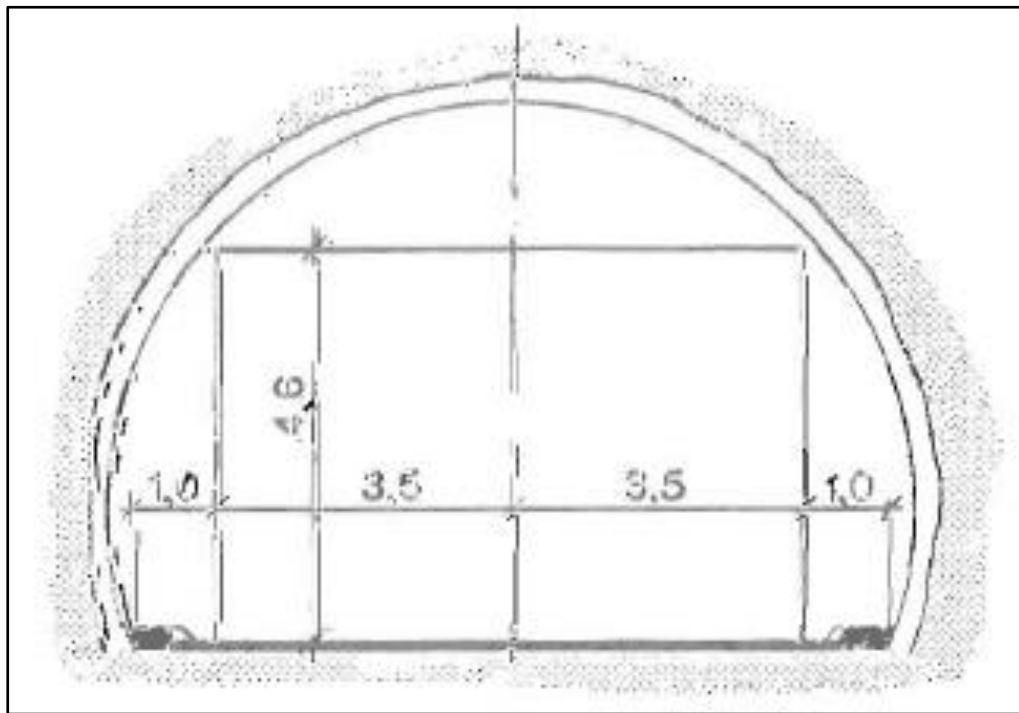


Figure A-6: Geometrical measures for tunnel profile T9 (Statens Vegvesen, 1992).

# Appendix B: Geological timescale - chronostratigraphic chart

The chronostratigraphic chart, figure B-1, is a detailed classification of geological time and is divided into Systems/Periods, Series/Epochs and Stages/Ages (International Union of Geological Science, 2013).

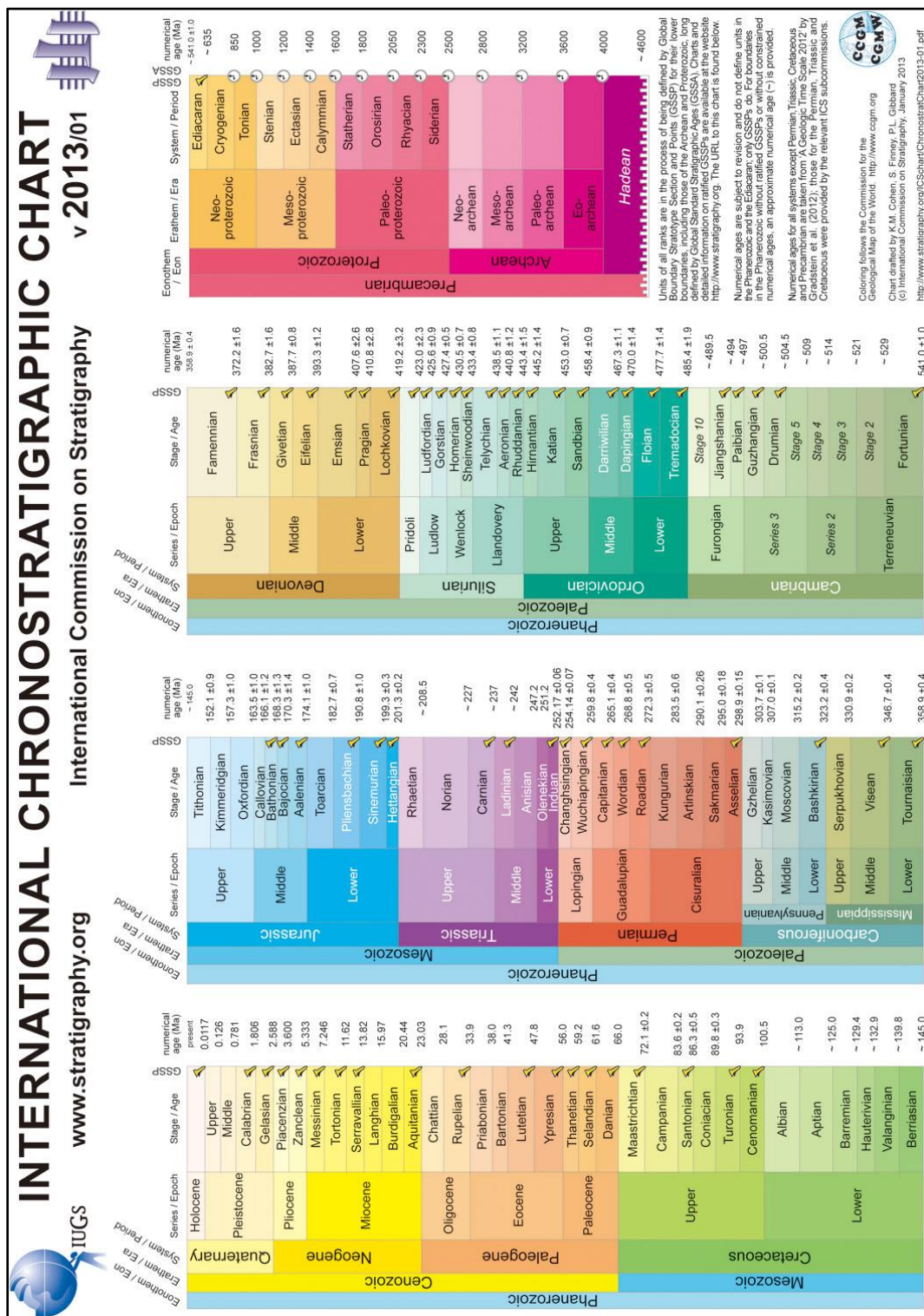


Figure B-1: Chronostratigraphic chart showing the geological timescale (International Union of Geological Science, 2013).



## Appendix C: Classification of swelling parameters of gouge material

The classification gives a quantitative determination of the swelling parameters of gouge material. Both free swelling and swelling pressure are performed under zero volume change conditions (Dahl et.al, 2013).

Table C-1: Classification of free swelling and swelling pressure (modified after Dahl et.al, 2013; based on NBG, 1985).

Classification	Free swelling [%]	Swelling pressure [MPa]
Very high	> 200	> 0,75
High	140 – 200	0,30 – 0,75
Moderate	100 – 140	0,10 – 0,30
Low	< 100	< 0,10

Table C-2: Fine grained material content and swelling parameters of gouge material from four project cases (modified after Nilsen, 2010).

Project	Material < 20 µm [%]	Free swelling [%]	Swelling pressure [MPa]
Hanekleiv tunnel	14	150	0,18
Oslofjord tunnel	34	167	0,55
Atlantehav tunnel	5	135	0,10
Frøya tunnel	-	800	1,55
“Inactive”		40 - 70	< 0,15
“Active”		> 100 - 200	> 0,30

<b>Journal nr:</b>			
<b>Prøve:</b>	Alunskifer		
<b>Fri svelling</b>			
			<i>[ml]</i>
Andel materiale	10		
Svelling	13		
<b>FS</b>	<b>130</b>		

<b>Journal nr:</b>			
<b>Prøve:</b>	Grønnskifer		
<b>Fri svelling</b>			
			<i>[ml]</i>
Andel materiale	10		
Svelling	10		
<b>FS</b>	<b>100</b>		

<b>Journal nr:</b>			
<b>Prøve:</b>	Tuff		
<b>Fri svelling</b>			
			<i>[ml]</i>
Andel materiale	10		
Svelling	13,5		
<b>FS</b>	<b>135</b>		

Figure C-1: Free swelling values from the Excel spreadsheet.





## Appendix D: Classification of rock composition, grain size, texture and silicate minerals.

---

Figure D-1 shows an interference color chart with increasing order to the right. The related minerals for each order are shown.

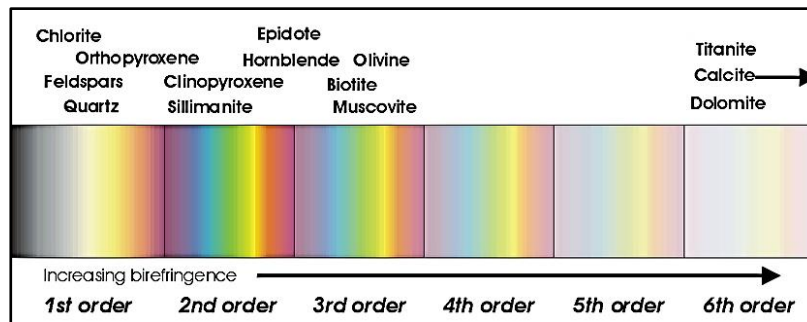


Figure D-1: Order of interference colours (Prestvik, 2009)

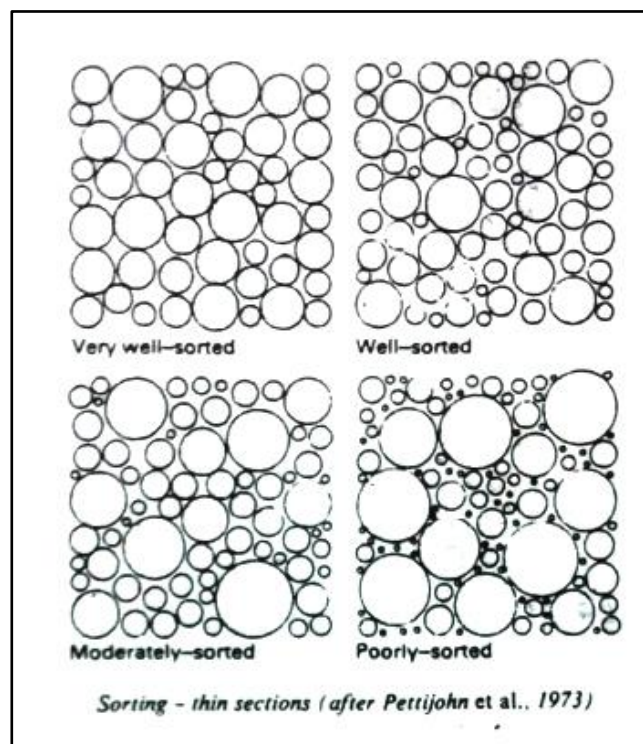


Figure D-2: Sorting of mineral grains (Prestvik, 2009).

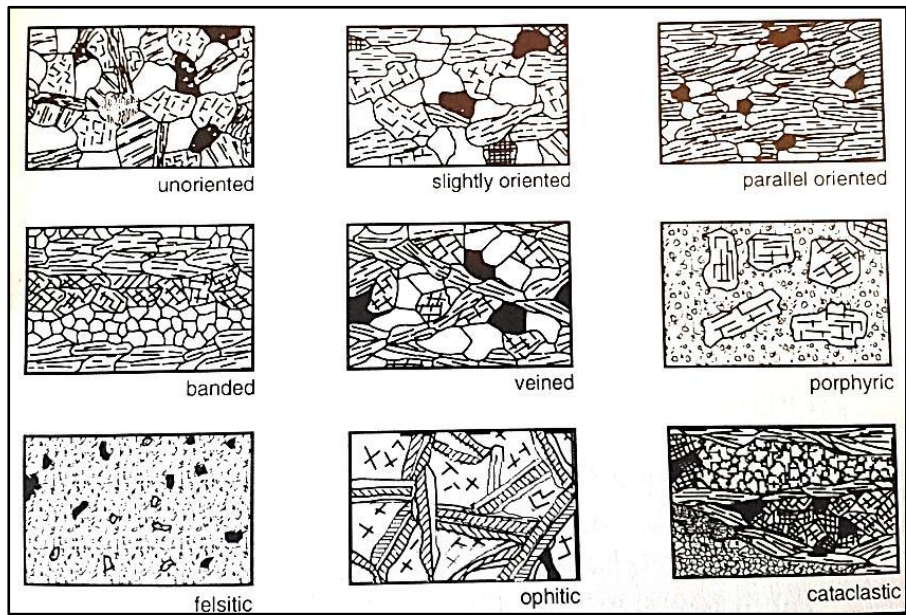


Figure D-3: Orientation of the mineral grains (NBG, 2000).

Grain size [mm]	Pyroclastic fragment	Pyroclastic rock type
> 64	Bombs and blocks	Agglomerate and pyroclastic breccia
2-64	Lapilli	Lapilli-tuff
0,06-2	Coarse ash	Tuff
0,004-0,06	Fine ash	
< 0,004		

Figure D-4: Classification of pyroclastic rock material by grain size, above, and by grain size relative to percentage, below (Modified after Prestvik, 2001).

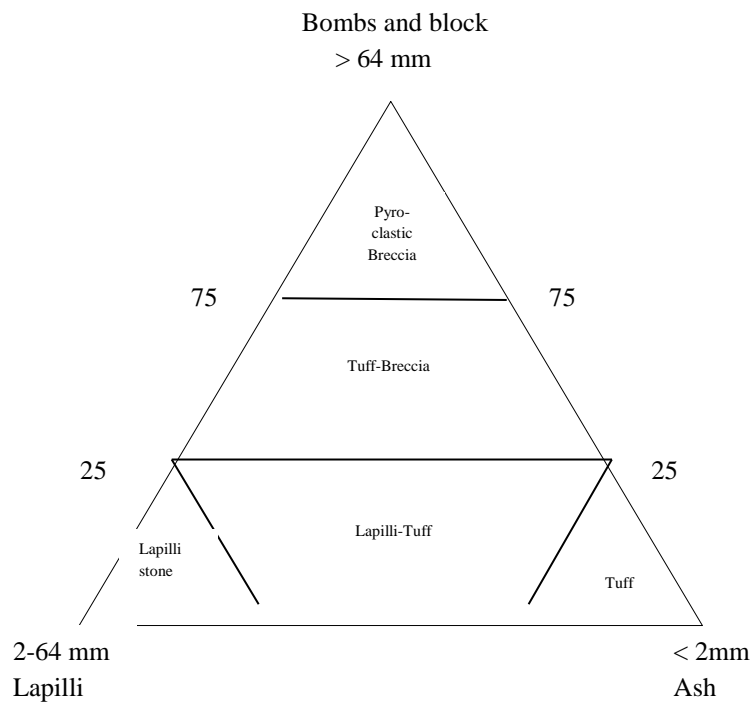



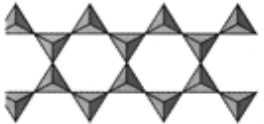
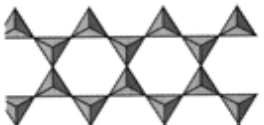

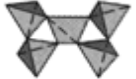


Figure D-5: Classification of silicate minerals (Earth Nerd's, 2014 and Prestvik, 2005).

<b>Silicate mineral</b>	<b>Structure</b>	<b>Si:O</b>	
Nesosilicates	Insular tetrahedrons bonded by positively charged cations	1:4	
Sorosilicates	Isolated double tetrahedrons	2:7	
Cyclosilicates	Ring structure of linked tetrahedrons, 3, 4 or 6 tetrahedrons	1:3	
Inosilicates, single chain	Chain structure	1:3	
Inosilicates, double chain	Two chains are bounded together	1:2,75	
Phyllosilicates	Parallel sheet structure	1:2,5	
Tectosilicates	3D structure, framework of tetrahedrons	1:2	



## Appendix E: Classification of point load strength

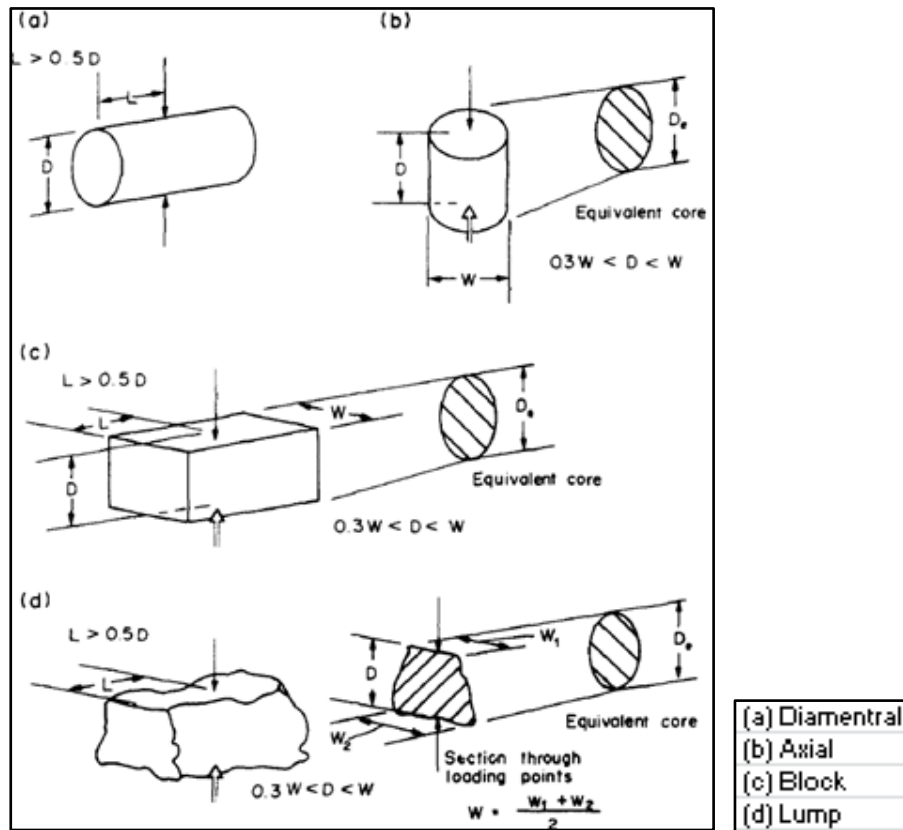


Figure E-1: Specimen shape requirements for the irregular lump test (ISRM, 1985).

Table E-2: Classification of point load strength  $I_s$  and suggested value of the factor  $k_{50}$  (NBG, 2000).

Category	Point Load Strength (Bieniawski, 1984)	Uniaxial Compressive Strength $\sigma_c$ [MPa]	Point Load Strength $I_{50}$ [MPa]	Suggested value of $k_{50}$
Very low strength	< 1 MPa			
Low strength	1 – 2 MPa			
Medium strength	2 – 4 MPa			
High strength	4 – 8 MPa			
Very high strength	> 8 MPa			
		25 – 50	1.8 – 3.5	14
		50 – 100	3.5 – 6	16
		100 – 200	6 – 10	20
		> 200	> 10	25


								
RESULTS - Point Load Strength								
Basis:		ISRM Suggested Method for Determining Point Load Strength						
Journal No.:		Master thesis						
Sample:		Alum shale						
Remarks:								
Technician:								
Date:								
Water content:								
Test No.	Test type	Width [mm]	Height [mm]	D <sub>c</sub> [mm]	Failure load [kgf]	Failure load [N]	Point Load Index I <sub>p</sub> [MPa]	Index of Strength I <sub>p,50</sub> [MPa]
1	Lump	21,85	9,9	16,6		1390	5,0	3,1
2	Lump	35,01	15,1	26,0		420	0,6	0,5
3	Lump	23,15	13,8	20,2		1850	4,5	3,0
4	Lump	36,83	18,1	29,1		710	0,8	0,7
5	Lump	46,66	18,6	33,2		3110	2,8	2,3
6	Lump	13,27	23,0	19,7		2080	5,4	3,5
7	Lump	30,05	20,9	28,3		1840	2,3	1,8
8	Lump	33,07	27,4	34,0		2780	2,4	2,0
9	Lump	42,9	16,7	30,2		3260	3,6	2,9
10	Lump	42,15	44,0	48,6		3800	1,6	1,6
<b>Mean</b>							<b>2,9</b>	<b>2,3</b>
Results indicate:				Uniaxial Compressive Strength			σ <sub>c</sub> [MPa]	31,7
				Tensile Strength			σ <sub>t</sub> [MPa]	1,8

Figure E-3: Excel spreadsheet showing the calculated of point load strength for the alum shale.


								
RESULTS - Point Load Strength								
Basis:		ISRM Suggested Method for Determining Point Load Strength						
Journal No.:		Master thesis						
Sample:		Greenschist						
Remarks:								
Technician:								
Date:								
Water content:								
Test No.	Test type	Width [mm]	Height [mm]	D <sub>c</sub> [mm]	Failure load [kgf]	Failure load [N]	Point Load Index I <sub>p</sub> [MPa]	Index of Strength I <sub>p,50</sub> [MPa]
1	Lump	57,69	20,1	38,4		18310	12,4	11,0
2	Lump	40,4	19,9	32,0		9670	9,5	7,7
3	Lump	63,09	29,3	48,5		20810	8,8	8,7
4	Lump	38,41	25,3	35,2		12110	9,8	8,4
5	Lump	68,74	29,1	50,4		7360	2,9	2,9
6	Lump	54,26	25,8	42,2		13080	7,4	6,8
7	Lump	46,75	37,5	47,2		12410	5,6	5,4
8	Lump	50,02	18,3	34,1		7200	6,2	5,2
9	Lump	43,61	26,7	38,5		11510	7,8	6,9
10	Lump	55,66	14,5	32,0		8870	8,6	7,1
<b>Mean</b>							<b>8,0</b>	<b>7,1</b>
Results indicate:				Uniaxial Compressive Strength			σ <sub>c</sub> [MPa]	141,1
				Tensile Strength			σ <sub>t</sub> [MPa]	5,6

Figure E-4: Excel spreadsheet showing the calculated point load strength for the green schist.



**RESULTS - Point Load Strength**

**Basis:** *ISRM Suggested Method for Determining Point Load Strength*

**Journal No.:** *Master thesis*

**Sample:** *Tuff*

**Remarks:**

**Technician:**

**Date:**

**Water content:**

Test No.	Test type	Width [mm]	Height [mm]	D <sub>c</sub> [mm]	Failure load [kgf]	Failure load [N]	Point Load Index I <sub>p</sub> [MPa]	Index of Strength I <sub>s,50</sub> [MPa]
1	Lump	38,79	38,4	43,5		6960	3,7	3,5
2	Lump	45,56	21,7	35,4		2160	1,7	1,5
3	Lump	41,85	23,6	35,4		3660	2,9	2,5
4	Lump	45,76	23,2	36,7		4170	3,1	2,7
5	Lump	22,43	20,3	24,1		3470	6,0	4,3
6	Lump	28,03	20,9	27,3		2560	3,4	2,6
7	Lump	15,39	18,7	19,1		3720	10,2	6,6
8	Lump	22,83	15,6	21,3		2890	6,4	4,3
9	Lump	16,76	14,8	17,7		1080	3,4	2,2
10	Lump	20,09	13,4	18,5		2530	7,4	4,7
<b>Mean</b>							<b>4,3</b>	<b>3,3</b>

Results indicate:

Uniaxial Compressive Strength

$\sigma_c$  [MPa]

46,4

Tensile Strength

$\sigma_t$  [MPa]

2,7

Figure E-5: Excel spreadsheet showing the determination of point load strength for the tuff.



# Appendix F: Classification of slake-durability index

Formula for slake-durability index, cycle 1, used when  $I_{d2}$  is between 0 and 10 % (ISRM, 1977):

$$I_{d1} = \frac{B-D}{A-D} \times 100\%$$

Formula for slake-durability index, cycle 2, used in rock classification (ISRM, 1977):

$$I_{d2} = \frac{C-D}{A-D} \times 100 \%$$

Table F-1: Slake-durability classification (modified after Dahl et.al, 2013)

Classification	Slake-durability Index ( $I_{d2}$ ) % retained*
Very low durability	0 – 30
Low durability	30 – 60
Medium durability	60 – 85
Medium high durability	85 – 95
High durability	95 – 98
Very high durability	98 – 100

\* % remaining rock material > 2.0 mm after 2 cycles of drying and wetting

RESULTS - Slake-durability Index ( $I_{d2}$ )	
<i>Basis: ISRM Suggested Method for Determination of the Slake-Durability Index</i>	
Journal No:	
Sample:	Alum shale
Remarks:	
Technician:	
Date:	
Slake fluid:	Tap water
<b>Mass</b>	<b>[g]</b>
Mass A (Sample + drum)	2365,1
Mass B (Sample after testcycle 1 + drum)	2346,0
Mass C (Sample after testcycle 2 + drum)	2338,0
Mass D (Drum - cleaned and dried)	1886,9
Mass of dried specimen before testing	450-550
<b>Slake-durability Index</b>	<b>% retained</b>
$I_{d1}$	96,0
$I_{d2}$	94,3
Remarks:	
<b>Category</b>	<b>Slake-durability Index (<math>I_{d2}</math>) % retained</b>
Very low	0 – 30
Low	30 – 60
Medium	60 – 85
Medium high	85 – 95
High	95 – 98
Very high	98 – 100

RESULTS - Slake-durability Index ( $I_{d2}$ )	
<i>Basis: ISRM Suggested Method for Determination of the Slake-Durability Index</i>	
Journal No:	
Sample:	Green schist
Remarks:	
Technician:	
Date:	
Slake fluid:	Tap water
<b>Mass</b>	<b>[g]</b>
Mass A (Sample + drum)	2402,1
Mass B (Sample after testcycle 1 + drum)	2395,9
Mass C (Sample after testcycle 2 + drum)	2392,3
Mass D (Drum - cleaned and dried)	1886,4
Mass of dried specimen before testing	450-550
<b>Slake-durability Index</b>	<b>% retained</b>
$I_{d1}$	98,8
$I_{d2}$	98,1
Remarks:	
<b>Category</b>	<b>Slake-durability Index (<math>I_{d2}</math>) % retained</b>
Very low	0 – 30
Low	30 – 60
Medium	60 – 85
Medium high	85 – 95
High	95 – 98
Very high	98 – 100

RESULTS - Slake-durability Index ( $I_{d2}$ )	
<i>Basis: ISRM Suggested Method for Determination of the Slake-Durability Index</i>	
Journal No:	
Sample:	Tuff
Remarks:	
Technician:	
Date:	
Slake fluid:	Tap water
<b>Mass</b>	<b>[g]</b>
Mass A (Sample + drum)	2369,8
Mass B (Sample after testcycle 1 + drum)	2366,9
Mass C (Sample after testcycle 2 + drum)	2364,9
Mass D (Drum - cleaned and dried)	1886,7
Mass of dried specimen before testing	450-550
<b>Slake-durability Index</b>	<b>% retained</b>
$I_{d1}$	99,4
$I_{d2}$	99,0
Remarks:	
<b>Category</b>	<b>Slake-durability Index (<math>I_{d2}</math>) % retained</b>
Very low	0 – 30
Low	30 – 60
Medium	60 – 85
Medium high	85 – 95
High	95 – 98
Very high	98 – 100

Figure F-1: Excel spreadsheet showing the determination of the slake-durability index  $I_{d2}$  for all three rock samples.

Slake Values for chart				
No.		1	2	3
Sample		Green schist	Tuff	Alum shale
Value		98,1	99,0	94,3
	30,0	30,0	30,0	30,0
	60,0	60,0	60,0	60,0
	85,0	85,0	85,0	85,0
	95,0	95,0	95,0	95,0
	98,0	98,0	98,0	98,0

Figure F-2: Chart values for the slake-durability testing

## Appendix G: Classification of density and compressive strength

---

Table G-1: Density for some Norwegian rocks (Nilsen and Broch, 2009).

Norwegian rock type	g/cm <sup>3</sup>
Gabbro and amphibolite	3,15
Anorthosite and chlorite schist	3,00
Greenstone	2,85
Mica and dolomite	2,80
Limestone and syenite	2,75
Tronhjemite	2,70
Granite and quartzite	2,65

Table G-2: Classification of rock hardness based on determination of the compressive strength (Modified after NBG, 2000).

Compressive strength for rocks		
Grade and term		Approximate $\sigma_c$ [MPa]
R0	Extremely weak rock	0.25-1
R1	Very weak rock	1-5
R2	Weak rock	5-25
R3	Medium strong rock	25-50
R4	Strong rock	50-100
R5	Very strong rock	100-250
R6	Extremely strong rock	> 250